COMPUTATIONAL STUDIES OF HOMOGENEOUS CHARGE COMPRESSION IGNITION, SPARK IGNITION AND OPPOSED PISTON SINGLE CYLINDER ENGINES

By

Ali Mubarak Al-Qahtani

A thesis submitted to

The University of Birmingham

For the degree of

DOCTOR OF PHILOSOPHY

Department of Mechanical Engineering

The University of Birmingham

Edgbaston, Birmingham, UK

September 2017

Abstract

In this research, possible improvements in engine specifications using the simulations developed on the AVL BOOST™ and Ricardo WAVE™ platforms were investigated. These modelling simulations help the author to predict the effect of any improvements in engine specifications without practical experimental challenges and difficulties. Firstly, HCCI and SI engines were modelled with the intention of maximizing the engine's efficiency and minimizing the emissions. Changes of valve timing and throttle angle influence emissions' reduction and the efficiency of the engine. In SI engines, the emissions of NOx can be reduced by using EGR, while only having a little effect on performance. The emissions from the HCCI, due to their intrinsically low emission output, were not improved. The effect of increasing the bore to stroke ratio in an opposed piston engine whilst maintaining a constant swept volume, port geometry and combustion timing, shows an increase of heat losses due to the lower ratio of exposed surface area to volume; an increase in thermal and mechanical efficiency; and most importantly, an improvement in fuel consumption. Also, in this research study, different strategies for opposed piston engines were investigated to increase the engine's efficiency. The effect of a variable compression ratio on an opposed piston engine's performance indicates different behaviour at various engine speeds and under different running conditions.

Dedication

To my lovely Family

Acknowledgments

This thesis would not have been possible without the contribution of a number of persons whom I would like to gratefully acknowledge.

Firstly and most importantly, I would like to express my sincerest gratitude my supervisor, Professor Miroslaw Lech Wyszynski for his invaluable and continuing support, guidance and encouragements during this PhD course. His guidance helped me in all the time of research and writing of this thesis. I could not have imagined having a better supervisor, advisor and mentor for my PhD. I would also like to thank my co-supervisor, Professor Hongming Xu. Dr Pawel Mazuro is also acknowledged for his insightful comments, data and encouragement. I would like to deeply thank Mr Omid Doustdar for his support throughout my research programme.

Finally I would like to thank all my family: my parents, my wife, my brothers and sisters for their endless support throughout my educational life.

'This thesis was copy-edited for the conventions of language, grammar and spelling by Janet's Proofreading Service.'

Table of Contents

List of Figures

List of Tables

List of Abbreviations

BTE   Brake Thermal Efficiency

BMEP   Brake Mean Effective Pressure

BSFC   Brake Specific Fuel Consumption

BDC   Bottom Dead Centre

CAD   Crank Angle Degree

CFD   Computational Fluid Dynamics

CI   Compression Ignition

C   Celsius

CO   Carbon Monoxide

CR   Compression Ratio

DI   Direct Injection

EGR   Exhaust Gas Recirculation

EVC   Exhaust Valve Closing

g/kwh   gram per kilowatt hour

GDI   Gasoline Direct Injection

HCCI   Homogenous Charge Compression Ignition

IC   Internal Combustion

ICE   Internal Combustion Engine

IDC   Inner Dead Centre

IMEP   Indicated Mean Effective Pressure

ISFC	Indicated Specific Fuel Consumption
ISO	International Standard Organization
IVO	Intake Valve Opening
IVC	Intake Valve Closing
K	Kelvin
kg	Kilogram
kJ	Kilojoules
kw	Kilowatts
kw/kg	Kilowatt per Kilogram
l	Litre
λ	Relative Air to Fuel Ratio
ME	Mechanical Efficiency
MFB	Mass Fraction Burnt
mg	milligram
mm	Millimetres
MPa	Mega Pascal
NOx	Nitrogen Oxides
ODC	Outer Dead Centre
OPE	Opposed-Piston Engine
OP2S	Opposed-Piston Two Stroke
P	Pressure
Pa	Pascal
PM	Particulate Matter
ppm	part per million by volume

ROHR	Rate of Heat Release
RPM	Engine Speed, Revolutions Per Minute
SFC	Specific Fuel Consumption
SOI	Start of Injection
SI	Spark Ignition
ɵ	Crank Angle
TDC	Top Dead Centre
$°aTDC_{COMB}$	After Top Dead Centre of Combustion, Crank Angle Degrees
$°bTDC_{COMB}$	Before Top Dead Centre of Combustion, Crank Angle Degrees
$°aTDC_{GE}$	After Top Dead Centre of Gas Exchange, Crank Angle Degrees
$°bTDC_{GE}$	Before Top Dead Centre of Gas Exchange, Crank Angle Degrees
USD	United State Dollar
USD/kw	United State Dollar per Kilowatt
ULSD	Ultra-Low Sulphur Diesel
V	Volume
VCR	Variable Compression Ratio
VCT	Variable Cam Timing
VVT	Variable Valve Timing
WUT	Warsaw University of Technology

Chapter 1 – Introduction

1.1 Overview

In the automotive industry, there is much ongoing research into areas such as engine efficiency improvements, emissions and economical products. This research concentrates on innovation in relation to the demand for efficient, stronger, cleaner and cheaper vehicles compared to modern power trains. These vehicles are equipped with more advanced internal combustion engines and most of their development research focuses on improvements of the systems of power, control and increasing the durability of engines. Hybrid and electric cars are in the most demand and are developing fast. Besides these electric cars, conventional internal combustion engines need some improvement so they can play an important role as they have done for the last few decades. The only unconventional engine produced in small quantities is a motor WANKEL [1]. Researchers in Poland decided to build a completely different engine from the classic piston engine which is called *bezkorbowymi.* These engines were considered for use in aerospace industry. After the Second World War the rapid development of the automotive industry and the high demand for an uncomplicated solution forced the focus onto the classic conventional engine because of its relatively simple structure, easily analysed kinematics and dynamics and extensive mass production. So nowadays, conventional engines are used commonly in modern cars but still researchers are working to develop them as much as they can.

Modelling is one of the best solutions in any industry to reduce production and investigation costs. Any industry design and build of a prototype needs very

comprehensive investigation and analysis to study its behaviour in the real world. All of these issues can be solved by carrying out simulation in suitable software packages. Many different types of software packages are used in vehicular companies.

This research envisages the future prospect of automotive industries' modernization to utilize OP advanced technologies.

The experimental methods used in this research have focused on exploring and exploiting previously used opposed-piston (OP) engine. Trusting the novel technique used in this research, innovation to envision potential fuel efficiency and environmentally friendly conditions for the future automotive industry will be presented. These experimental exploits have discovered techniques and introduced promising technologies for the opposed-piston 2-stroke (OP2S) engine, to endorse its fuel efficiency and to offer an advance formation, power density, thermal efficiency whilst sustaining its lower cost and weight. Today thermodynamic modeling remains an indispensable and cost-effective route in the development and optimization of internal combustion engines (ICEs). To illustrate a distinctive engine and to comprehend the performance of a single cylinder two-stroke opposed piston engine's capabilities to improve its performance and its effect on the environment were enormously challenging.

1.2 Research Objectives and Approaches

The main purpose of this thesis is to compare two simulation software platforms, AVL BOOST ^{TM} and Ricardo WAV E^{TM} to simulate HCCI and SI GDI engines with the intention of maximizing the engine's efficiency and minimizing the emissions. Additionally, AVL boost software has been used to simulate a single cylinder two stroke opposed piston engine. It is aimed to achieve the most optimal set-up (high bore\stroke ratio and variable compression ratio). The main advantage of this research is allowing an option to be built and tested in real world conditions without the need for an expensive prototypes system.

The OP2S engine thermodynamic model was simulated and validated against experimental results in AVL Boost^{TM}, which provides the most consistent and advanced engine simulation tools in particular the analysis of the piston dynamics, heat release, scavenging and heat transfers are highlighted in discrete sections of this thesis. The unambiguous results indicate that heat losses decreased by increasing stroke to bore ratio, because of the surface area-to-volume reduction in the cylinder, undoubtedly improved ITE and mechanical efficiency, by means of reduced ISFC.

In addition to the compression ratios, the effect of stroke-to-bore (S/B) ratios on the OP2S's performance is investigated with various values of S/B ratios, whilst maintaining a constant swept volume, port geometry, and combustion timing, and thereafter, the effect on fuel consumption and heat loss are also analyzed in this thesis.

The overall aim in this research is to develop the most efficient simulation based on some assumptions in order to improve the engine's efficiency. The broad spectrum purpose of this thesis is to deliberate the implementation of a novel engine pattern. This brand of engine is unique, totally visualised by the author and has not yet been described in the open literature. It contains two opposed pistons in a single cylinder two-stroke structured by wobble plate mechanism to generate the obligatory piston motion aimed at an engine mechanical efficiency increase within thermodynamics performance improvements. The individual investigated objectives include:

- Build and simulate a model of a single cylinder engine by using a computer program called AVL boost software.

- Model a simple single cylinder opposed piston two-stroke engines.

- Investigating the combustion analysis by altering high bore /stroke ratio

- Investigating the combustion analysis by altering the variable compression ratio

- Examine the effect of efficiency when altering the parameters.

- Generate pattern performance data from engine data analysis.

- Match the AVL boost software model performance specifications with the experimental result from Warsaw University of Technology

The University of Birmingham as well as the Warsaw University of Technology have provided all of the correlated contact to allow the above assimilated method to be accomplished.

1.3 Thesis Outline

This thesis is organized into eight chapters as follows:

1.3.1. Chapter 1: Introduction

The research's background, aims, objectives and approaches have been explained in this first chapter.

1.3.2. Chapter 2: Review of Literature

This chapter is divided into two main parts, the first part introduces an overview of internal combustion engines (CI, HCCI and SI) and the second part reviews the literature related to opposed piston engines and the importance of the investigated engine.

1.3.3. Chapter 3: Experimental Setup

The detailed description of the experimental facilities that were used in this research study is presented in this chapter. The experimental section is divided in to two main sections, the first part explains the single cylinder diesel engine which was tested at the University of Birmingham and the second section explains the opposed piston engine which called the PAMAR engine, which is based at the Warsaw University of Technology in Poland.

1.3.4. Chapter 4: Modelling and Simulation Software Packages

Detailed descriptions of two software packages which were used in this research study are presented in this chapter. It describes the model geometry, boundary conditions, governing inputs, assumptions and any procedures needed for simulations.

1.3.5. Chapter 5: Thermodynamic Simulation Comparison of AVL BOOST and Ricardo WAVE for HCCI and SI Engines Optimisation

This chapter explains the HCCI and SI engines performances, combustion and emission analysis and some possible improvements using the developed simulation in AVL BOOST and Ricardo WAVE. Experimental and simulations results will be compared to find the optimum modelling setup to reach a minimum amount of error.

1.3.6 Chapter 6. Investigation into the Effect of Bore to Stoke Ratio on the Performance of a Single Cylinder Two-stroke Opposed Piston Engine

This chapter investigate the opposed piston engine's promising fuel efficiency. The AVL model was built and the effect of bore to stroke ratio on performance of the engine studied to find the optimum engine design parameters was examined.

1.3.7 Chapter 7. Evaluation of the Effect of Variable Compression Ratios Performance on an Opposed Piston Two-stroke Engine

The main aim of this chapter is to model and simulate a simple single two stroke opposed piston engine and then investigate the effect of the variable compression ratio on the engine's performance. The AVL BOOST package was used as modelling software.

1.3.8 Chapter 8. Summary, Conclusions and Recommendations for Future Work

According to the research results, in this chapter conclusions of the modelling work performed in this thesis's scope are shown and also recommendation and suggestions for future studies are presented.

Chapter 2 – Review of

Literature

In this study, the review of the literature is divided into two main parts to show the main objectives of this study. The first section provides the relevant history and literature of HCCI and SI engines, which mainly is relevant to Chapter 5. The second section is related to opposed piston engines, which is mostly the topic for the investigations in Chapters 6 and 7. The literature concerning the opposed piston engine is not comprehensive because the novelty of the investigated engine.

2.1. Internal Combustion Engine

The internal combustion engine as power machinery plays an important role in modern society; almost all cars are powered by internal combustion engines (although there are electric cars and hybrids, the vast majority powered by internal combustion engines). There are also large scale trains and ships are based on internal combustion engines as the driving force. This type of engine has a long history; and is now widely used in aviation, transportation, agriculture, the military, general machinery and in other areas in the world where economic development plays an important role. The history of the invention of human technology tells us that any successful invention is not achieved at the first stage and it takes many attempts to achieve perfection. The internal combustion engine has experienced development stages, time and time again being improved.

The earliest appearance of the internal combustion engine used coal gas as fuel. In 1860, Belgian Jean Joseph Etienne Lenoir (1822–1900) produced the first commercial gas machine (single-cylinder, two-stroke, no compression or electric ignition, the output power of 0.74-1.47 kw, speed 100 rpm), but because there was

no compression stroke, the thermal efficiency was only about 4%. From 1861 to 1862, the German Nikolaus Otto (1832-1981) built a copy of the Lenoir engine, to try to structure compressed charge four cycle engine and manufacture a free piston and no compression gas Lenoir engine. In 1864, Nikolaus Otto's and Eugen Langen's (1833-1895) cooperative developed a free piston engine and exhibited it at the Paris Exhibition in 1867. In 1876, they created a four-stroke gas machine (single cylinder, horizontal, with coal gas as fuel, power at about 2.21 kw, 180 rpm), which had four times the thermal efficiency than the machine built by Lenoir, up to 6%. It is acknowledged as the world's first true internal combustion engine. German engineer Gottlieb Daimler (1834-1900) manufactured a constant volume internal combustion engine as per the principle of Otto's engine in 1885. Using the supercharger, which he invented, petrol became evaporates before combustion. The speed went up to 800 rpm and the compression ratio to 3:1. Increasing the compression ratio means that the engine will have a greater impetus; At the same time, the constant volume internal combustion engine speed was correspondingly improved and this thermodynamic law, based on the internal combustion engine has been widely used. Karl Benz (1844-1929) manufactured the first reliable two-stroke gas engine in December 1879 (speed of 200 rpm, power of about 0.7 kilowatts). He improved Otto's four-stroke engine to trial the world's first single-cylinder engine three-wheeled car in 1886. In the same year, he invented the mixer and electric ignition device, so that the gasoline engine became more perfect. In 1892, Rudolf Christian Karl Diesel (1858-1913) developed the first compression ignition engine which injected fuel into a combustion chamber and ignited the fuel by being greatly compressed. To improve the power and reduce the weight-to-power ratio, engineers

have tried to improve the internal combustion engine. One of these important measures is to increase the speed and the number of cylinders. Karl Benz invented the boxer engine, also named as the flat engine, or the horizontally opposed engine in 1896. The horizontally opposed engine has corresponding pistons which reach top dead centre at the same time, thus balancing each other in momentum.
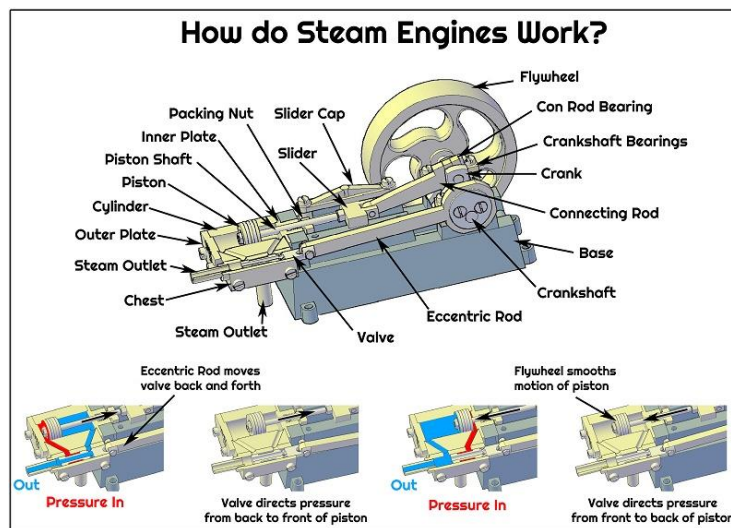
Figure 2-1: Schematic diagram of steam engine [2]

Watt had obtained the first patent on the manufacture of steam engines in 1769 as shown in figure 2-1, after he continued research and improvement which lasted 100 years, only to make it more perfect. The improvement of the steam engine is basically carried out under the guidance of the developing thermodynamic theory, along the direction of raising the vapour pressure, the multi-stage section expansion and increasing the rotational speed. The first improvement was made in 1802 by the British engineer Trevizick who made the "high-pressure steam engine" as a symbol. He improved the boiler so that the vapour pressure increased from 0.8 to 3.5 atm. The second major improvement was made by the British engineer Wolf in 1816; he

made a "composite steam engine", it is saved more than half fuel and improved mechanical efficiency compared to the Watt steam engine (that is, the mechanical energy into mechanical energy and total heat). After the third, fourth and fifth big improvement, up to the early 20th century, the vapour pressure reached 20 atmospheric pressure, the mechanical efficiency increased to 23% and the power to more than 2400 horsepower. By the 20th century, 20 years later, with the internal combustion engine and the rapid development of steam turbines, the steam engine was gradually replaced. In the steam engine's continuous improvement and development process, people gained more and more profound understanding of the steam engine's "natural" shortcomings: The steam engine must have a boiler, it is bulky, has poor mobility; heat is derived through the steam medium and then converted into machinery. These drawbacks are related to the fact that the fuel must be combusted outside the cylinder -" external combustion ". Therefore, it has long been studied of the internal combustion engine into the external combustion engine, the boiler and the cylinder into one, eliminating the steam medium, so that gas combustion expansion of high-pressure gas directly to the piston does the work - this is the internal combustion engine. Around 1860, the invention of the internal combustion engine was envisioned by many, but most failed to solve the practical problems. This is because the work of the internal combustion engine at that time was little researched and there was a lack of theoretical guidance and also the lack of fuel in the cylinder quickly burned. In 1862, the Frenchman Drogheda published his theory of an internal combustion engine. The conditions for improving the efficiency and economic performance were put forward: boosting before ignition; rapid expansion to maximum expansion ratio after combustion. He also proposed the

working process of the four-stroke internal combustion engine as follows: the piston down into the gas and then piston up to compressed gas and finally ignition, rapid combustion expansion of gas to promote the piston down work; but unfortunately he did not create the internal combustion engine.

The first four-stroke internal combustion engine was developed by the German Otto in 1876 according to the principles that Drogheda produced. In 1861, he made the first gas internal combustion engine. Three years later, in cooperation with Langen, he developed the engine, and in 1867 at the Paris Expo Gold Award Otto made the first four-stroke internal combustion engine, which is the first to replace the steam engine of the practical internal combustion engine. Otto's internal combustion engine had a compact structure and gave a stable and reliable performance, with a speed of 80 to 150 rpm, mechanical efficiency of 12% to 14% and a weight power ratio of 200 kg/hp. It usually used gasoline as fuel and is also known as the gasoline engine. In 1859, the United States discovered the first oil well. Since then, the oil industry developed rapidly; Gasoline and diesel gradually become common commodities and also the material basis for the development of internal combustion engines.

The history of the development of the internal combustion engine involves continuous improvement and the history of technological invention. In 1885, Daimler developed a constant volume internal combustion engine, according to Otto's machine, using his invented surface carburettor gasoline mist as fuel, with a speed of up to 800 rpm and a compression ratio of 3:1. During the 20th century, to

meet the needs of the automotive industry and aircraft industry, the internal combustion engine made great progress.

The first 20 years of development improved the power and reduced the weight-to-power ratio. The main measures taken to increase the speed increased the number of cylinders. At this stage, the internal combustion engine's speed reached 1500 rpm; the proposed ignition, starting, vaporization and cooling and other technical problems were also one by one resolved. A "multi-cylinder system" was the main technical measure to reduce the weight-to-power ratio. The 4-cylinder, 8-cylinder linear, V-type arrangement and 12-cylinder, 16-cylinder V-shaped arrangement appeared successively, and the weight-to-power ratio was reduced to 4kg/hp, which reached a practical level for aircraft.

The main research topic in the 1930s to the 1950s was to solve the "blast barrier" problem of the internal combustion engine, in order to further improve the compression ratio. The compression ratio is the ratio of the volume of the mixture of the intake cylinder to the volume of the compressed air mixture, which affects the power and mechanical efficiency of the internal combustion engine. However, when the compression ratio is increased to about 4:1, the high temperature generated by the compression allows the mixture to ignite without significant ignition. Deflagration of the engine has a severe impact on the normal operation and can damage the engine. The "blast barrier" problem is the United States General Motors Corporation of Migrai and Bao Yi De's solution. They mixed a small amount of tetraethyl lead in gasoline to interfere with the process of combining oxygen and gasoline molecules, increasing the compression ratio from 4:1 to 8:1, making the

octane number (also known as antiknock value, in the anti-detonation performance indicators) increase from 55 to 85, between 1920 and 1950, greatly improving the gasoline engine power and efficiency.

In this period, there was a research project concerning the installation of a supercharger gasoline engine. A serious obstacle to the development of aircraft was shown in high-altitude flight, due to thin air and insufficient oxygen supply. In the United Kingdom a gas compressor with air compressor gas supply equipment changed the air pressure to 1.5 atm. With the invention of the late 1930's gas turbine, with its drive turbocharger, the pressure was increased to 1.6 atm. The use of the supercharger reduced the power-to-weight ratio of the gasoline engine to 0.5 kg/hp and increased the power to 3500 hp at 3400 rpm. The fuel consumption was reduced to 0.2 kg/hp and the service life from 200 hours in the 1920s to 3000 hours in the 1970s.

In 1956, in the history of the development of the internal combustion engine there appeared a revolutionary new design, where the German Wankel (F. Wankel) invented the rotary piston engine, also known as the rotor engine. In a Wankel rotary engine, an equilateral triangle rotor rotates in a specially shaped cylinder. A crescent shaped combustion chamber is formed between the rotor side and the curved wall of the cylinder. The three corners of the rotor are fitted with springs and sealing plates, which are in sliding contact with the inner wall of the cylinder. The volume of the combustion chamber increases and decreases in sequence as the rotor rotates. From the carburettor inhalation of the combustion chamber mixture, with the rotor rotation for reduction, the combustion chamber is compressed to a minimum spark plug

ignition, and then promotes the rotor rotation to increase the volume of combustion chamber. This engine directly make the output shaft to rotate, greatly reduces the vibration while removing the crankshaft connecting rod and valve mechanism. The numbers of parts were reduced by 40%; there was a 50% weight reduction and then also half the size of small/ high speed, power, fuel consumption, which attracted attention.

The spark ignition (SI) engine worked on the principle of the operating cycle invented by Nicolaus A. Otto in 1876. The compression ignition (CI) engine worked on the principles established by Rudolf Diesel in 1892.

For the engine to work properly, it must continue to perform some periodic operations. Spark ignition (SI) - the operating principle of the engine was invented by Nicolaus A. Otto in 1876; therefore, the SI engine was also known as the Otto engine. Rudolf Diesel discovered the working principle of a compression ignition engine (CI) in 1892; so the CI engine is also known as a diesel engine. The SI and CI engines work almost the same, except for the fuel combustion process that occurs in both engines. In the SI engine, the combustion of the fuel occurs through the spark generated by the spark plug located in the cylinder head. The fuel is compressed to high pressure and its combustion takes place in a constant volume. In the CI engine, the combustion of the fuel occurs because the fuel is compressed to an excessively high pressure, which does not require any spark to initiate the ignition of the fuel. In this case, the combustion of the fuel occurs under constant pressure.

The Spark Ignition and Compression Ignition engines can operate in two-stroke or four-stroke cycles. Two loops have been described below:

1. Four-stroke engine: in a four-stroke engine, the engine's running cycle is completed in four strokes of the piston in the cylinder. The four strokes of the four-stroke engine are: fuel intake, fuel compression, expansion or power stroke and exhaust stroke. In a four-stroke engine, power is generated when the piston performs an expansion stroke. During the four strokes of the engine, two revolutions of the crankshaft of the engine are generated.

2. Two-stroke engine: in the case of two strokes, the suction stroke and the compression stroke occur simultaneously. Similarly, the expansion and exhaust strokes occur at the same time. Power is generated during the expansion stroke. When the two strokes of the piston are completed, a turn of the engine crankshaft is generated.

In a four-stroke engine, the engine burns the fuel once for two rotations of the wheel; and in a two-stroke engine, the fuel burns once when the wheel rotates one turn. Therefore, the four-stroke engine is more efficient than the two-stroke engine. However, the two-stroke engine generates more power than the four-stroke engine.

2.2. Homogenous Charge Compression Ignition Combustion

The HCCI combustion has been investigated by many researchers and was found to be one of the best solutions for the requirement of cleaner and fuel efficient

internal combustion engines in current cars. The reason behind it is that HCCI has almost the same fuel economy as diesel with less nitrogen oxides and soot emissions [3]. In HCCI un-throttled operations, there are reduced pumping losses compared to spark ignition operation; so this leads to high fuel efficiency [4].

2.3. Spark Ignition Combustion

Spark ignition combustion engines are used in various car industries as a practical combustion system because of their wide range of capability and their specification in using many kind of fuels, provided a suitable combination of compression ratio and spark timing is chosen. These fuels include gasoline, ethanol, methanol, hydrogen and many other possible fuels. This kind of engine produces a very low amount of soot and particulate matter due to the homogeneous mixtures of the fuels, unlike conventional compression ignition combustion. The SI engine's thermal efficiency is slightly slower than that of CI engines. In spark ignition combustion, the load is controlled by throttling the intake air, which increases the pumping losses and reduces efficiency [1, 5]. In SI engines' combustion, phasing is controlled by the timing of the spark discharge. For maximum efficiency the combustion needs to be phased so the optimum balance of compression and expansion work is obtained [6].

2.4. Opposed Piston Engine

This literature review was written in order to better understand the background and current development of opposed piston engines. These OP engines were used for a wide range of applications, since the 1890s. They were considerably developed and

improved in the first half of the last century. However, the emission regulations in the 1970s discouraged the use of OP engines and their growth gradually ceased. To tackle the energy crisis of fossil fuels and save fuel costs, engines with better fuel economy and higher thermal efficiency are in great demand. Additionally, hybrid vehicles, which are growing rapidly, also need the development of highly-efficient small-sized engines to work as range extenders or backup engines. Contemporary needs have resulted in the re-examination of OP engines; they have inherent advantages in low fuel consumption, compactness, high specific power output etc. In recent years, there has been a significant increase in published literature regarding OP engines, and technology breakthroughs overcoming the historical drawbacks of OP engines. It is of importance to conduct a literature review to identify the strengths, weaknesses and research gaps of the cutting-edge modern OP engines. The literature selected includes a book entitled 'Opposed Piston Engines: Evolution, Use, and Future Applications' published by SAE International and also many SAE technical papers [7]. The review was organized around several themes including background, history, advantages, challenges, solutions and applications.

The opposed piston two-stroke engine (OP2S) concept can be tracked back to the late 1800s. The OP2S concept saw a rapid development in the first half of the 20th century across many countries for a wide range of applications, although stringent regulations on emissions halted the growth of two-stroke engines in the latter half. Despite their issues with emissions, OP engines had already set the benchmark for power-to-weight ratio, multi-fuel tolerance, packaging, fuel efficiency and manufacturing simplicity for ICEs [7].

The opposed piston (OP) architecture is characterised by two reciprocating pistons opposite to each other sharing a single cylinder, minus the cylinder head and valve train, which results in reduced heat loss for greater wall temperatures. The OP configuration inherits its exceptional engine balance due to the asymmetric motion of the pistons [7, 8].
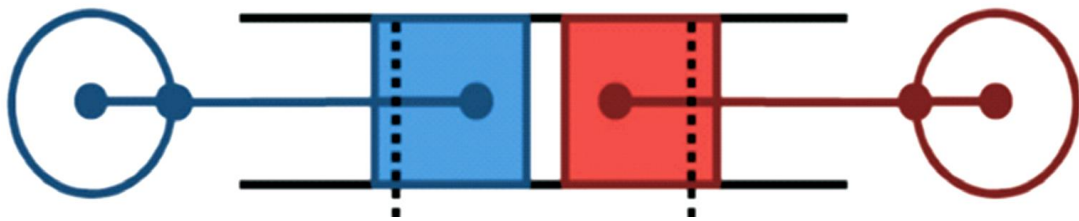
Figure 2-2: Opposed Piston Engine [7]

The advantages of opposed piston engines are described in the book, Opposed Piston Engines: Evolution, Use, and Future Applications:

"OP engines evolved because of their ease of manufacture, excellent balance, and competitive performance and fuel efficiency relative to comparable four-stroke engine. With the progressive development of OP engine, other significant advantages also emerge. Among these advantages were cutting-edge specific output, high specific torque, very high power density, and very high power-to-bulk ratio. Other OP two-stroke advantages, compared to the four-stroke engine, were relatively low heat-to-coolant ratios, high reliability and low maintenance, relative ease of servicing, excellent multi-fuel tolerance, low injection pressures, and simple fuel injection nozzles." [7]

The first OP engine, engineered by Wittig, was deemed to have appeared for public use in Germany in 1878, although it was only commercialised during the

1900s for land, marine and aviation purposes. Prolific OP engines have typically functioned on a two-stroke cycle, as they were prominent in achieving high thermal efficiency as well as high power density [7].

Two-stroke opposed piston engines are arranged in such a way that two pistons are reciprocating opposite to each other, both working in one cylinder. A combustion chamber is located between the pistons near the top dead centre. Scavenging is controlled by piston-ported valves. The intake and exhaust ports are located at opposite ends of the liner. There are no classic poppet valves and cylinder head compared to conventional SI engines [9].

The first opposed piston two-stroke engine was successfully manufactured for public use in Germany in 1878. It was characterized by its ease of manufacture, inherently balanced architecture and fuel efficiency, during its development period around 1890. From 1900 to 1970, more advantages of OP engines were developed such as high specific torque, high power density and high power to bulk ratio. These OP engines have been globally and extensively used for land, marine and aviation purposes from the last century till this present day [7].

However, their use has greatly decreased at the present because of the emission regulations put forward in the 1970s. Nevertheless, current and future emission laws and the development of engine technologies have prompted a re-examination of opposed piston engines, due to their substantial potential advantages such as thermal efficiency, low cost etc. [10].

Witting engineered the first OPE to have appeared for public use in Germany, in 1878. Although it was only commercialised for land, marine and aviation purposes in the 1900s. Pinault and Flint [7], interpret that Witting's OPE has a classic three-throw crank with the centre throw linked to the inner piston, which operated on a four-stroke cycle. Prolific OP engines have typically functioned on a two-stroke cycle, as they were prominent in achieving high thermal efficiency as well as high power density. In 1888, Oechelhaeuser and Hugo Junkers revolutionised OPEs with the consideration of two-stroke operation. This OP2S engine produced some immense figures with a mechanical efficiency (ME) of 77% and a 40% reduction in fuel consumption, in comparison to a modern-day four-stroke engine. Between 1930 and 1945, Hugo Junkers developed and manufactured OPEs for use in German civil and military airplanes. In World War Two, Junkers 205 and 207 aviation engines were record-breaking, in terms of fuel efficiency and reaching altitudes of 20,000 feet [10]. The basic concept from Hugo Junkers, has been employed in many applications with a trend towards very large capacity installations [11].

During the early 1900s, only a few OPEs were developed with a varying degree of success. One of which was the Doxford engines. William Doxford and Sons Ltd, was a British shipbuilding and marine engineering company. Doxfords developed vertical, OP2S diesel engines for ships (up to 8000 bhp). This design became a standard unit for British flag-carriers. However, in the early 1960s, the licence-built Sulzer and B&W engines challenged their pistons. The single-crankshaft engines had connecting rods for both the lower and upper pistons, with two rods for the upper piston. The factor which differentiates Doxford's OPE to Junkers' OPE is that in

Doxford's the upper pistons are connected to the single crankshaft by connecting rods each side of the main cylinder. One of the advantages of Doxford's OPEs, over the traditional four-stroke engine, was that the two-stroke running enables a low operating speed (115 rpm), which eliminates the requirement for a reduction gearbox between the engine and the propeller. In addition, no reverse gear was required since the engine was reversible. The Doxford engine was predominant until its decline in the 1980s [12].

The Stelzer engine was proposed by Frank Stelzer. It uses conjoined pistons in a push-pull arrangement which allows for fewer moving parts and simplified manufacturing. There are two combustion chambers and a central pre-compression chamber. Control of the air flow between the pre-compression chamber and the combustion chambers is made by stepped piston rods. In 1983, a prototype engine was demonstrated in Frankfurt. A prototype car with a Stelzer engine and electric transmission was shown at a German motor show in 1983; it achieved an electrical efficiency of 56%.

An exhaustive thermodynamic investigation has been presented by Herold et al. [13], entitled "Thermodynamic Benefits of Opposed-Piston Two-Stroke Engines". It demonstrates the fundamental efficiency advantages of the OP2S engine over a four-stroke engine with noticeable power output and geometry. From the simulation results, it can be observed that a 10.4% reduction was noted in indicated-specific fuel consumption (ISFC) over the four-stroke engine. Along with the geometric advantage of reduced heat transfer of OP architecture, the double firing frequency of the two-stroke cycle allows linear operating conditions. This enables the two-stroke

cycle to maintain a high ratio of specific heat during combustion and reduced energy release density. The OP2S engine demonstrated an indicated thermal efficiency (ITE) of 53%; which is 5.5% greater than its four-stroke counterpart.

Another intriguing piece of work was carried out by Rishikesh Venugopal in 2013; utilising three-dimensional (3D) computational fluid dynamics (CFD) integrated with state-of-the-art spray, turbulence and combustion models. Venugopal [14] analysed the effects of injection pattern design on piston thermal management, through a combined experiment and analytical approach.

Achates Power is based in San Diego, California and was founded in 2004 by James Lemke. At Achates Power, modern analytical tools, materials and engineering methods have been employed to develop an OP2S compression ignition engine for use in commercial and passenger vehicles. According to the 'Achates Power Opposed-Piston Two-Stroke Engine: Performance and Emissions Results in a Medium-Duty Application' [12, 15], "the engine design has demonstrated a 15-21% brake-specific fuel consumption improvement compared to a state-of-the-art 2010 medium-duty diesel engine at similar engine-out emissions levels". Moreover, "oil consumption has been measured to be less than 0.1% of fuel over the majority of the operating range". With the two-stroke cycle, each combustion event is shorter in duration, thus closer to optimum timing, as compared to the four-stroke engines. While development of historic OPEs ceased for use in on-road car and truck applications with the introduction of modern emissions' standards, Achates Power says that it has patented many modifications to the original architecture in order to meet current standards. A detailed numerical simulation of the Achates Power 1.64 L

single cylinder research engine is executed and validated against existing experimental data.

Most recently, Warsaw University of Technology (WUT) is developing a new type of barrel engine called PAMAR-4 under a Polish-Norwegian research programme. This is an iteration of a successor of the PAMAR-3, which was a 3.0 L, 340 kW engine built for the purposes of aviation. The PAMAR-3 accomplished a test bench efficiency of 44% and has successfully functioned on LPG, propane, alcohol, CNG, gasoline and diesel fuels. One of the many reasons for the great output of the PAMAR-3 engine was due to an OP2S engine, which meant unnecessary strokes were eliminated; uniflow scavenging; and no valve train. In addition, the elimination of a crankshaft reduced piston side thrust. All of these factors led to an increased ME, henceforth increased engine efficiency. Another reason for the great output of the PAMAR-3 engine is due to its axial symmetry of its cooling system, keeping a constant thermal condition in all cylinders; and inlet and exhaust axial symmetry, keeping a constant volumetric efficiency and equivalence ratio in all cylinders. Consequently, there is equal work from cylinders; thus HCCI, at a whole range of loads. The manufacturing costs of the PAMAR-3 engine were reduced by an incredible 40%. Opaliński et al. [16] refers to a comparison of gas-dynamics of this engine, which has been modelled and quantified using Ricardo WAVE (1D) and Ansys Fluent (3D CFD).

According to Pirault and Flint [7], the very first opposed piston engine, which used a three-throw crankshaft, was made by Witting in 1878, in Germany. The pre-1900 period is an exploratory phase for OP engines, which substantially improved

two-stroke engines and improved their efficiencies to around 30%. In 1892, an OP engine of the three-throw crank type was successfully built. Its mechanical efficiency was 77% and its fuel consumption was 40% lower than that of a typical four-stroke engine of the time.

From 1900 to 1915, diesel opposed piston engines were introduced for land and marine purposes. In the meantime, a common rail injection system was invented by Vieckers of Newcastle in 1910. Fullagar improved the OP engines in packaging and weight reduction through a new crankshaft arrangement. Several engines of this concept were put into use for power generation in 1913. The technology progress at that time improved the mechanical efficiency of OP engines to 80%. It is noteworthy that Doxford engines were tested as a submarine drive unit in WW1 and reached brake thermal efficiency up to 32% in 1920 [9].

After WWII, plenty of OP engines were manufactured and used for all kinds of applications such as marine, rail and military. These OP units might be the first medium-sized diesel engines that showed BTE over 40%. Its low heat-rejection-to-coolant ratio aroused the interest of UK designers to explore the multi fuel capability of OP engines [7].

2.4.1 Advantages of Opposed Piston Engines

Achates Power (2010) stated that OP engines have advantages of simplicity, compactness, high torque capability and ease of servicing. These features are essential for mobile use. In addition, less heat is rejected to coolant in OP engines,

thereby enabling smaller radiators. Moreover, it is proven that OP engines have a long lifetime and multi-fuel capability. The advantage of OP engines regarding power density per unit cylinder displacement and engine weight are one of the main benefits of this engine. From 1900 to 2005, the specific outputs of OP engines have been significantly better than that of four-stroke counterparts without the use of turbocharging. Also, the brake thermal efficiencies of OP engines exceeded that of four-stroke engines for many years. Moreover, OP engines have better power/bulk values versus four-stroke engines throughout their history.

Similarly, Kalke et al., [9] also claimed that OP engines have thermodynamic benefits and multi fuel capability. Additionally, they detailed and justified the main advantages of OP engines as listed below.

The elimination of cylinder head obviates heat losses due to poppet valves, camshafts etc. reducing the emission of unburned hydrocarbons and carbon monoxide, which are mainly formed at the cylinder head. Similarly, Achates Power [10] stated combustion waste rejection is generally lower than equivalent power four-stroke engines. This will enable reduced radiator size, decrease the engine volume and hence increase the power/bulk values.

Both Achates Power [10] and Kalke et al. [9] pointed out the SA/V factor is nearly twice lower in OP engines than in conventional engines, where heat losses are proportional to the surface area and the heat generated is proportional to the volume. The smaller surface area of cylinder walls in OP engines will absorb less combustion heat and hence enables OP engines to have higher thermal efficiency. Herold et al.

[13] used a custom zero-dimensional thermodynamic engine analysis tool and obtained a result that OP two-strokes (OP2S) have less SA/V ratio than four-strokes, as illustrated in Figure 2.3.
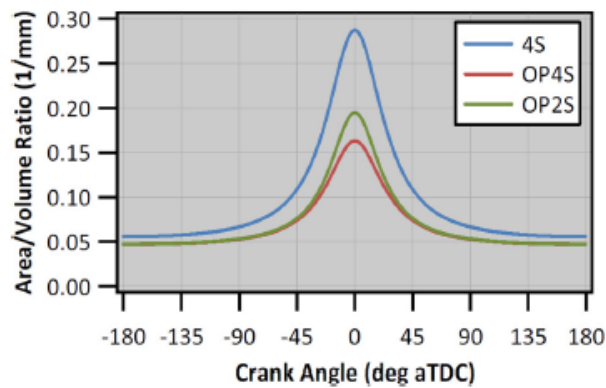
Figure 2-3 : Area/Volume Ratio at different Crank Angles [13]
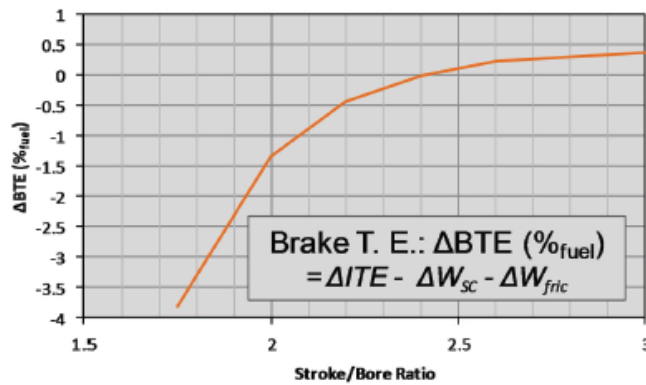
Figure 2-4 : Impact of Stroke to Bore Ratio on Brake Thermal Efficiency [13]

As induction and exhaust strokes are overlapped in OP engines, it is of crucial importance to minimize fresh air losses. According to Kalke et al. [9], uniflow scavenging gives the best trapping and scavenging efficiencies. Achates Power [10]

added the long strokes of OP engines also help cylinder scavenging and fresh air filling.

Achates Power [10] stated the stroke-bore ratio of 3 is the usual case for two-stroke engines. Importantly, Regner et al. [15] found through experiments that the higher the stroke-bore ratio is, the better the brake thermal efficiency, as shown in Figures 2.3 and 2.4.

Regner et al. [12, 15] stated that OP engines are less costly to manufacture because of their fewer parts than conventional four-strokes. In addition, Achates Power [10] claimed the medium and heavy-duty OP engines have approximately 12% lower product cost compared to four-stroke diesel engines, which have equivalent torque, power and emissions. The reasons are as follows: the numbers of cylinders are half; cylinder heads, valve trains and high-pressure gaskets that account for 13% of the four-stroke base engine cost are eliminated; 34% lower part numbers leads to 34% less machining time; besides, fewer parts improve the serviceability and mechanical efficiency [9]. Table 2.1 shows that with equivalent engine power, two-stroke OPs weigh and cost less.

Furthermore, it is mentioned by Kalke et al. [9] that running on multiple fuels requires the engine to have variable compression ratio and be able to withstand widely changing conditions. Both of these conditions are met in OP engines. The VCR is incomparably easier to adapt in OP engines. Fewer parts, simple combustion chamber shape and the compactness of OP engines make them robust.

Table 2-1 Four Stroke and Two Stroke OP (32 kw and 400 kw) [9]

Utility Engine 32 kw	4-Stroke	2-Stroke OP
Weight (kg)	174	113
Cost (USD @ 500 unit per year)	2306	1853
kw/kg	0.18	0.28
USD/kw	72	58
Utility Engine 32 kw	4-Stroke	2-Stroke OP
Weight (kg)	1425	945
Cost (USD @ 500 unit per year)	11713	10314
kw/kg	0.28	0.42
USD/kw	29.28	25.79

Herold et al. [13] investigated the pumping work difference between OP two-strokes and conventional four-strokes in meeting an equivalent NOx constraint. The intake pressure of OP two-strokes was found inherently lower so that concurrently met the NOx constraint. The simulation results of Herold et al. [13] showed that the pumping work for OP two-stokes (3.3% fuel) is lower for four-strokes (3.9% fuel)

and the brake specific fuel consumption of OP two-strokes is 9% lower than four-strokes.

2.4.2 Challenges of Opposed Piston Engines

The emission regulations in the 1970s were difficult to overcome for two-strokes, which discouraged the use of two-stroke engines and led the four-strokes' development to be more favoured [15].

It was believed in the latter half of the twentieth century that the scavenge air and resultant excess air in the exhaust in two-strokes, would cause the exhaust temperature to be too low for catalyst operation. Oxygen rich air would also be rendered and this is incompatible with the then-prevailing after-treatment [7].

Due to the fact that the lubricating oil was lost through the induction and exhaust ports, high oil consumption has been a traditional challenge for two-strokes. Moreover, the lubricating oil prior to 2000 contained additives that poison catalysts and had high ash residues plugging the flow passages in the catalyst [7]. Regner et al. [12, 15] stated that this issue can result in more problems. Firstly, a large amount of aerosolized oil will form significant particulate emissions. Secondly, additives in the oil create ash residue contaminating after-treatment devices.

According to Regner et al. [15], as shown in Figure 2.5, the fuel injector must be installed in the cylinder liner as a result of the absence of cylinder heads. The large distances across the diameter of the cylinder combined with relatively low injection

pressures in the 1970s-1990s made it difficult for the fuel to access all the air in the combustion chamber, which resulted in uneven fuel distribution and inefficient combustion. Due to the side injection structure, the spray is close to the cylinder wall and this will form more low NOx, particulate and smoke emissions. Furthermore, the low injection pressure forced the use of coarse sprays in order to make the large droplets to fully traverse the cylinder bore. However, the large droplets are not favoured for rapid fuel evaporation [7]. Due to these issues, Kalke et al. [9] pointed out that the side injection would lead to fuel impingement on the cylinder liner and pistons, which results in locally high thermal loads and locally rich combustion zones. Achates Power [10] also argued that the off-axis spray and poor fuel-air mixing will worsen the exhaust emissions as well. However, these issues are not existent in four-strokes, as their central position of the injector enables easier fuel-air mixing.
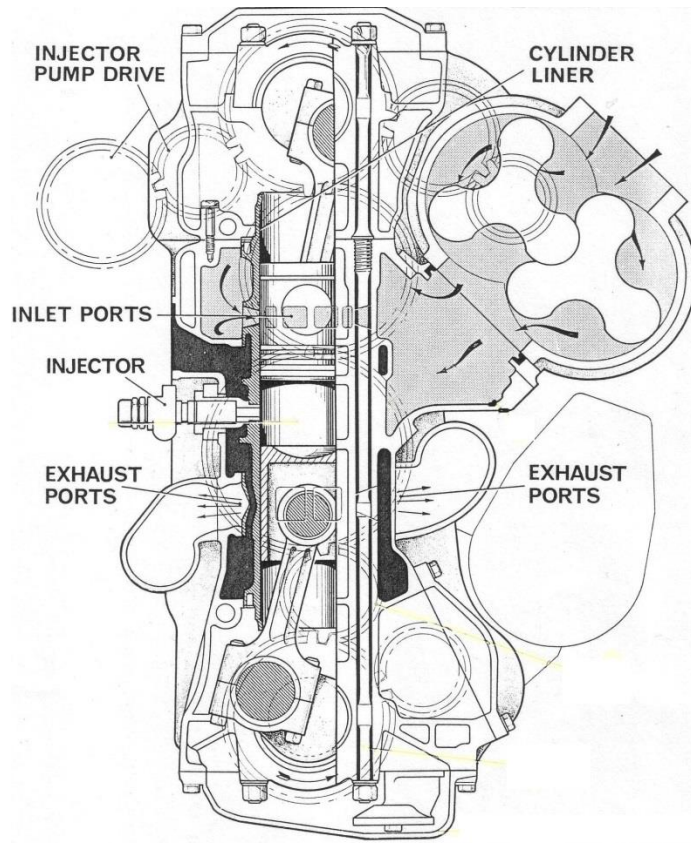
Figure 2-5: Section through Leyland L60 Liner, Piston and Injector [12]

As two-stroke engines fire during every engine revolution and dispense with intake and exhaust strokes, high thermal loads tend to act on the piston and cylinders [7]. The high-power concentration will lead to problems of durability and piston head wear.

To reduce the oil consumption of four-strokes, many technologies such as improvements in cylinder bore materials, cylinder bore finishing, piston ring technology, use of synthetic oils, crankcase breathing systems and management of cylinder bore oil impingement have been developed. All these improvements are applicable to two-strokes as well [7, 13]. Regner et al. [15] have proposed some

detailed mitigation techniques to reduce oil consumption, including modifying oil ring tension, scraper element conformability, ring end gaps, end chamfers, land chamfers, ring grove tilt, pinch, keystone angle, texture, flatness and cylinder cooling design. Especially, the advent of low ash and phosphorus oils further reduce the metal poisoning and cell plugging of after-treatments. The SCR technique, that is largely applied for NOx reduction, is also applicable to the OP engines [15, 17]. Moreover, Achates Power used a Da Vinci sulphur trace system to measure the oil consumption in real time. The cycle-averaged fuel-specific oil consumption was 0.114%, which is believed to be an exceptional value for a two-stroke engine and close to the best values of four-strokes.

With the development of modern tools and advanced fuel systems, Regner *et al*. [11] believed that OP architecture has turned from a technical challenge into a unique opportunity. It is nowadays easier to manufacture asymmetric injector nozzle hole directions and achieve high pressures of the injection. These improvements enable the fuel spray to better mix with the air in the combustion chamber and mitigate the wall impingement. Moreover, the use of computational fluid dynamic software makes it achievable to quickly and accurately design the combustion chamber geometry and configure the nozzle, so as to achieve clean and efficient combustion [11]. Notably, two piston crowns can be shaped and there are multiple fuel injection locations on the liner in OP engines; thereby providing a larger design space than conventional four-strokes.

Regner et al. [11] proposed some methods to reduce the thermal loads. The combustion in OP engines is designed to occur away from the piston and liner

surfaces, which reduces the cooling requirement of the components as well. Moreover, conjugate heat transfer simulations are used to analyse the cooling circuits of the engine so that an effective cooling system can be engineered; this better protects components and prevents oil degradation. Regner et al. [11] stated that thermal loadings can be alleviated by use of high-pressure fuel injection systems with several sprays per injector, that can reduce the fuelling and burning concentration near the cylinder liner and outer edges of piston. The thermal problems are addressed by providing cooling to relative components and selecting steel-based material for pistons as well as cylinder liners. The appropriate injector spray patterns and oust on bowl geometries can reduce heat flux into the piston crown. Port timing, air-fuel ratios and other parameters need to be accurately configured to manage the piston and liner temperatures. The flow rates of cooling and fill ratios for galleries need optimization as well. Introducing the impingement cooling to the area of highest heat transfer will maintain a uniform temperature of the cylinder. Achates [10] published a paper about the methods of controlling maximum piston temperature including how to prevent oil degradation, ring jacking and carbon build-up. Modern analytical models are used to evaluate and manage the thermal loadings of components in OP engines, which will develop OP engines more rapidly.

Regarding lubrication issues, the bearing is now designed with greater surface area and spreader grooves to transfer oil to highly loaded regions. Achates Power [10] put forward a design of a bi-axial wrist pin, which is illustrated in the figure below. This design can make different portions of the bearing alternatively loaded

and unloaded so that lubricating oil is able to migrate to more surfaces of the pin and prevent premature wear.

Modern design tools will greatly help the development of OP engines. These engines have more parameters which can be configured compared to conventional engines. Some parameters are difficult to obtain during testing, but their trends can be simulated using modelling software. The use of modern design tools will not only hasten the design process but also save the hardware and iteration costs. Only a small number of configuration testing needs fabrication and dynamometer tests. An optimal combustion system can be therefore designed with decreased time, effort and cost [11].

For instance, computational fluid dynamics can be used to simulate the scavenging process of the engine and calculate the scavenging efficiency. A single simulation can save weeks of procurement and testing [11]. Fuel injection and air-fuel mixing are altered by varying additional parameters. Besides, a piece of software, for example KIVA 3 can be used to chemically and three-dimensionally analyse the reactive fluid. It can model the effect of parameter change on fuel consumption. In addition, to ensure the fidelity of inputs, a laser Doppler anemometry system is used to measure the droplet size and spray penetration.

Venugopal et al. [14] successfully investigated the effects of injection pattern design on piston thermal management in an OP engine. They firstly employed a telemetry system to measure the temperature distribution on the piston surface from research engine testing. A chemistry-based combustion CFD model was then

correlated and used to study the impact of varied injection clocking angles and spray angles. Although this study is still in progress, it can be seen that CFD can also be used to improve the piston thermal management.

Regner et al. [12] stated that by injecting the fuel into a pressurized chamber, the cylinder is simulated. Lasers are used to determine the distribution, dispersion, size and velocity of the fuel droplets. The characteristics of spray and air flow are input into KIVA-based code to predict the combustion performance. Using analytical tools like KIVA-based code can analyse and evaluate the effect of different combustion system parameters, for instance, stroke-to-bore ratios. Regner et al. [12] summarised that the advances in engine simulation, modelling and analysis tools enable quicker and more accurate design for OP engines; which make it realizable for OP engines to achieve satisfying thermal efficiency and meet environmental restrictions.

Many simulation software packages can be used to model engine. In this study AVL BOOST and Ricardo Wave, as the leading combustion engine modelling packages have been used; because of their capability of modelling in various situation. They can easily predict effect of any improvements or changes of engine design.

2.4.3 Applications of OP Engines

Opposed piston engines have been successfully applied to vehicles and in aviation and marine uses. These engines are also used for stationary applications including power plants and pumping. Modern OP engines are suited for these applications due to their compelling advantages in cost, compactness, high specific power output and

thermal efficiency at low emission levels. According to Kalke et al. [9], there are several companies currently developing OP engines. A UK company called Fair Diesel was established in 2000. This company mainly develop and produce engines for industrial and aviation uses. He claimed that Fair Diesel is currently designing engines from 2 to 32 cylinders. EcoMotors, founded in 2008, have been invested in by Khosla Ventures and Bill Gates. Commercial OP engines for cars and trucks are developed by this company. Moreover, EcoMotors established a joint research and development centre with Huhan University in order to better adapt the technology into its main target market, China. It also cooperates with Chinese automotive parts' companies.

Pinnacle Engines has cooperated with another company called FEV and commercialized four-stroke OP engines. Their target market is developing countries. They aim at reducing emissions of engines without increasing the engine cost. They began to produce scooter engines in Asia in 2014.

Achates Power [10] is a USA company established in 2004. It started engine testing in 2005 and began designing a light-weight and compact engine for UAV in 2007. This design had reached 5000 hours of dynamometer testing in 2014. A two-stroke, three-cylinder OP diesel engine was developed by Achates Power. They tested a one-cylinder engine on the dyno and simulated three-cylinder performances with the aid of modelling software.

One particular market for OP engines is the medium-duty truck [15]. A comparison analysis of a two-stroke engine and a conventional four-stroke engine,

both of which meet similar emissions' standards and have equivalent manufacturing volumes, was done by a team from Achates Power. They conducted a benchmarking study to compare the component number, engine weight and engine cost. It can be seen from the figure 2.7, a 40% component cost reduction was achieved by the OP engine. Each part was weighted and the total weight comparison is indicated by Figure 2.6. There was approximately a 30% weight advantage for the OP engine versus the four-stroke counterpart. It is shown by Figure 2.7 that the cost of the OP engine was 10% lower than that of a four-stroke engine of equivalent power. The analysis takes the material cost, matching complexity and finishing processes into consideration. Notably, the cost advantage of OP engines will be magnified because significant savings can be achieved when the production volume is quite high. Also, it is concluded that the vehicles can remarkably benefit from the fuel economy of OP engines.
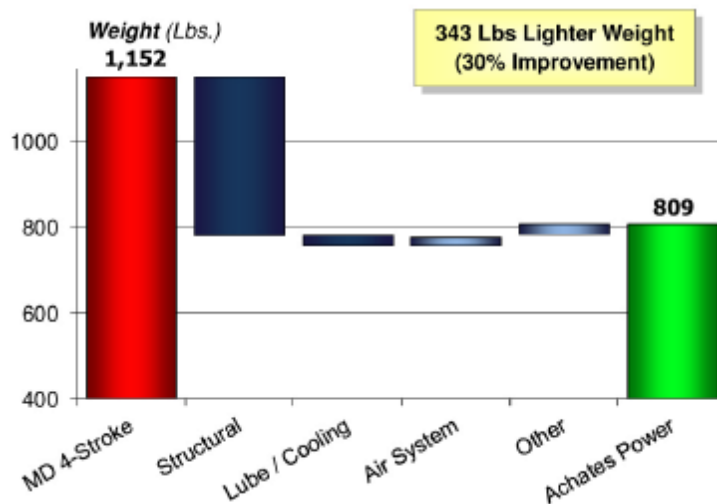
Figure 2-6: Weight comparison of different engines [15]
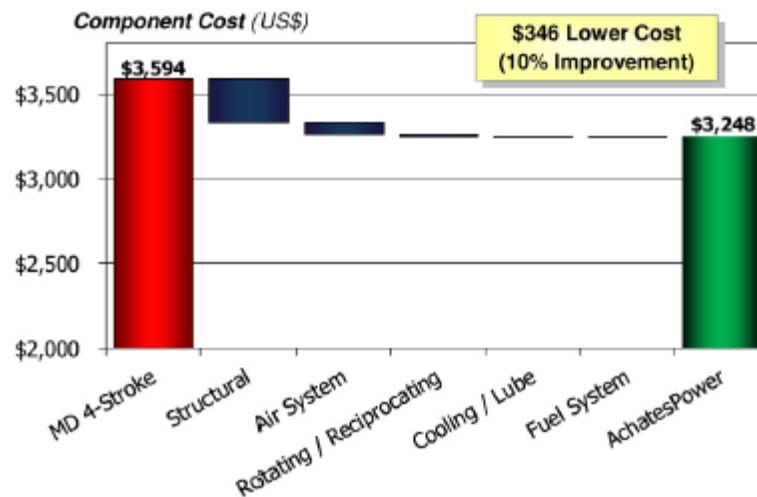
Figure 2-7 Cost comparison of different engines [15]

Kalke et al. [9] believed OP engines have significant advantages in three applications. They are range extenders, distributed power generation and a highly flexible piston power plant. The growing popularity of hybrid vehicles makes a place for small engines with high efficiency for the application of range extenders. The range extender drives an electric generator to charge the battery for the electric motor of hybrid vehicles. It is used to extend the vehicle range in case the battery in the car is used up. The OP engines can beat the competition in this field due to their high power-to-weight, power-to-volume ratios, compactness, simple architecture and high thermal efficiency.

The inherent advantages of OP engines also make them applicable to be used for distributed power generation and power plants. Variable compression ratios enable the engines to work on multiple fuels. Compared to the range extenders of a small size, the emissions of power generation and power plant are easier to manage. For

instance, the engine is able to use biogas as its main fuel and switch to natural gas or other fuels in case of need.

It can be concluded from all the literature mentioned that opposed piston two-stroke engines are widely considered to feature in low fuel consumption, low manufacture and servicing cost, high thermal efficiency and high-power density. Nowadays, the development of engine technology has overcome lots of historical challenges for OP engines; such as side injection, thermal loads, and oil consumption and emission issues. Additionally, the advent of modern design tools significantly helps perfect the engine architecture and optimize the combustion system. Due to these reasons, opposed piston engines are believed worthy of re-examination by more and more research institutions and companies. There has been a soaring rise in published literature regarding opposed piston engines in recent years, which has proved the fundamental characteristics of OP engines and put forward feasible solutions to improve the engines' performance. A large amount of prototype OP engines has been manufactured and considerable research is being undertaken. These OP engines are beginning to revive and they are promising alternatives to conventional four-stroke engines in the field of hybrid-vehicles, power plants etc.

Chapter 3 – Experimental data

This chapter describes the means by which the experimental results from the research contained in this thesis were collected. The details of the equipment used in this study are given. The engines, various test criteria, emissions' analyser, as well as the combustion behaviour, will be explained. The first part of this chapter concerning the Jaguar engine is gathered from Dale Michael Turner's PhD thesis [6].

3.1 Jaguar Thermal Engine

The experimental part of Chapter 5 of this thesis was conducted utilising nearly identical thermal single cylinder research engines. The experimental thermal analysis throughout this research thesis was done on a Jaguar single cylinder thermal engine. Figure 3.1 indicates a schematic image of the single cylinder engine set-up and its specification is listed in Table 3.1

Figure 3-1 Thermal Single Cylinder Engine

Table 3-1 Engine Specification

Thermal Engine (Jaguar DI 4v VCT)	
Cylinders	1
Displacement Volume	0.57 l
Clearance Volume	0.05 l
Bore	90 mm
Stroke	88.9 mm
Connecting Rod Length	160 mm
Compression Ratio	11.5:1
Intake Camshaft Duration	130 °CA
Exhaust Camshaft Duration	110 °CA

Intake and exhaust camshafts were controlled by the implemented continuous (within shaft range) variable cam timing systems simultaneously and independently. As seen from Table 3.1 the intake and exhaust camshafts, their profiles and lifts are variable in this range for this specific engine.

In addition, a centrally mounted third-generation Bosch gasoline solenoid operated multi-hole direct injection injector type was used as the direct injection system. For this DI system, which is high pressure operation in the piston accumulator, nitrogen as a gas was installed to pressurise the fuel. Furthermore, near to the DI system, the port fuel injector was located close to the intake valves; this enables further injection strategies' investigations. This port fuel injection system is a low-pressure operation condition at around 5 bars.

Moreover, this engine is connected to a DC dynamometer, which can operate in constant speed mode; for this investigation in Chapter 5, a speed of 1500 rpm is studied. Before any experiments were carried out, the engine was warmed up at low load in spark ignition mode until the water and oil were at their proper operating temperatures: oil at 85±5 °C and water at 95±3 °C.

3.1.1 Combustion System

The combustion system for this single cylinder engine consists of a centrally mounted, six-hole injector. The spark plug is mounted beside the injector at an angle of 18 degrees to the cylinder axis, as shown in Figure 3.2 (blue indicates intake and red shows exhaust ports). The complete orientation and details of the spray plumes are indicated in Figure 3.3. From this picture, it can be clearly seen that the nozzle pattern consists of two groups of three holes, with the line of symmetry coinciding with the crankshaft axis. Spray plumes one and six pass either side of the spark plug.
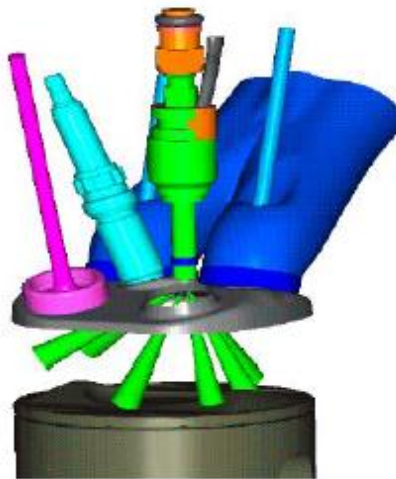
Figure 3-2 Layout of Combustion System
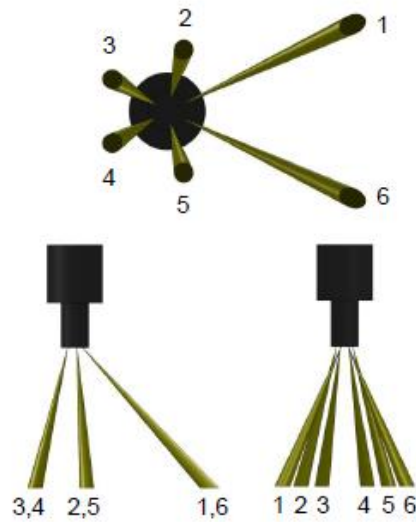
Figure 3-3 Injector Spray Plume Orientation

3.1.2 Crankshaft Encoder Set-up

The crankshaft encoder needs to be precise enough as it is used by the engine control software for injection and spark timings. The variable valve timing software is used for the generation of the timing of the once per revolution. The timing of the signal (relative to combustion Top Dead Centre) is attained by setting spark timing at 0º bTDC in the engine control software. This measures the actual position of the spark by using a stroboscope and 1/degree markings on the engine flywheel. Then, it is entered in to the engine control system where the 0º $bTDC_{COMB}$ spark will occur at TDC; the 1/degree markings on the flywheel are investigated by measuring the location of the piston relative to top dead centre at different positions and by calculation of the angular distance from TDC, from the geometry of the crankshaft.

3.1.3 Valve Train

For Chapter 5's experimental results, a variable cam timing system was set up on the engine. The engine was equipped with two different sets of camshafts: one set for the homogenous charge compression ignition and the other for the spark ignition operation conditions. More information and details are provided in the sections below:

3.1.3.1. Variable Cam Timing (VCT) System

For changing the offset of the camshaft relative to the camshaft pulley, the crankcase oil pressure was used in the variable cam timing system. For both the intake and exhaust camshafts, the camshaft timing can be delayed by a maximum of 50 crank angle degrees. To control the variable cam timing system, a custom LABVIEW script, in conjunction with a National Instruments counter-timer card (model 6202) is used. The software displays the camshaft position (relative to the cycle marker) once a cycle (two revolutions of the crankshaft) and makes adjustments to the cam timing by changing the pulse width of the signal sent to the variable valve timing oil control solenoids. Typically, for stable engine operation, the cam position can be maintained to within ±0.1 crank angle degrees.

3.1.3.2. Spark Ignition Camshafts

The geometry of the intake and exhaust camshafts used for the spark ignition investigations are shown in Table 3.2. These values are typical for a production engine of this cylinder size. For Chapter 5's experiments, the HCCI load control method was chosen involving the use of trapped exhaust residuals in the cylinder.

This is done by closing the exhaust valve early and opening the intake valve late. The duration of the intake and exhaust camshafts has to be reduced compared to the SI method to allow this strategy, so that the compression and expansion strokes are not adversely affected. This duration has to be undergone with a reduction in maximum valve lift to conserve proper valve acceleration values. The geometry of the intake and exhaust camshafts used for the homogenous charge compression ignition investigation is indicated in Table 3.2.

Table 3-2 Intake and Exhaust Valve Specification

Valve	Intake		Exhaust	
	Low Lift	High Lift	Low Lift	High Lift
Inner Seat Ø (mm)	36.0		30.0	
Max Lift (mm)	2.65	10.50	2.10	9.30
Duration (CAD)	130	250	110	250
VCT timing range (CAD)	Opens 54° to 104° aTDC	Opens 26° bTDC to 24° aTDC	Closes 104° to 54° bTDC	Closes 6° aTDC to 46° aTDC

3.1.4 Fuel System

For Chapter 5's investigations, the engine is equipped with a port fuel injection system as well as a direct injection system. The port fuel injection system is used for

warming up the engine; however, it is also used to measure the mixture preparation performance of the DI system, such as wall wetting and fuel evaporation.

A direct injection fuel system is based on a free piston accumulator. From a tank, fuel is delivered via a pump to the volume in the top of the accumulator cylinder above the piston; in addition, the top of the cylinder is connected to the direction injection system. There is a space below the piston which is pressurized with oxygen free nitrogen. For any unused fuel to be delivered back to the fuel tank, the system was designed with some circuits with the ability to flush the complete system and clean it with compressed nitrogen gas. The system is controlled manually by operating the proper valves. The fuel pressure which was used for Chapter 5's investigations is 150 bar gauge.

3.1.5 Lambda Meter System

An ETAS lambda meter, model LA3 and a Bosch heated wideband oxygen sensor on this engine was used to measure the lambda values. This lambda meter permits the preprogramed fuel properties to be changed to suit the fuel being used. Hydrogen to carbon ratios, oxygen to carbon ratios and stoichiometric air to fuel ratios are the main parameters. This is particularly important when oxygenated fuels such as alcohols or other blends are used.

3.1.6 Control

In any experimental set-up, the control room plays a vital role in controlling every step and the environment of the operational conditions. For this issue, LABVIEW is used to control the injection and spark timing parameters. The start of injection

timing and injection pulse width, also spark timing and coil charge time can be defined while the experiments are running on the engine. The system is capable of various operational conditions, controlling two separate injections per cycle by having independent pulse widths. Load control for spark ignition is done by the operator modifying a butterfly throttle valve that is situated in the inlet track. For homogenous charge compression ignition, the load is controlled by the mixture strength (λ) and the number of trapped residuals (ER), via the VCT control system. Indicated mean effective pressure is calculated online by the high-speed data acquisition software. The IMEP is calculated from the in-cylinder pressure, which is measured with a water cooled Kistler pressure transducer (type 6041A). This is connected to the data acquisition system via a Kistler 5011 charge amplifier. Some K-type thermocouples are used to measure the temperatures at various points on the engine, such as the intake, exhaust, engine oil and coolant. The engine coolant temperature was controlled with a proportional integral derivative (PID) controller to drive a solenoid valve that regulated the flow of cold water through an heat exchanger. The oil temperature was maintained by using a heat exchanger connected to the engine's cooling system.

3.1.7 Data Acquisition System

In any experimental set-up, a data acquisition system is used and a brief description is provided in each section of the two data acquisition systems used for this study. The first is a high-speed system for cycle resolved parameters and the second is a low-speed system for the measurement of steady-state parameters.

3.1.8 High Speed

Cylinder pressure and intake pressure were recorded with a high-speed data acquisition system as cycle resolved data. For the purpose of checking the correct operation of the VCT system, output data from the camshaft position sensors are also measured. The system consists of a custom LABVIEW script and a National Instruments data recording card, model 6251. The input signals are connected to the data acquisition card via a National Instruments breakout box, model BNC 2090. The data is recorded with a resolution of 0.5 CAD, for 100 consecutive cycles [6].

3.1.9 Low Speed

The low-speed data acquisition system records the signals that have a time period greater than an engine cycle. These signals are principally temperature (intake, exhaust, etc.), volumetric intake airflow, the atmospheric conditions (temperature, pressure and humidity) and the output from the emissions' tower. The signals from the thermocouples were passed through a thermocouple amplification circuit before going to the data recorder. The acquisition system consists of a custom LABVIEW script and a National Instruments data recording card, model 6220. The data is recorded at a rate of 10 Hz, for 10 seconds for the HCCI investigations and for 30 seconds for the spark ignition studies. These approximate to the times required for the high-speed data to be recorded for the respective investigations [6].

3.1.10 Data Processing

Data processing involves the manipulation of the data recorded by the high and low-speed data acquisition systems. All the necessary parameters such as IMEP, heat

release rate, rate of pressure rise and maximum in-cylinder pressure are measured for every recorded cycle and then averaged to find the final answer.

The method used for the calculation of the IMEP is the standard method that can be found from any reference books such as in Heywood and Stones. More details on some of the calculations are presented in the sections below.

3.1.11 In-Cylinder Pressure Referencing

To measure the in-cylinder pressure, the piezo electric pressure sensors are used. Due to the temperature fluctuations, the signal from the sensor can be susceptible to drift; therefore, the signals from the sensor need to be pegged to the reference values. The common method which was used for this measurement is based on the assumption that at the intake before top dead centre, the in-cylinder pressure is the same as the intake pressure. The in-cylinder pressure trace for each individual cycle is shifted to achieve the referencing; so as a conclusion, the pressure at the intake before top dead centre is equal to the intake pressure at the same crank angle.

3.1.12 Heat Release Analysis

For all of the investigations in this thesis, the heat release rate analysis is conducted in two parts with the first being the calculation of net heat release rate (Equation 3.1), as can be found in [1, 5]. The second part is the cumulative summation and normalisation of the heat release rate to obtain the mass fraction burned (MFB) data (Equation 3.2) [1, 5]; where k is approximated to be the polytropic exponent of compression and expansion, for which a different value is calculated for the respective parts of the cycle.

$$\frac{dQ_n}{d\theta} = \frac{\bar{k}}{\bar{k}-1} P \frac{dV}{d\theta} + \frac{1}{\bar{k}-1} V \frac{dP}{d\theta}$$
　　　　　　　　　　　　　　　　　　　　　　　　Eq.3.1.

$$MFB = \frac{\sum_0^n \frac{dQ_n}{d\theta}}{\sum_0^N \Delta \frac{dQ_n}{d\theta}}$$
　　　　　　　　　　　　　　　　　　　　　　　　Eq.3.2.

where:

Q_n: Heat release rate

θ: Degree of crank angle

$\bar{k}$: Polytropic index

P: In-Cylinder pressure

V: Cylinder volume

And, MFB: Mass fraction burnt

3.1.13 Fuel Consumption

The amount of fuel usage cannot be directly measured by the use of simple techniques, such as a mass balance, because of the nature of the high-pressure direct injection fuel system. Fuel consumption is calculated from the inducted air flow rate and the air to fuel ratio. The volumetric inducted air flow is measured with a rotary flow meter, which is converted to a mass flow rate by using the ideal gas law and having the ambient environment air pressure and temperature. Then, the inducted air mass flow rate is divided by the gravimetric air to fuel ratio; which is found from the gravimetric stoichiometric air to fuel ratio and the recorded lambda value from the lambda meter.

3.1.14 Exhaust Recirculation Rate for HCCI Combustion

For the homogenous charge compression ignition engine investigations the exhaust recirculation rate is estimated based on the method described by Risberg et al.[18]. The mass trapped in the cylinder at the point of the exhaust valve closing is estimated using the ideal gas law. At the exhaust valve closing time, the in-cylinder pressure is known along with the trapped volume from the crankshaft geometry, with the in-cylinder temperature being estimated as the same as the exhaust gas temperature. So, the mass of the trapped exhaust gas rate can be estimated from this method, with the exhaust recirculation rate being given as a percentage of the total mass of the trapped charge.

3.1.15 In-Cylinder Temperature

The in-cylinder temperature is only calculated for the homogenous charge compression ignition investigations. This is due to the difficulties in estimating the amount of trapped exhaust residuals when a positive valve overlap valve timing strategy is used, like for the spark ignition investigation for the Chapter 5 investigations. From the ideal gas law, by knowing the total trapped mass, total in cylinder volume and the in-cylinder pressure, the in-cylinder temperature is estimated. In calculating the temperature, the blow-by losses are considered as zero.

3.1.16 Fuel Properties

The pertinent properties of the unblended fuels used in Chapter 5's study are listed in Table 3.3. Shell Global Solutions UK provided the fuel used throughout the

experiment: ultra-low sulphur diesel (ULSD). The fuel's key properties are shown in Table 3.3.

Table 3-3 Properties of Fuel [6]

Properties	ULSD
Cetane Number	53.9
Density at 15 K (kg/m^3)	827.1
Viscosity at 40 K (cSt)	2.5
50% Distillation (K)	264
90% Distillation (K)	329
LCV (MJ/kg)	42.7
Sulphur (mg/kg)	46
Total Aromatics (wt. %)	24.4
C (wt. %)	86.5
H (wt. %)	13.5
O (wt. %)	0
H/C Ratio (Molar)	1.88

3.2 PAMAR Barrel Engine

The experimental part of Chapters 6 and 7 of this thesis was conducted utilising a PAMAR barrel engine. The experimental analysis of Chapters' 6 and 7 simulations

was done on the PAMAR barrel engine based in Politechnika Warszawska, WYDZIAŁ MECHANICZNY ENERGETYKI I LOTNICTWA, ZAKŁAD SILNIKÓW LOTNICZYCH, Poland [19]. Most information is provided from this university and they are greatly acknowledged for their kind cooperation. Figures 3.4 a, b, c and d present a real view picture of the engine. A PAMAR-4 engine is a two cylinder, opposed piston two stroke barrel engine. This engine has been designed under Polish Norwegian Cooperation Research conducted by the National Research and Development Centre. The engine prototype was built to carry out preliminary studies and identify weakness of the prototype. The main aim of this design was to build two stroke engines and use a double acting piston.
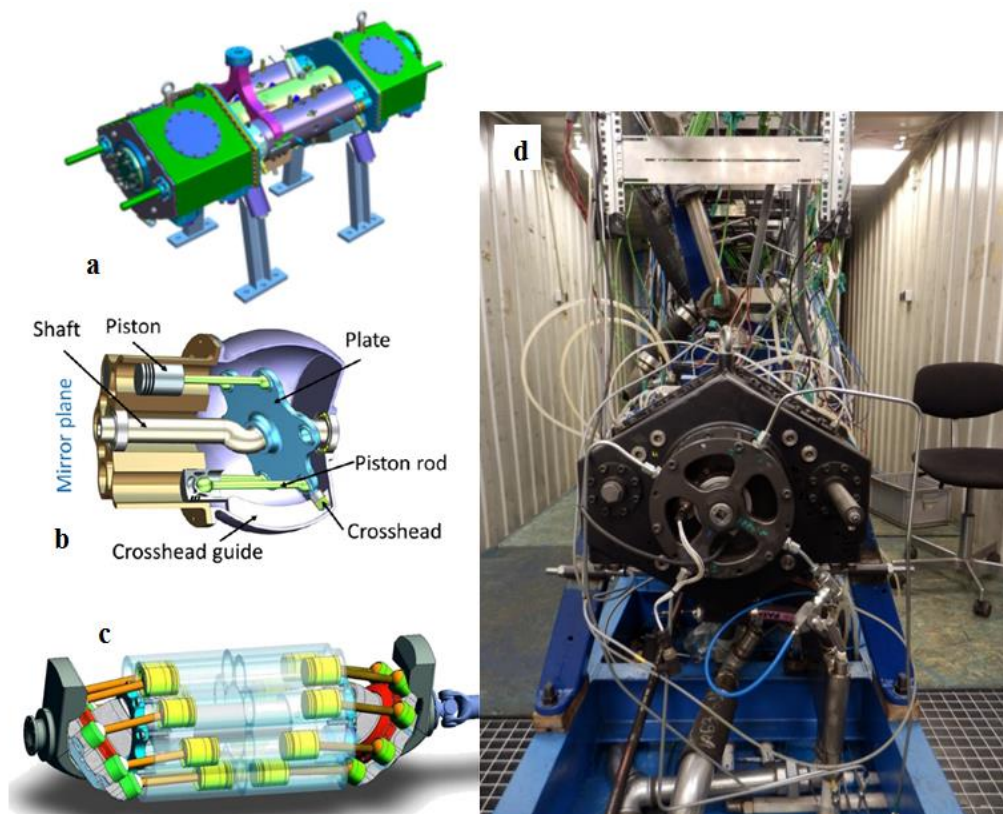
Figure 3-4: (a) PAMAR-4 CAD Model without Auxiliary Equipment (b) PAMAR-4 Wobble Plate (blocked by crosshead, half of the engine) (c,d) Engine Picture and Schematic Diagram

In OP engines injection is made perpendicularly to the piston motion in comparison to standard symmetrical central injection 4-stroke engines. Such injectors have problems with even fuel distribution in the combustion chamber and can lead to inefficient combustion. Moreover, there is a risk of cylinder liner/piston rings' fuel impingement, which results in non-uniform charges and generates local high thermal loads. Even worse, such fuel impingement can destroy the lubricant film, leading to increased emissions, oil consumption, and faster piston-cylinder wear [9].
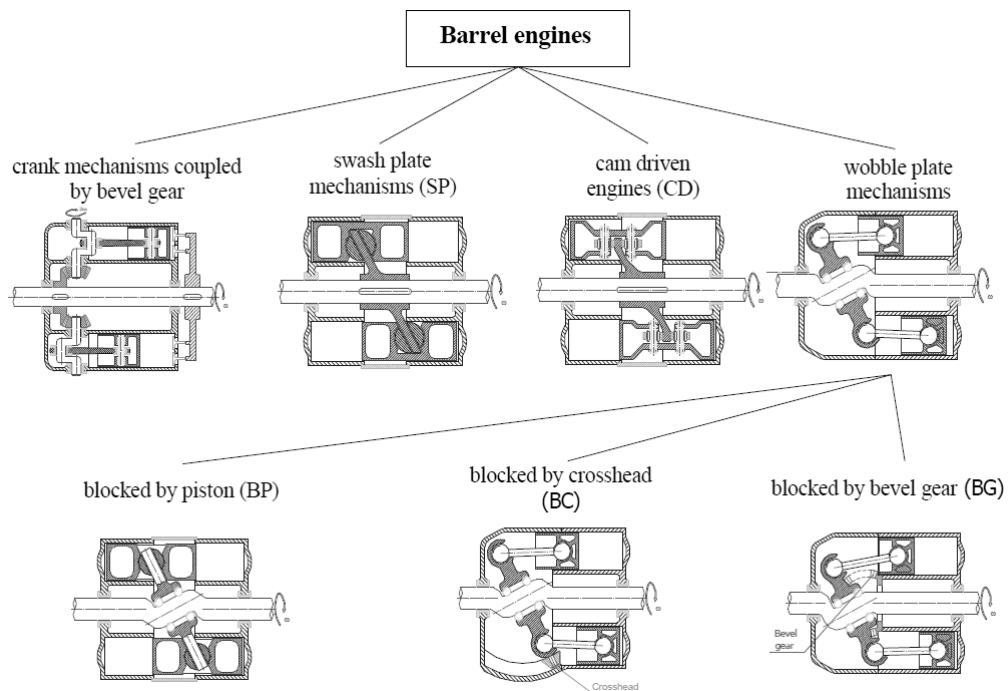
Figure 3-5: Examples of Barrel Engines [13]

During the PAMAR 4 project in Poland, it turned out that there are no readymade tools which can be used for analysing the 2-stroke opposed piston engine operation, so AVL BOOST is considered to compare the first experimental results with simulation results.

An opposed piston engine is a subtype of an internal combustion engine with no cylinder head. Two pistons reciprocate exactly opposite to each other as shown in Figure 3.4. The combustion chamber is located between the moving pistons.

Differences between a barrel engine and an opposed piston engine can be summarised as follows: a barrel engine has high power concentration and an opposed piston has high thermodynamic efficiency. Other main properties of barrel engines are: simpler technology, less required parts, axial symmetry geometry of the engine and low vibration level, which make the engine quieter than other types of engine. Opposed piston engines do not have a cylinder head; no valves are required for this type of engine. Also, one of its main specifications is its high stroke to bore ratio; the effect of its efficiency will be investigated in Chapter 6.

As a summary, the main properties of this engine are as follows: homogenous charge compression ignition combustion on gasoline under various loads, power of 100 kilowatts at 1500 rpm; multifunctional potential for both liquid and gaseous fuels, variable compression ratios; variable valve timing; and variable phase shift.

It can clearly be seen from Figure 3.4.b that this engine is using a wobble plate mechanism. The shaft inside the engine is not straight but bent with an appropriate angle; this makes the plate rotate in the other axis rather than the shaft axis. The plate is equipped with a special pin (crosshead) which moves on a crosshead guide. This slider blocks the plate's rotation and makes the shaft rotate, while the plate's pin only has a pendulum-like motion.

A PAMAR barrel engine is a mixture of these two beneficial engines which were investigated over several years when it was being built in the Politechnika

Warszawska. The research was started in 2000, then in 2003, the first PAMAR barrel engine with a 50 cm^3 capacity was built. In 2006 and 2009, PAMAR 2 and 3 with a capacity of 600 cm^3 and 3000 cm^3 respectively started running. The PAMAR 2 was the first opposed piston barrel engine. Now the research is based on a clean combustion mode (HCCI) and distributed energy generation; this relates to the PAMAR 4 and PAMAR 5, respectively.

The combustion chamber in the PAMAR engine is equipped with a piezoelectric gasoline direct injector (VDO Siemens) which has the ability to use direct water injection as well. To ensure the pressure inside the cylinder, a piezoelectric pressure transducer (Kistler) is used.

Results from PAMAR 3 were achieved with a compression ratio of 8-15, boost pressure 1-3 bar and maximum combustion pressure 200 bar, by using gasoline, diesel, CNG, LPG and ethanol as fuels. All the calculations for heat release and mass fraction burned were explained in the previous section and were also used for Chapter 6.

PAMAR 4 is run with ultra-high combustion pressure 300 bar, variable compression ratio, variable valve timing, HCCI combustion mode, direct water injection and with liquid gasoline and diesel as fuel, or gaseous methane and biogas.

The engine crank position is measured by two Heidenhein ERN 130 3600 HTL UQAD incremental encoders connected to the NI 9411 module. Also, the PXI-7853R FPGA coupled encoder signal with pressure aquisition is used to record the pressure versus crank angle data.

In-cylinder pressure is measured by a piezoelectric Kistler 6055C80 pressure transducer with a diaphragm that even measures the pressure during any knocking. The pressure signal is acquired by both Dewetron and National Instruments' systems [19, 20].

Chapter 4 - Modelling and

Simulation Software Packages

This chapter describes the means by which the research modelling and simulation results contained in this thesis were collected. It gives details of the software packages used in this study: Ricardo WAVE and AVL BOOST.

4.1 Introduction

The main aim of the modelling of the engines in this thesis is investigation of engine modifications' effects on the performance and emissions without doing expensive experiments. The main purpose in modelling the modifications of engines is to quantify the effects of each one. These modelling results allow vehicle engineers to make more educated decisions about how to build engines with minimum emissions, maximum performance and economy.

One of the least expensive and quickest methods of achieving accurate data based on reasonably accurate assumptions is the modelling of engines through proper software such as AVL BOOST and Ricardo WAVE.

4.2 Ricardo WAVE^{TM}

Ricardo WAVE^{TM} is the one of the best simulation software packages on the market for use in the simulation of gas dynamics and engine simulation. It has the capability to analyse the dynamics of pressures, mass flows and energy losses in ducts, plenum and also manifolds of various systems and mechanical systems. It is used widely in industry, including vehicular technology, trucks, motor sport, marine engines, locomotive engines and power generation systems [21].

Ricardo WAVE was used to create the SI, HCCI and diesel model in the chapter 5. WAVE is a comprehensive engine modelling package which has a very high-

quality application in the automotive industry, to develop and improve engines and determine levels of efficiency and performance of engines before they are actually built. Valves, injectors, compression ratios, fuel type, number of cylinders, position of the pistons and the heat release rate due to the combustion, can all be modified to investigate their positive and negative effects. A simulated engine can be created at different speeds and load points with enough iteration at each point to reach more precise convergence of all factors [21].

4.2.1 Engine Performance in WAVE^{TM}

WAVE is widely used in the engine design process from the beginning of the conceptual designs to the detailed design of production engines. The design of engines in WAVE improves the volumetric efficiency, transient response and performance of the engines. It has various applications in torque response studies, intake and exhaust manifold geometric designs, prediction of fuel consumptions, variable valve timing strategies, turbocharger analysis, exhaust gas recirculation studies and also various piston geometric analyses [21].

4.2.2 Acoustics and Noise

WAVE is able to predict intake and exhaust noises as well. In this thesis, the investigation of the engine noise is not the main purpose, but in this chapter, it is mentioned to show the capacities of this software package for any future research in this area. WAVE allows the simulation of static and noise tests, location of the intake and exhaust resonances and most importantly, the prediction of performance and sound pressure levels of the simulated engine. Some of the main application of WAVE in acoustic and noise investigation are: pressure loss reduction which means

transmission losses, intake system component design, exhaust system component design, catalysts, pipelines, design of engine noise signatures, transient noise analysis in various engine speeds [21].

4.2.3 Combustion and Emissions

Advanced combustion models for any type of engines are another property of WAVE. It includes secondary sub models for the investigation of direct injection, SI turbulent flame propagation, engine exhaust gas emissions and also knocks studies. In addition, it contains a suite of exhaust after-treatment sub models. These allow full detailed chemical kinetic simulation of advanced emission control technologies. In the combustion systems, the designer can investigate a concept level of bore to stroke ratio. Chapter 6 aims to study the effect of bore to stroke ratio on special engine performance. Other applications which can be investigated in this software package: pin offset, bowl design, injector placement study using full three-dimensional chamber, fuel strategy developments, emissions' trade-off studies, performance studies and after-treatment system designs. All of the mentioned features make Ricardo WAVE capable of studying engine improvements' strategies which are not possible to do experimentally [21].

4.2.4 Thermal Analysis

Another application of WAVE includes structural conduction models for the engine structure: such as head, cylinder, piston, valves and manifolds. Exhaust system's investigation such as catalysts light-off studies which are more focused on the emission analysis and the study of the intake and exhaust manifolds'

temperatures, all of them affect the engine's performance and emissions' legislations [21].

4.3 Modelling in Ricardo WAVE

WAVE contains three main parts: pre-processors, solvers and post processors. The pre-processors are programs used to set up the simulation model and analysis. In the main window of the software it has series of values, inputs and parameters required to define the simulation and perform the analysis. The pre-processor converts the provided data into the input format of the model for the solver section of the software package. The second section of the package is the solver. Solvers are programs used to analyse the data which are provided by the pre-processors. In this section, they are largely non-interactive and print text output to the progress of the simulation. The last section of the simulation package is the post processors; they are programs used to view and interpret the results which are provided by the solvers for the simulation [21]. All the results can be exported in the desired version for further investigations.
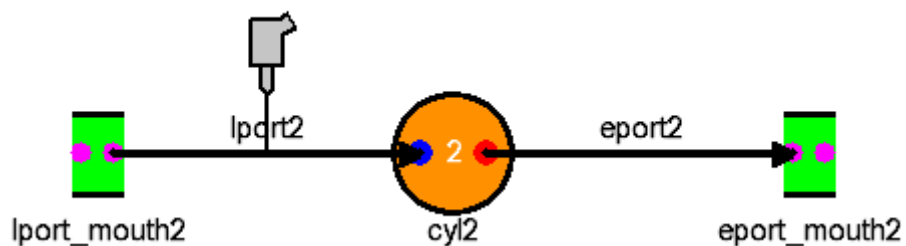
Figure 4-1 Simple Model in WAVE

There are many input parameters in the model which affect the engine efficiency and performance. These parameters are duct length, temperatures, thermal

conductivities, crankshaft speed, valve timing, cylinder dimensions' compression ratio, fuel to air ratio, injection timing, combustion timing, combustion heat release rate, EGR valve timing, frictional losses, wall heat losses, pressures profiles, fuel properties, environment conditions and any other engine specifications.

Output results can be exported after running the simulation; and can consist of pressure traces, temperature traces, regulated emissions, output power, fuel consumption, volumetric efficiency, mechanical efficiency, scavenging efficiency, indicated mean effective pressure, exhaust gas temperatures and any another model results. All of these results can be extracted and then the effects of the variables on these results can be found.

4.3.1 Building a WAVE Model

To build a model in WAVE, it is necessary to gather the data, prepare it and construct the model. Before making a model in WAVE, a wide variety of information is required relating to the system to be simulated. These data are categorized in three main parts including geometric data, engine data and operating parameters.

Geometric data collection is the most time-consuming part of any model building. For an engine, the dimensions of all intake and exhaust systems are required. All of the engine specifications' dimensions and their geometries are very important, but the most necessary parts which need more precise dimensions and specifications are the inlet and exhaust manifolds' pipe length especially for noise prediction simulations. Engine detailed specifications are needed for most accurate modelling.

Cylinder head and exhaust ports are the actual engine characteristics for which the required information is as follows: bore, stroke, connecting rod length, wrist pin offset, compression ratio, valve timing and mechanical friction details. The ports require more information such as port flow coefficient, valve diameters, valve event timings and valve lift [21].

To operate the parameters in the conditions in which the simulation will be run, typical data required for an engine are the inlet and exhaust wall temperatures, engine operation speed, fuel flow rate, piston head, ambient conditions and combustion data. These are the minimum conditions required to get the basic model running. At the end, dynamic intake and exhaust pressures, cylinder pressure traces, engine performance, volumetric efficiency and IMEP are required to perform any needed correlation of the model.

At the end of modelling it is essential to check the defined parameters to make sure that everything is described precisely. These main important parameters are mentioned in Table 4.1 [21, 22].

Before starting modelling, it is important to understand the various blocks in the package for the best application. Junctions are the first main part which is necessary to learn. Junctions have many uses, including connecting ducts and representing engine cylinders. These are numerous types of junctions which can be used in the package. The basic common junctions are described in Table 4.2.

Table 4-1: Ricardo WAVE Parameters

Power Cylinder	Intake and Exhaust Geometry	Valve and Port Data	Turbocharger
Bore, Stroke, Connection rod Length, Piston Pin Offset, TDC combustion chamber volume, Compression ratio, Number of Cylinders, Number of Stroke, Heat transfer area of combustion, Clearance height between top of piston and top of cylinder	Intake piping and manifold geometry, Exhaust piping and manifold geometry, EGR circuit geometry	Lift profile versus crank angle, Valve timing events, Maximum valve lift, Flow coefficient versus L/D, Number of ports of the same type, Port geometry and precise location	Compressor map showing operating points, Compressor reference temperature and pressure, Compressor inlet and exit diameters, Compressor speed, Turbine speed, Turbine inlet and exit diameters, Mechanical efficiency

Table 4-2: Ricardo WAVE Common Junctions

Junction	Orifice	Ambient	Engine Cylinder	Y-Junction
Applications and properties	To link two ducts, ducts on either side can be of different or the same diameter, the only required input is the diameter of the orifice. It is used for joining a duct to duct with no change other than diameter or a restriction.	Used to represent the atmosphere ends of the model or flow terminations, it can have only one duct or multiple exhaust muffler, for joining a duct to atmosphere conditions.	Used to represent the power cylinder of an IC engine; every cylinder has its own properties and can have multiple duct connections signifying multi-valve engines.	Used to model complex geometrical parts. Simple y junctions are used to model arbitrarily shaped volumes. It is used to model junctions where more than two ducts come together. Main applications are air cleaners, inlet manifolds, catalysts and exhaust mufflers; used for modelling an exhaust collector.

It is important to choose the right type of junctions when modelling an engine. In the above table, full detailed information was provided to help the designer to find the correct junction.

Ducts have two primary purposes; which are to model pipe geometry and to connect sub volumes together when modelling large volumes. It is very important that the ducts will be defined with complete details and use of the proper connections [21].

Wave Build is the processor used to build geometric models and provides all of the input data for the models which is required to perform the analysis. It consists of many features which can be edited each time to have more accurate results. When the model is complete it can be run from the Wave Build environment in any variety of modes. In the final step, any prepared model has the capability to calibrate it with the existing experimental results.

4.3.2 WAVE model for JLR Engine

Following on from the above explanation, now the aim is to design the experimental set-up in Ricardo WAVE to analyse the effect of the input data. Figure 4.2 shows the engine model in the software package for simulation. This indicates the two ambient junctions at the start and end of the model which is connected to the atmosphere. Orifice junctions are used for different duct sizes, which were mentioned in Chapter 3 as the experiment set-up geometries; Y junctions connect the ducts with different diameters and with different numbers of input and output pipes. The engine cylinder also includes the full detailed specification of the engine which

was defined precisely to start running the simulation. Different thermocouples and injector also were defined in the specified location for further investigations. It is essential before the start of the modelling of any engine to understand what we have and what we want from the simulation results. In this step, our model was built and the results can be analysed without carrying out any expensive experiments; but it is very important before making any predictions, that the model is calibrated and validated with the existing experimental results.

4.4 Modelling in AVL BOOST

BOOST is a simulation program developed for the modelling and simulation of the entire engine. The whole engine can simulate the complete engine cycle including the combustion and emissions. The AVL Company have created many categories of this simulation package such as FIRE, CRUISE and BOOST. For our investigation BOOST is used; which is applied for thermodynamics' analysis. It offers a graphical user interface, an interactive pre-processor; an interactive post processor for fast analysis of the results and comparison with experimental data; extensive interactive context; efficient simulation; and animated display of pressure profiles.

BOOST is a powerful tool for engine performance analysis, it can be applied to a range of tasks; such as comparison of various engine concepts, optimizing component geometry (inlet, exhaust, valves etc. with respect to power, torque and fuel consumption), valve timing and cam profiles, supercharge and turbocharging systems, orifice noise optimization and evaluation of engine performance.

AVL provides many features which are summarised below and table 4.3:

- Pipes and junctions

- Perforated pipes

- Flow restrictions

- System boundaries

- Plenums and crankcases

- Air cleaners and air cooler

- Turbocharging and supercharging: single and multiple entry turbines, variable geometry turbines, power turbine

- Combustion model: vibe function, two-zone vibe for NOx, experimental burn rate input, constant pressure, constant volume

- Control functions: BOOST internal engine control unit, PID controller

Table 4-3: AVL Boost elements trees

Element	Symbol	Specification
Engine	E ( )	Engine element
System Boundary	SB (⊢)	Provides the conditions of the calculation model to a user-definable ambient.
Measuring Point	MP (X)	Access to allow data and gas conditions over crank angle at a certain location in a pipe.
Element	**Symbol**	**Specification**

Monitor	MNT ( )	Is used to produce transient results in the results folder and in online monitor for arbitrary number
Plenum	PL ( )	An element in which spatial pressure and temperature differences are not considered
Cylinder	C ( )	Cylinder element
Restriction	R ( )	Consider a distinct pressure loss at a certain location in the piping system
Throttle	T ( )	Controls the air flow in a pipe as a function of throttle angle
Junction	J ( )	Used to connect three or more pipes. In the case of three pipes, a refined junction model may be used. This considers geometric information such as the area ratio of the connected pipes and the angles between the pipes. In other cases a simple constant pressure model is available
Pipe	numbers	Pipes to connect different features

AVL BOOST is capable of the analysis of the calculation results in different modes, such as message analysis, transient analysis, traces analysis, series analysis and acoustic analysis. Transient analysis takes the average results for each cycle calculated versus cycle number or time. Any traces are shown in the graphs versus crank angle which can also be exported as a text file. It is aimed in Chapter 5 to

compare all the results of the measurement and experimental results with the simulation results.

4.4.1 Building a BOOST Model

BOOST simulates a wide variety of engines; so for most of the modelling this software is used due to its wide applications. As with Ricardo WAVE, this software has many features in the package. The model can be designed by placing the elements in the workbench and then connecting the elements with proper pipes.

The main features which need to put in the simulation plan are the plenum, restrictions, injector, junction, system boundary and pipes. All of mentioned features have the same usage as in WAVE. All of them can be midfield at each stage by changing their specification.

4.4.2 BOOST Model for JLR and PAMAR Engine

After the above explanation, now the aim is to design the experimental set-up in AVL BOOST to analyse the effect of the input data. Figure 4.3 shows the engine model in the software package for simulation. This indicates the two system boundary at the start and end of the model which is connected to the atmosphere. The engine cylinder also includes the full detailed specification of the engine which was defined precisely to start running the simulation. Different thermocouples and injectors also were defined in the specified location for further investigations. It is essential before the start of the modelling of any engine to understand the set-up and conditions at the beginning and what we want to achieve from the simulation results. In this step, our model was built and the results can be analysed without performing

any expensive experiments, but as previously, it is very important before doing any prediction that the model has to be calibrated and validated with the existing experimental results. In the monitor section, different types of traces can be defined to see the results. The AVL BOOST also has the capability for emission analysis; by defining the two-phase vibe function, all emissions will be predicted based on the engine type, engine running conditions and the types of fuel which are used [22, 23].
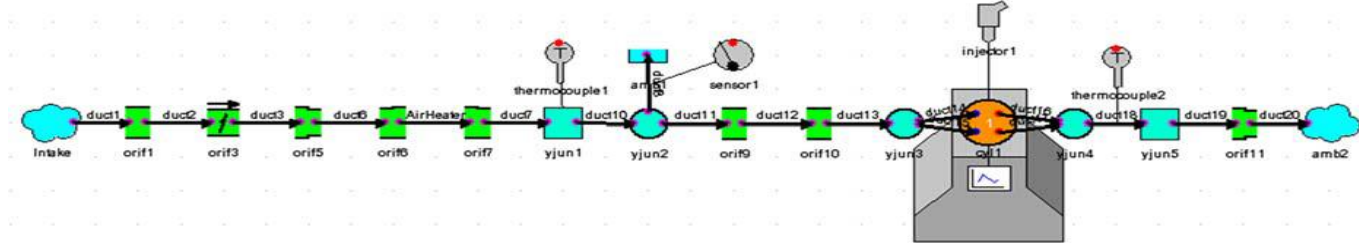
Figure 4-2 Designed Model in Ricardo WAVE
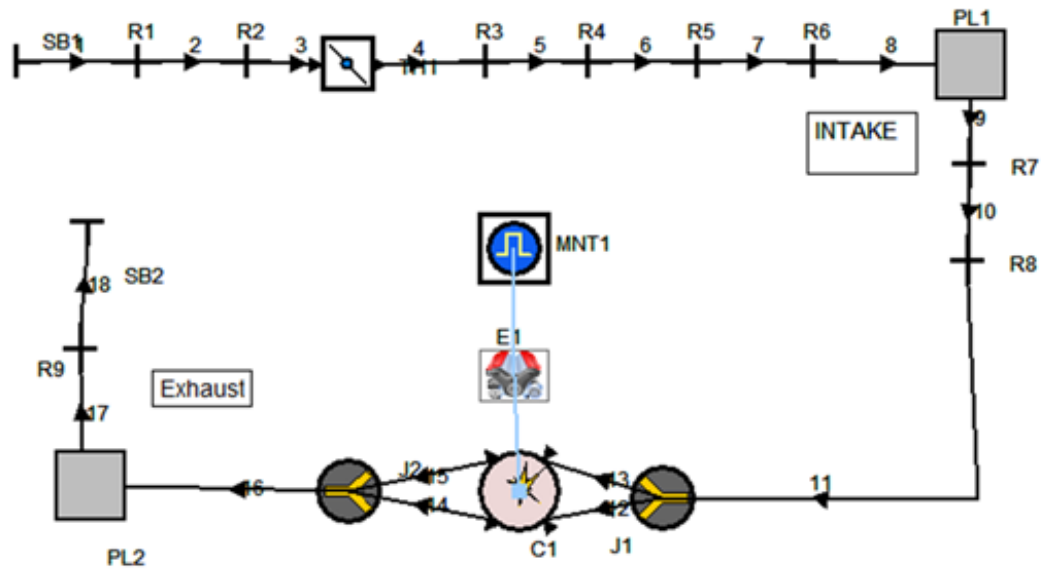
Figure 4-3 Designed model in AVL BOOST

Chapter 5 – Thermodynamic Simulation Comparison of AVL BOOST and Ricardo WAVE for HCCI and SI Engines' Optimisation

Most of this chapter contains the results which are part of a published paper by the author in the PTNSS journal [24].

This chapter describes the HCCI and SI engines' performance, combustion and emission analysis and also possible improvements using the developed simulation AVL BOOST and Ricardo WAVE programs. A full description of AVL and Ricardo WAVE software was presented in Chapter 4. By using the simulations programs, the limitations of the test engine in relation to the design and operating variables could be studied. The aim of this chapter is to compare two simulation software platforms, AVL BOOST and Ricardo WAVE as used to simulate HCCI and SI GDI engines, with the intention of maximising the engine's efficiency and minimising the emissions. This chapter compares these platforms in an experimentally validated model to analyse a spark ignition engine and a homogeneous compression ignition charge (HCCI) single cylinder 4-valve engine with multiple configurations and running parameters.

The most optimal set-up for the engine will be found with the prospect of allowing an optimum engine to be built and tested in real-world conditions without the need for multiple expensive prototypes and long delays. Software can then be used to predict improvements that can be made to the model and reduce the emissions of the engine. The effect of inlet valve timing in an SI and HCCI engine on NO_X emissions was also investigated, highlighting the key differences between the combustion modes. Results from the simulation showed that engine outputs were accurately replicated with minimal error for the SI and HCCI engines, validating the model and permitting the analysis of the emissions. From the intake valve opening of the SI engine, it was found that NO_X could be significantly reduced due to the

increase in residual gases, with a limited effect on IMEP and torque. On the other hand, altering the HCCI engine's IVO had a minimal effect on NO_X caused by the already reduced NO_X production [23].

5.1 Introduction

Recently in the design process of new engines, there was little analytical work and the majority of the development was physically carried out on rigs and workhorse vehicles in on-road trials. This meant that any experimental changes and any development to the engine design had to be implemented and tested out on the rig or vehicle, leading to great expense. With the advent of the computer and increased computing power, the design process has shifted to a more analytical approach. Nowadays engines can be quite accurately simulated on a computer (as this chapter aims to show), which has meant engine manufacturers can view the effects of changing engine parameters on engine performance very quickly, without it costing vast sums of money and time. There is no need to build the product completely, but by doing some simulations; researchers and manufacturers can investigate any work on the final products.

In this chapter, AVL BOOST and Ricardo WAVE were used to simulate the engine in different experimental conditions and find calibrate the modelling setup for further investigations.

5.2 Aims and Objectives

The main aim of this chapter was to create a realistic computer simulation of a single cylinder engine operating in two modes: spark ignition (SI) and homogeneous

charge compression ignition (HCCI). By using geometry, data and experimental data from the Jaguar DI Engine, which was, as explained in Chapter 3, at the University of Birmingham, Department of Mechanical Engineering. The experimental results were gathered from the engine by using the specific instruments which were all explained in Chapter 3. The rate of heat release and the mass fraction of burned fuel were to be calculated and used to model the engine in Ricardo WAVE. It was then to be calibrated and validated by comparing simulation results to experimental values obtained from the engine. Once validated, improvements to the engine design in terms of emissions were to be suggested and tested. As well as this, all of the operating cases were also to be modelled in AVL BOOST. At the end, the results of the experiment, AVL BOOST and WAVE are used to compare the differences between software packages and experimental data. In this work cases one to three refer to HCCI mode, cases four to seven represent the SI mode. In summary, the main aims of this chapter can be listed as: 1. Creation of a model in AVL and WAVE for specified combustion modes and conditions from defined engine geometry. 2. Mathematically calculate combustion profiles such as rate of heat release (ROHR), pressure rise and mass fraction burned (MFB) for validation. 3. Calibrate engine models to provided experimental data and validate obtained results. 4. Explore and investigate NO_X emissions through altering inlet valve opening times. Engine emissions can be improved by recirculating exhaust gases (EGR) back into the cylinder to reduce NO_X emissions. This can be conducted internally via valve timing, resulting in the increase in cylinder residual gases. It is expected that the higher EGR causes lower NO_X.

5.3 Engine General Parameters

A thermal Jaguar DI 4v VCT single cylinder engine was used, which is fully explained and all of its main specification which were used for modelling were mentioned in chapter 3.

Intake and exhaust valve specification were mentioned in chapter 3 with full detailed information. Figures 5.1 right and left show port ducting; again all of them were fully described in Chapter 3. The high lift intake, low lift intake, high lift exhaust and low lift exhaust data are presented in Appendix A.5.1 at the end of this thesis.
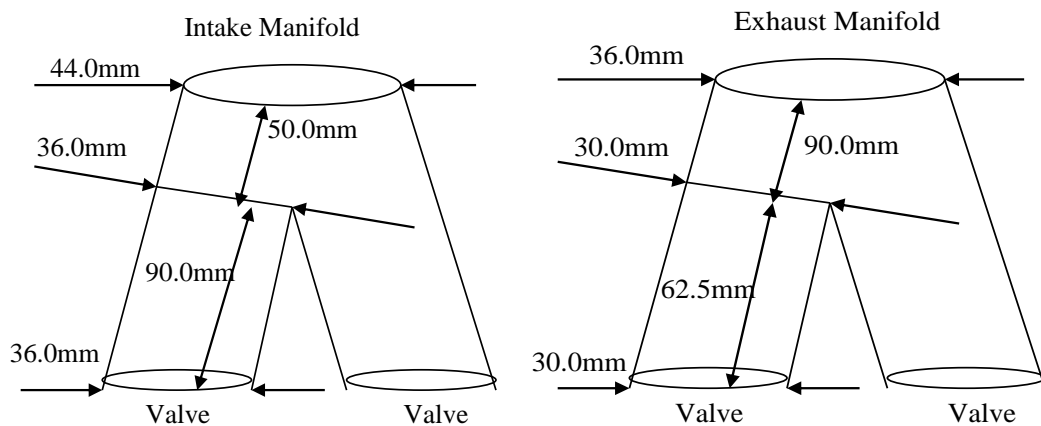
Figure 5-1 Port Ducting: Intake Duct (in head), Exhaust Duct (in head)

5.4 Analysis of Experimental Results

In order to complete the model, WAVE and AVL needed information about the combustion process; therefore, the mass fraction burned fuel (MFB) had to be calculated for each engine experiment case. Tables 5.1 and 5.2 indicate the seven different cases of the experiment which was run and then their results are compared

with modelling for validation of the simulation results. All of the experiments were run at 1500 rpm.

Table 5-1 Experimental Conditions

Case	Comb Mode	Camshaft	IVO (° bTDCge)	EVC (° aTDC ge)	SoI (° bTDC co)	Spark Timing (°bTDC)	λ
1	HCCI	Low Lift	-100	-100	330	-	1.19
2	HCCI	Low Lift	-90	-90	270	-	1.20
3	HCCI	Low Lift	-75	-75	330	-	1.31
4	SI	High Lift	10	10	280	9	1.00
5	SI	High Lift	10	10	280	36	1.00
6	SI	High Lift	10	10	280	34	1.01
7	SI	High Lift	10	10	280	34	1.00

5.4.1 Cylinder Volume

Using the geometry and equation shown in Equation 5.1 below, the volume of the cylinder was calculated at 0.5° crank angle increments and figure 5.2 (right) shows cylinder volume changes based on crank angle. [1].

$$V(\theta) = V(0) + \frac{\pi}{4}b^2(l + \frac{S}{2} - y - x)$$ **Eq. 5. 1**

where:

$V(\theta)$: Cylinder volume in different crank angle (θ)

$V(0)$: Cylinder volume in 0 degree crank angle

b: Bore

l: Conrad length

s: Stroke

y *and* x: As defined in Figure 5.2
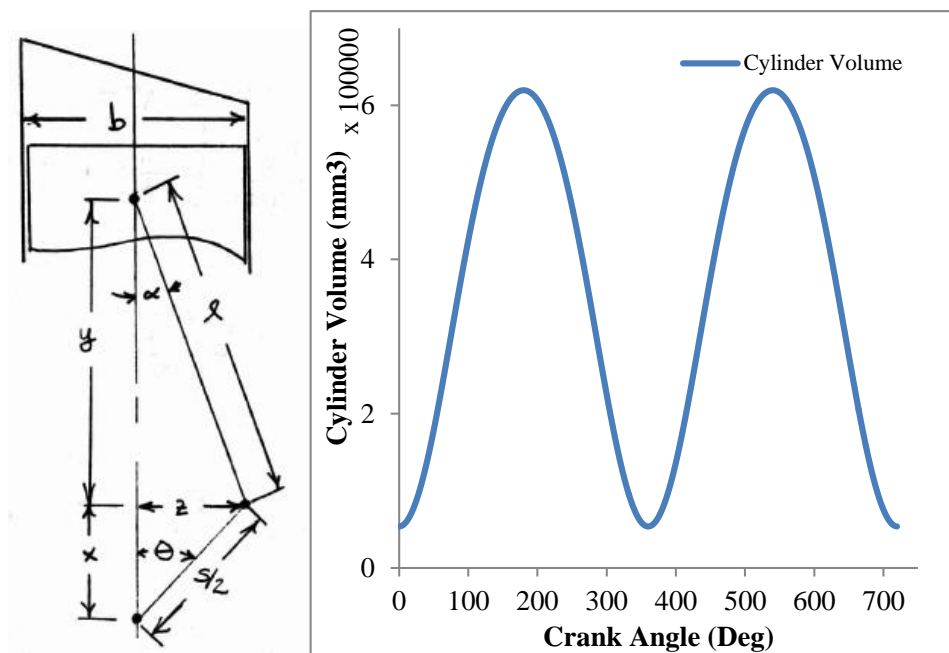
Figure 5-2 Cylinder Specification

5.4.2 Cylinder Pressure

The cylinder pressure was analysed in seven different cases, which were shown in Table 5.1 and Figure 5.3. These figures represent the change of pressure by changing the experiment conditions.
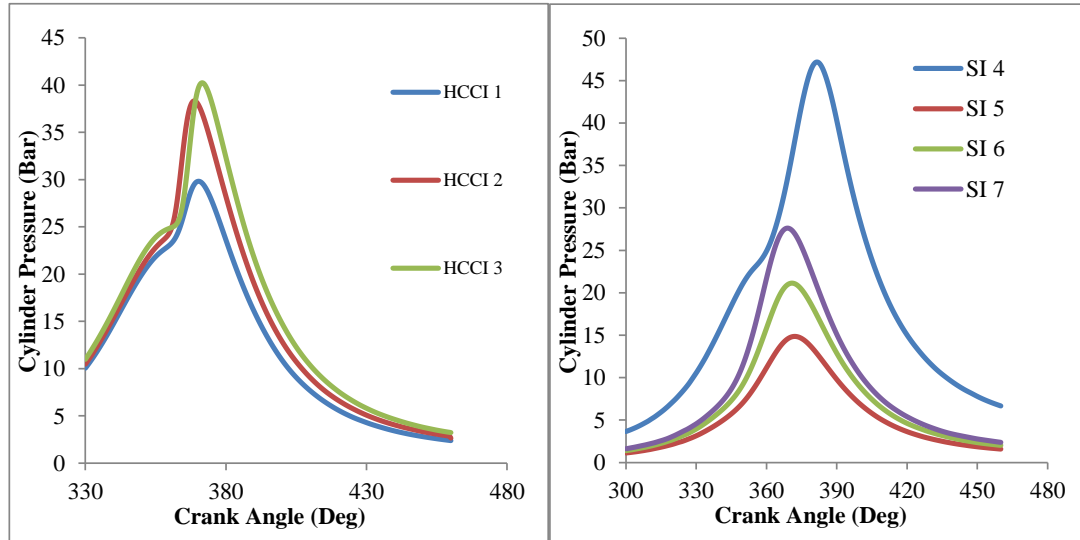
Figure 5-3 Cylinder Pressure versus Crank Angle of HCCI and SI conditions

Table 5-2 Experimental Conditions

Case	IMEP (bar)	BMEP (bar)	PMEP (bar)	COVimep (%)	RPR (bar/°)	Pmax (bar)	Pmax CAD (°)	Pmax CAD (°)	mfb5 (°aTDC)
1	1.81	-	0.40	3.01	1.82	29.8	371.0	11.0	1.7
2	2.80	-	0.38	1.46	3.55	38.3	369.5	9.5	0.9
3	3.48	-	0.46	1.29	4.42	40.2	372.0	12.0	4.0
4	10.04	9.56	0.11	2.04	2.49	47.2	382.0	22.0	3.7
5	1.73	1.16	0.70	3.96	0.80	14.9	372.5	12.5	-6.2
6	2.58	2.15	0.64	2.17	1.15	21.1	371.5	11.5	-7.7
7	3.25	2.95	0.59	1.69	1.67	27.6	369.5	9.5	-8.8

5.4.3 Heat Release Rate

Figure 5.4 indicates the heat release rate of different cases. The maximum heat for the HCCI and the SI cases are around 30 Joule/degree 35 Joule/degree respectively.
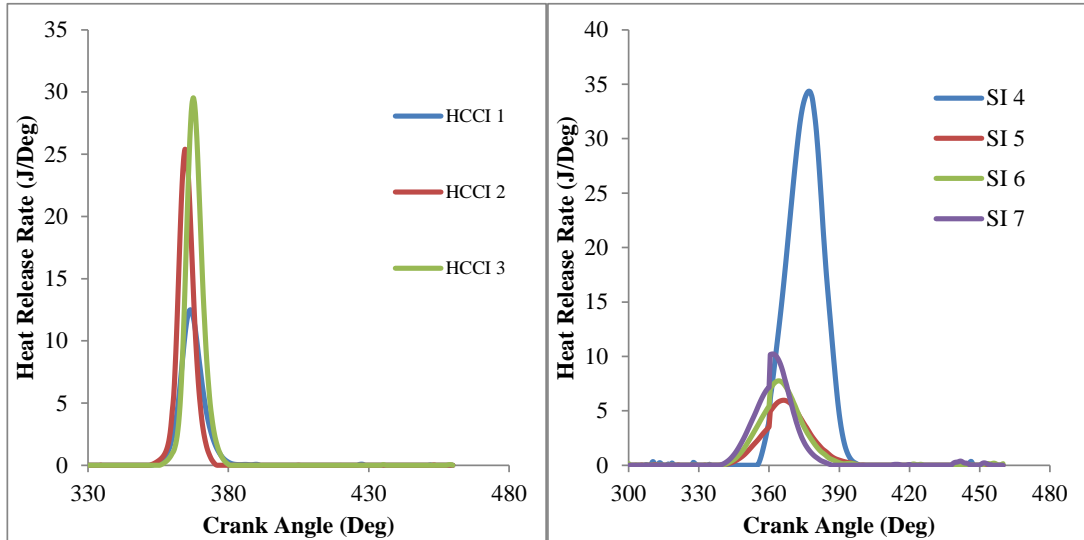
Figure 5-4 Heat Release Rate versus Crank Angle of HCCI and SI Conditions

Figure 5.5 indicates the mass fraction burnt of seven different cases, which were calculated based on Chapter 3's information and equation, used from references for calculation.
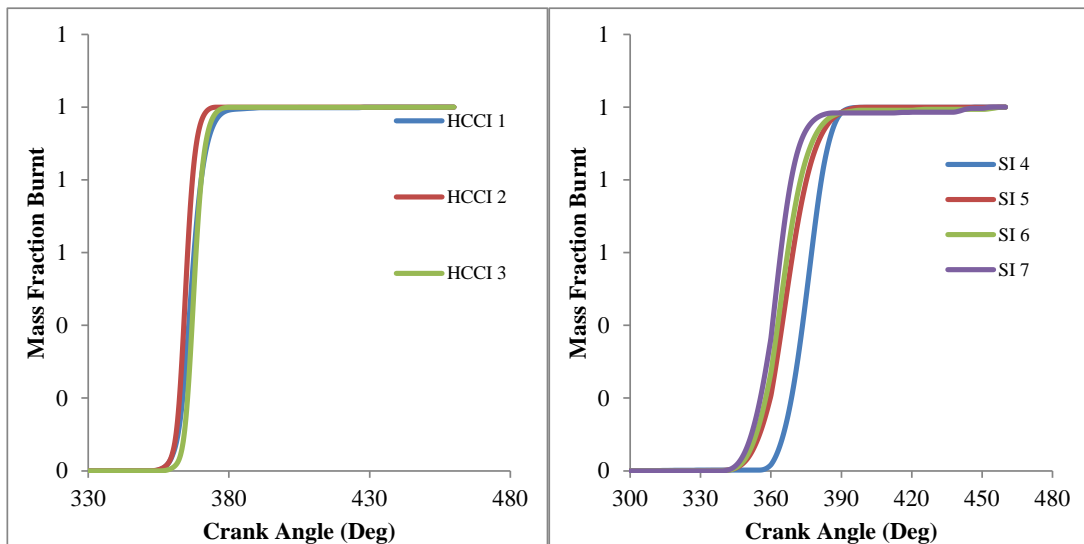
Figure 5-5 Mass Fraction Burnt versus Crank Angle of HCCI and SI Conditions

5.5 Analysis of Calculated Results

By using the experimental pressure data and also cylinder volume in different crank angles, a graph of the ln (pressure) versus ln (volume) was drawn in seven cases shown in Figures 5.6 and 5.7. From these graphs, it was possible to obtain the polytropic indices (k) of the compression and expansion by finding the magnitude of the gradients in the straight lines. For each case, an average k of the two polytropic indices was calculated.
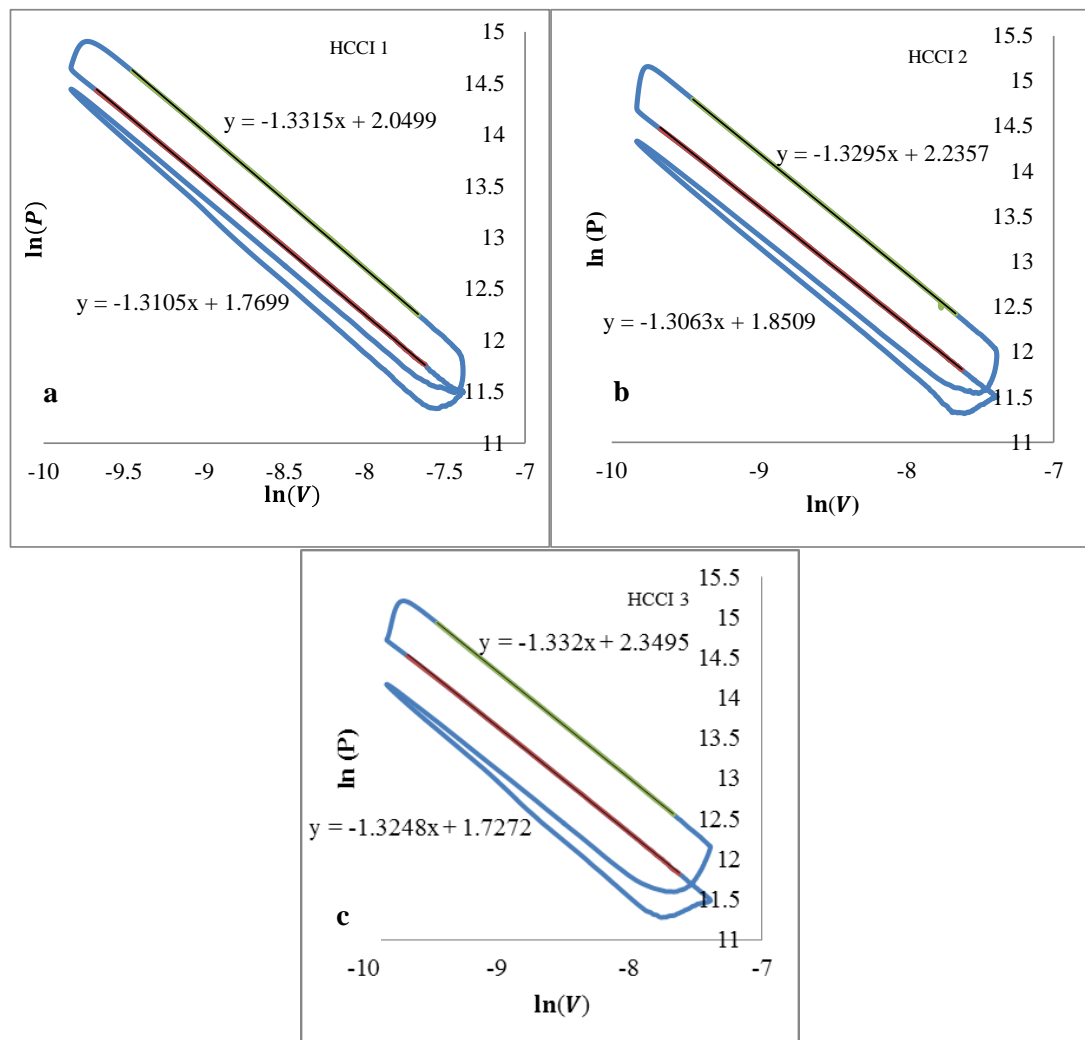
Figure 5-6 Compression and Expansion Polytropic Index k Calculation from Graph ln (v) versus ln (p) for HCCI Conditions
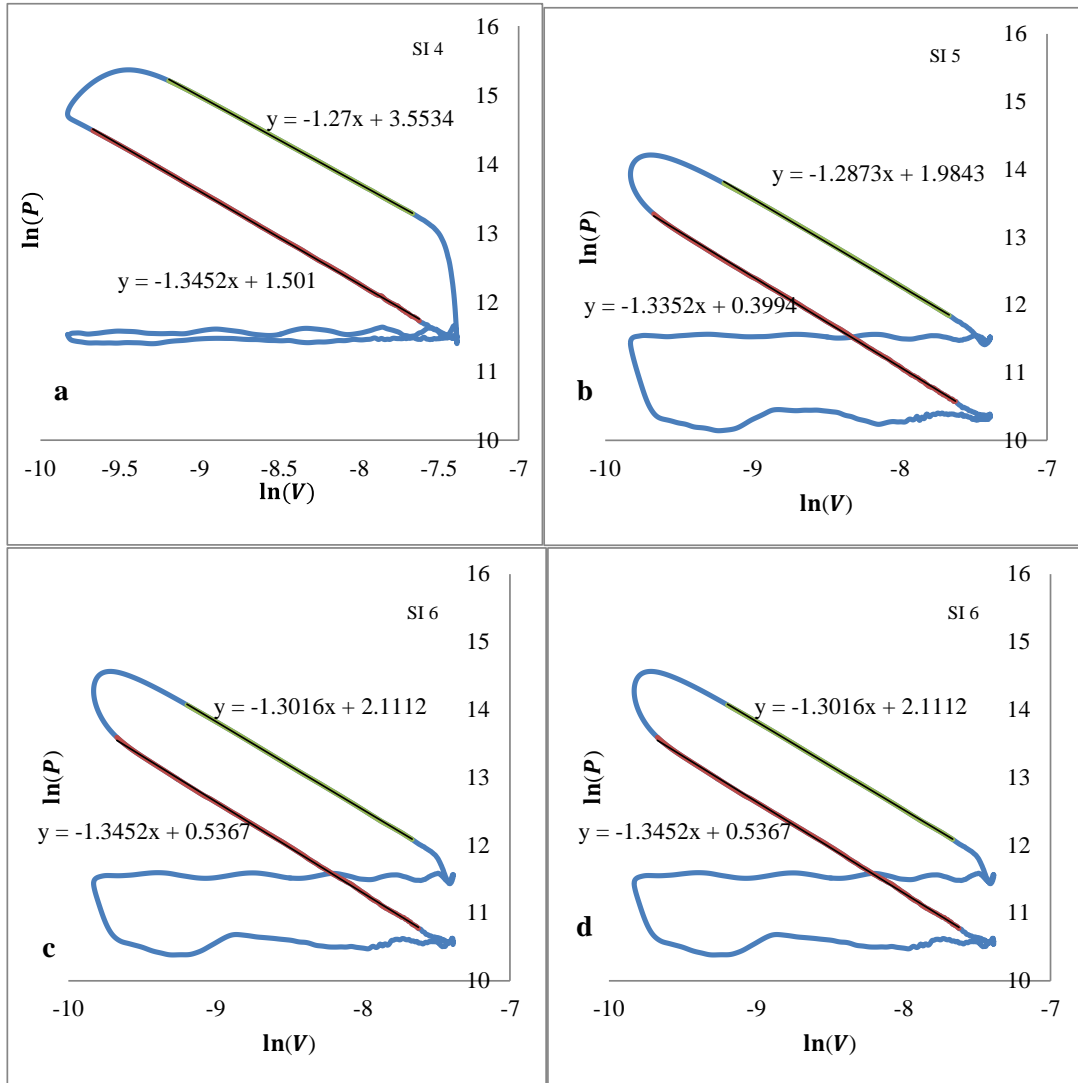
Figure 5-7 Compression and Expansion Polytropic Index k Calculation from Graph ln (v) versus ln (p) for

SI Conditions

By using the polytrophic index and Equations 5.2 and 5.3 the mass fraction burnt was calculated to compare with the experimental data. Equation 5.4 was used for the heat release rate [1].

$$\Delta P^*_C = P_{i+1} - P_i \left(\frac{V_i}{V_{i+1}}\right)^{\overline{k}} \left(\frac{V_i}{V_{Clearance}}\right) \qquad \textbf{Eq. 5.2}$$

$$MFB = \frac{\sum_0^i \Delta P^* c}{\sum_0^N \Delta P^* c} \qquad\qquad \textbf{Eq.5.3}$$

$$\frac{dQ_n}{d\theta} = \frac{\bar{k}}{\bar{k}-1} P \frac{dV}{d\theta} + \frac{1}{\bar{k}-1} V \frac{dP}{d\theta} \qquad\qquad \textbf{Eq.5.4}$$

where:

Q_n: Heat release rate

θ: Degree of crank angle

$\bar{k}$: Polytropic index

P: In-Cylinder pressure

V: Cylinder volume

And, MFB: Mass fraction burnt

5.6 Comparison of Experimental and Calculated Results

For each case, data from the experimental results, which was shown in Figures 5.8 and 5.9, and Figures 5.10 and 5.11, were used to validate the calculated mass fraction burned and the rate of heat release results, too. There was good agreement between the two, showing that the method of calculating the MFB and rate of heat release rate was correct.
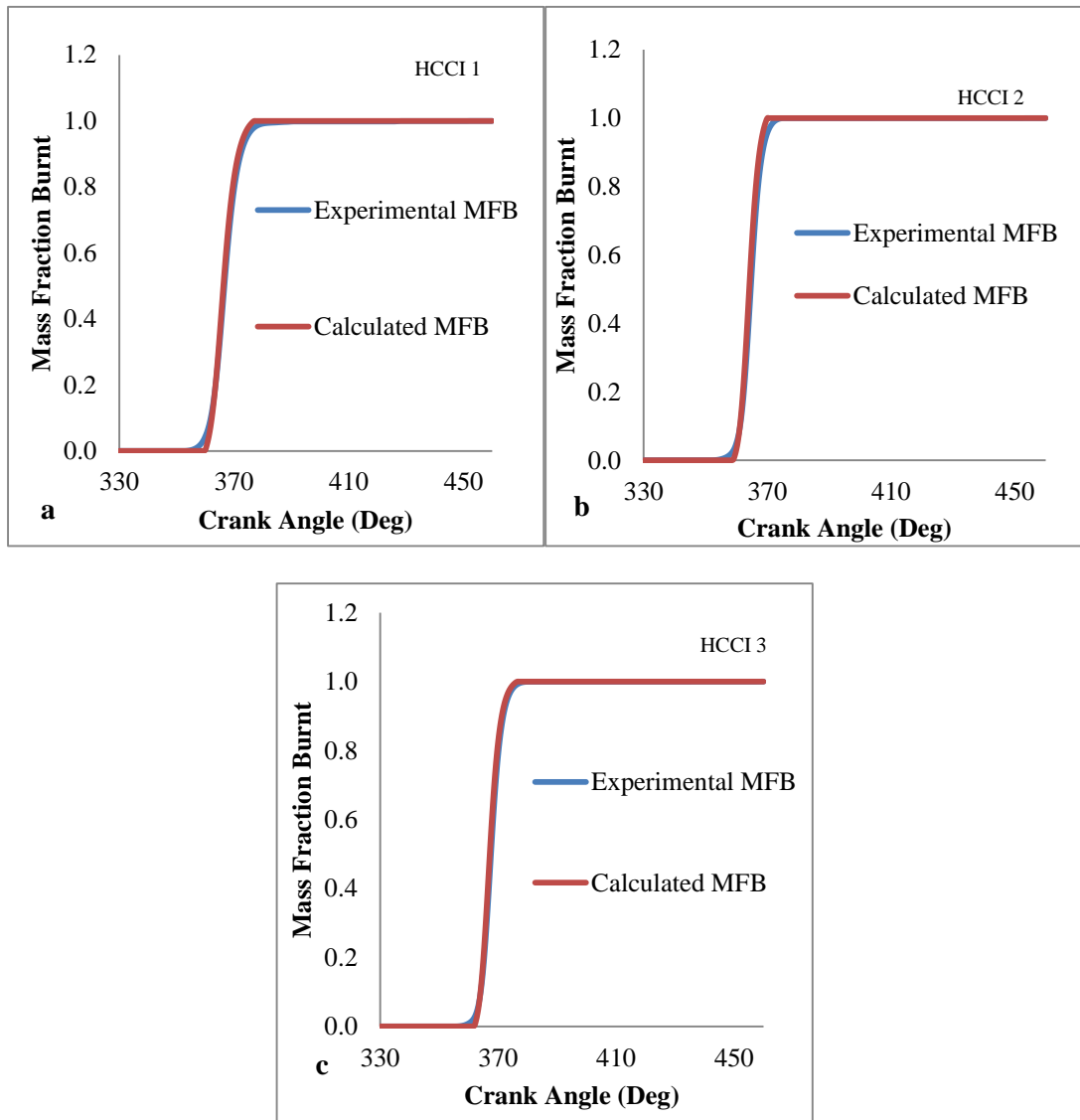
Figure 5-8 Comparison of the Experimental and Calculated Mass Fraction Burnt in HCCI Conditions
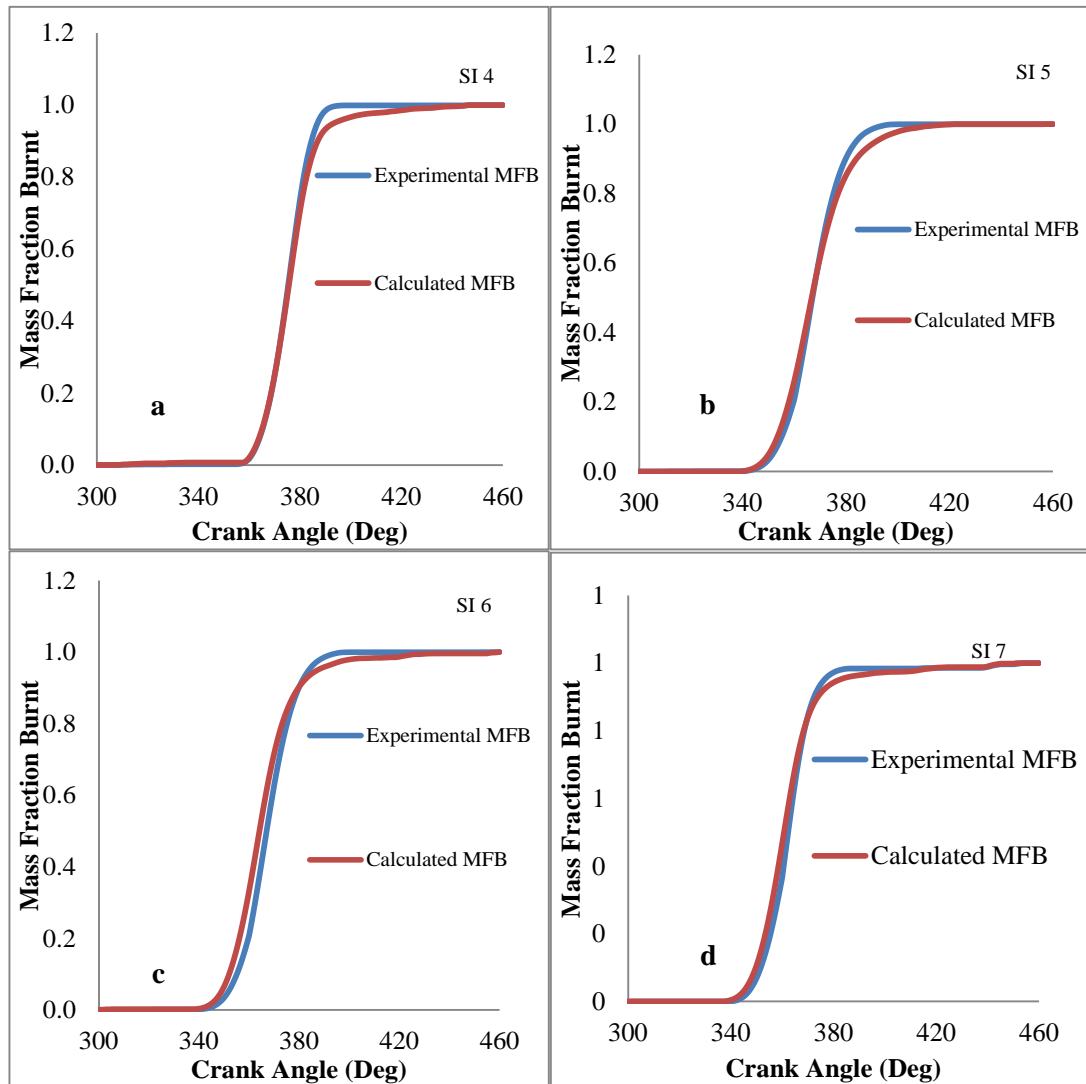
Figure 5-9 Comparison of the Experimental and Calculated Mass Fraction Burnt in SI Conditions
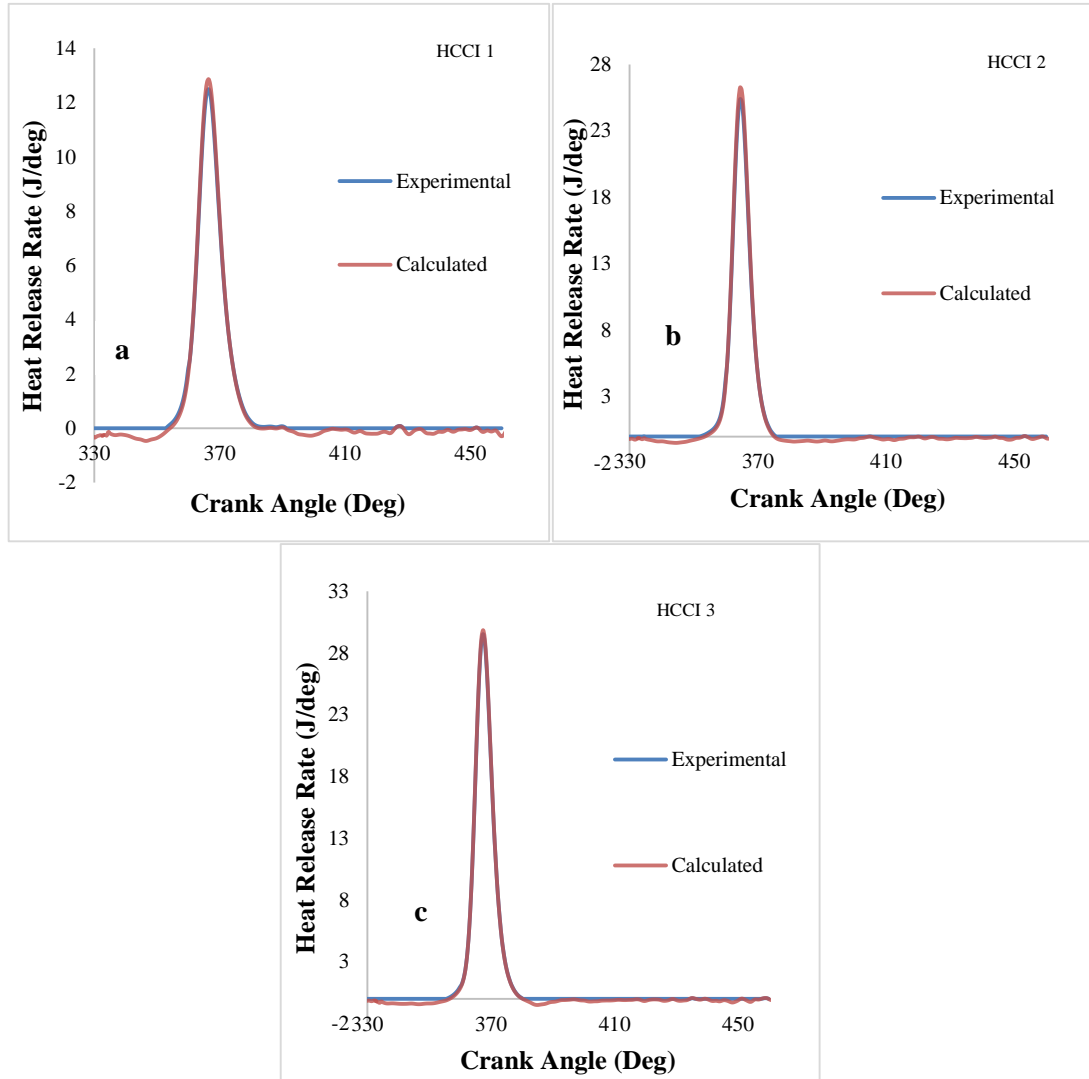
Figure 5-10 Comparison of the Experimental and Calculated Heat Release Rate in HCCI Conditions
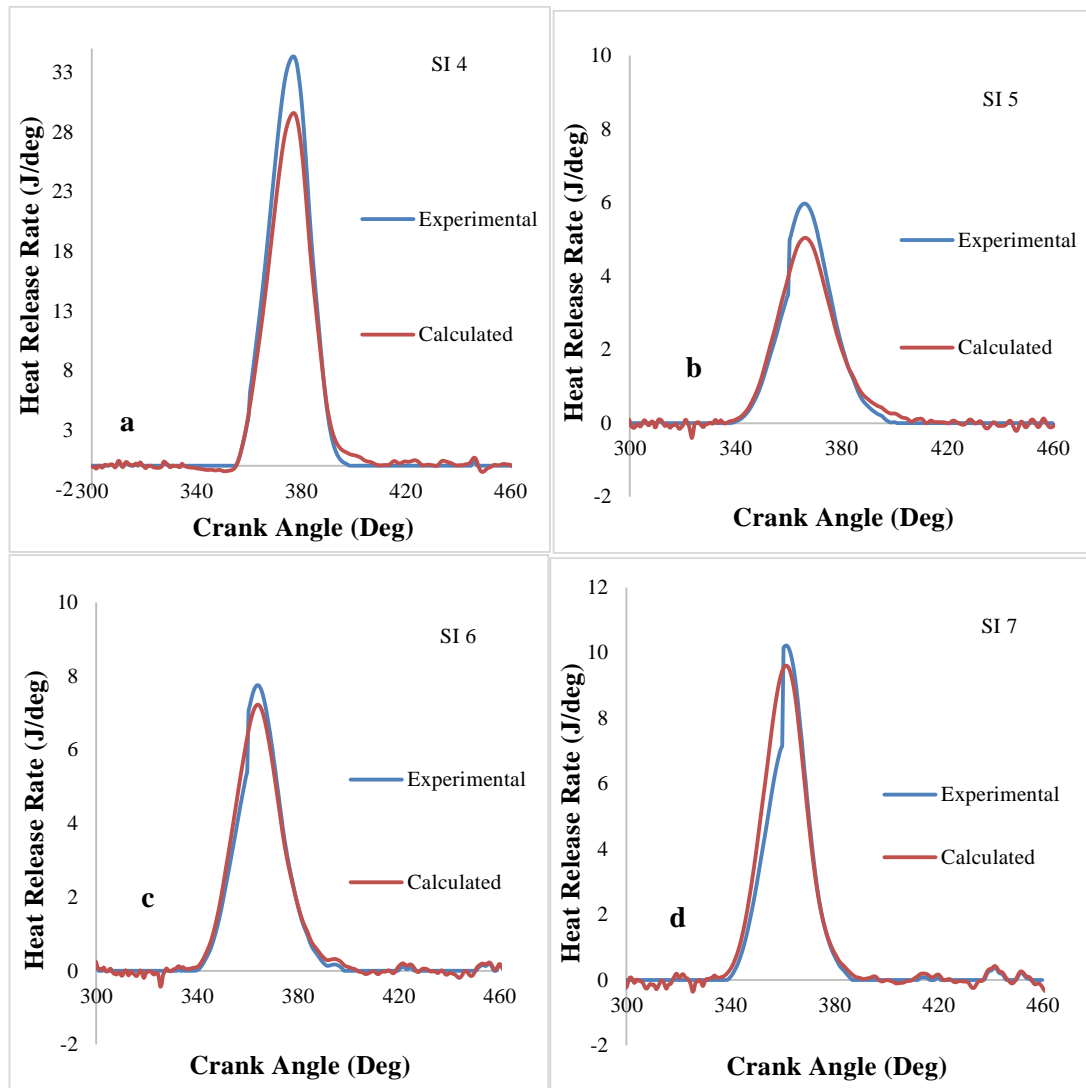
Figure 5-11 Comparison of the Experimental and Calculated Heat Release Rate in SI Conditions

5.7 AVL BOOST and Ricardo WAVE Modelling Set-up

According to Ricardo, "WAVE is the market-leading ISO approved 1D engine & gas dynamics simulation software package from Ricardo Software. It is used worldwide in industry sectors including passenger cars, motorcycles, trucks,

locomotives, motor sports, marine and power generation. WAVE enables performance simulations to be carried out based on virtually any intake, combustion and exhaust system configuration, and includes a drivetrain model to allow complete vehicle simulation."

The procedure of modelling in the software packages was fully explained in Chapter 4, but it is mentioned here as a summary for easy understanding of the main aim of this chapter. To start the simulation and make the model, the exhaust and inlet were modelled as a combination of orifices, "Y" junctions and ducts in Ricardo WAVE and restrictions in AVL BOOST, from the experimental data and junctions, plena and connections in AVL BOOST. The discretion lengths, heat transfers, temperatures of the piston walls and cylinder were calculated from equations in WAVE Help. Indolene was the chosen fuel as it is the closest representation to gasoline that is available in the software. A constant table was created so that it is easy to change the variables. The model was set to run for 100 engine cycles for SI and 50 for HCCI to allow for convergence of the results in the simulation. The fuel is directly injected into the cylinder for HCCI and due to the similarity of the intake and exhaust systems, the same fuel injector was used for the SI model, as many gasoline cars now use direct injection. The SI engine system as modelled in Ricardo WAVE can be seen in Figure 5.12 and as modelled in AVL BOOST can be seen in Figure 5.13. The main difference between the SI model and the HCCI model is that the throttle and the two ducts that are connected to it have been removed and replaced by one duct. The spark timing has been removed as HCCI auto ignites during compression. The model was to be a four-stroke engine capable of two modes. The first was DISI mode, where fuel is injected directly into the combustion

chamber, where it mixes with the inducted air at a near stoichiometric ratio (14.7:1) and combustion is initiated by an arc in the spark plugs. The second mode was HCCI mode, where fuel is also directly injected into the combustion chamber and mixes with the inducted air; however, in this mode, there is a large excess of air (λ>1.19) and combustion is initiated by auto ignition of the fuel, similar to a compression ignition engine. This makes HCCI clean and efficient, with low NOx, throttling and pumping losses.

Using the intake, exhaust and engine layout which was explained in Chapter 3 and briefly in the previous section for the engine, the model was built and defined in WAVE using ducts, orifices, complex and simple Y-junctions, sensors, injectors and cylinders. The valve lift data from the experimental data was imported for the intake and exhaust sides. The simulation was set to run for 50 cycles as time was not an issue in this case; however, the simulation would stop if convergence occurred earlier than this. WAVE allows for multiple cases of a model to be run in one document, so all SI conditions could be run together in one file and HCCI in another. A table of constants was therefore made to make it easy to change parameters such as λ, throttle position, start of valve openings and the start of combustion between cases without having to remake models. The HCCI model is similar, except the throttle valve is left fully open at 90° for all cases, the diameter of the air heater is slightly reduced, the valves have lower lift profiles with negative valve overlap and the engine operation is changed to compression ignition, removing the spark.

The MFB was then input into WAVE as the combustion model. As WAVE does not have a predictive combustion model, this process of calculating the MFB and inputting the data into WAVE was repeated for all seven SI and HCCI cases.

5.8 Model Calibration, Validation and Recommendation for Improvements

To obtain accurate results, the model was calibrated to the experimental results for cases 1 and 4 as they required no throttle. Calibration was accompanied by adjusting the engine temperatures, piston and cylinder head surface areas, as these values were unknown from the experimental conditions. It was decided to not change the combustion shift for any cases as the calculated/experimental ROHR was assumed to be accurate and representative of a real engine. Validation was achieved through correct IMEP values and MFB traces, peak pressure angle and alight permission to error of the maximum pressure (Pmax). For cases 5-7, the throttle value was adjusted to control the IMEP.

In Ricardo WAVE, the model was then run for a single SI case (case 4) in order to calibrate it. After the simulation converged, the pressure trace was analysed using WavePost, which was then used to compare with the experimental pressure trace. If the pressure traces did not align, then the simulation was repeated; however, an appropriate number of degrees moved the start of combustion so that the pressure traces would align. This process was repeated. Once aligned, the pressure peak was then calibrated by varying the throttle position to raise or lower the maximum pressure and other engine settings could be changed including surface area multipliers and heat transfer coefficients. Once it looked like there was reasonable agreement between pressure traces, both in phase and magnitude, the .out file was examined to find the exact maximum pressure (Pmax), the crank angle at Pmax and the IMEP. Again, even finer tuning was carried out to calibrate these three values to

match as closely to the experimental values as possible. It became slightly cumbersome to keep opening the .out file, therefore a Python script was developed to pull out the data and display it in the terminal. The model was then run on the other SI engine cases while only varying the throttle position and the start of combustion. The resulting pressure traces were then plotted and key data tabulated to compare with the experimental data.

The same process was repeated in order to calibrate the HCCI model using Case 1; however, as the throttle remains fully open in the HCCI case, the only parameters that can be changed are heat transfer coefficients of the open and closed valves and piston and cylinder head surface area multipliers. Again, these were changed in an iterative manner until the pressure traces were in reasonable visible agreement after being exported from WavePost. Then the .out file was examined using the Python script and finer tuning of the coefficients was carried out to match the model with the experimental values as closely as possible. Once the model had been calibrated and IMEP, Pmax and the crank angle at Pmax were in good agreement, the model was then run on the other engine cases while only varying the air-fuel ratio (provided in the supplied test conditions) and the start of combustion. Again, the resulting pressure traces from all cases were then plotted and key data tabulated to compare with the experimental data. The following table shows a comparison of the key experimental values and those obtained from WAVE.

Emission reductions can be achieved by changing the inlet and exhaust valve opening and closing times. As the geometries are kept near identical for all the investigated SI and HCCI cases, it is expected that changes due to the mode of

combustion will be observed. The model will show the advantages of HCCI over SI and is likely to display an improvement in pollution emissions over the SI cases.

5.9 Comparison of Modelling and Experimental Results

Finally, by finishing the validation of the modelling results in the seven different cases, main parameters such as the cylinder maximum pressure and indicated mean effective pressure were compared. As can be seen from the figures and tables below, the HCCI and SI models have produced accurate results with a near zero percent IMEP error. However, the Pmax produced a maximum error of 6.1%, which could not be removed without calibrating the model to unreasonable operating temperatures. The timing of the Pmax CAD was within 0.5%. In addition, all cases were successfully modelled in AVL BOOST. This was done using plena and restrictions and calibrated in the same iterative manner as in Ricardo WAVE.

5.9.1 Pressure Traces

Figures 5.14 to 5.20 show cylinder pressure from the experiment and simulation in seven different conditions. The good agreement between the AVL, WAVE and the experiments indicates that the cylinder geometry and engine parameters are accurately modelled in the simulation; since the indicated mean effective pressure also has good agreement. It should be distinguished that the difference between WAVE and the experimental results could be due to the use of indolene instead of gasoline and therefore, using a different fuel may also reduce emissions further; a change of fuel will affect any experimental and simulation results.
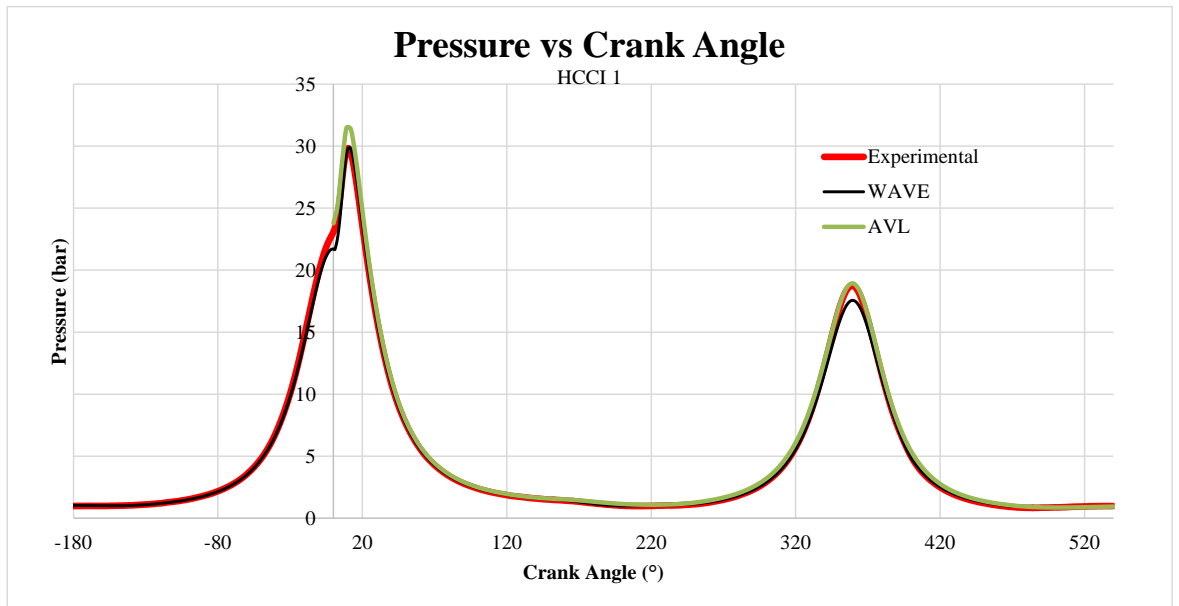
Figure 5-12 Cylinder Pressure HCCI 1 (AVL-WAVE-Experimental)
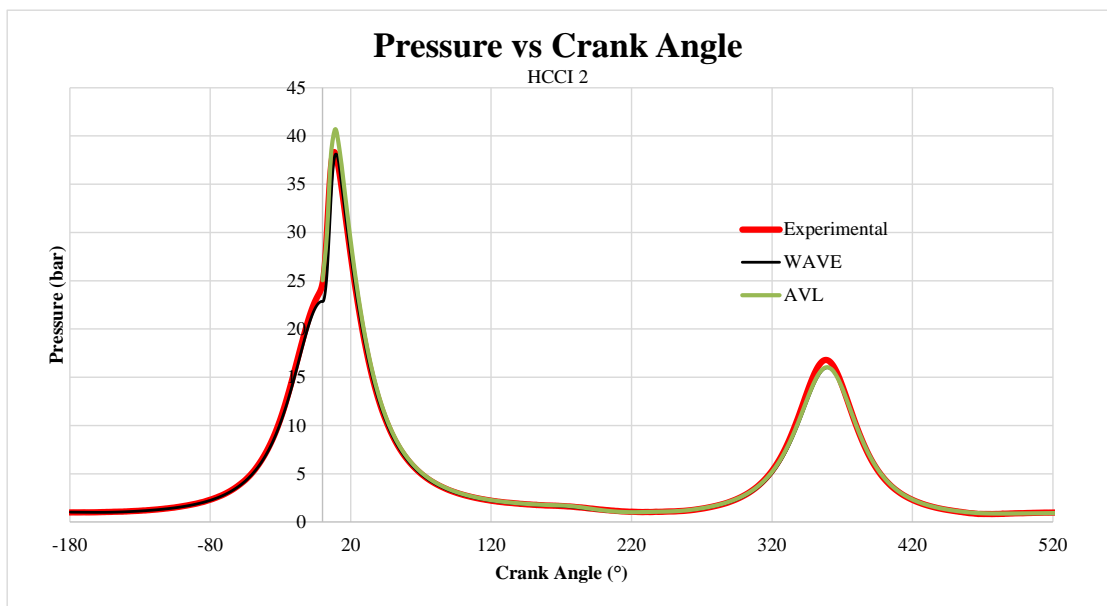
Figure 5-13 Cylinder Pressure HCCI 2 (AVL-WAVE-Experimental)
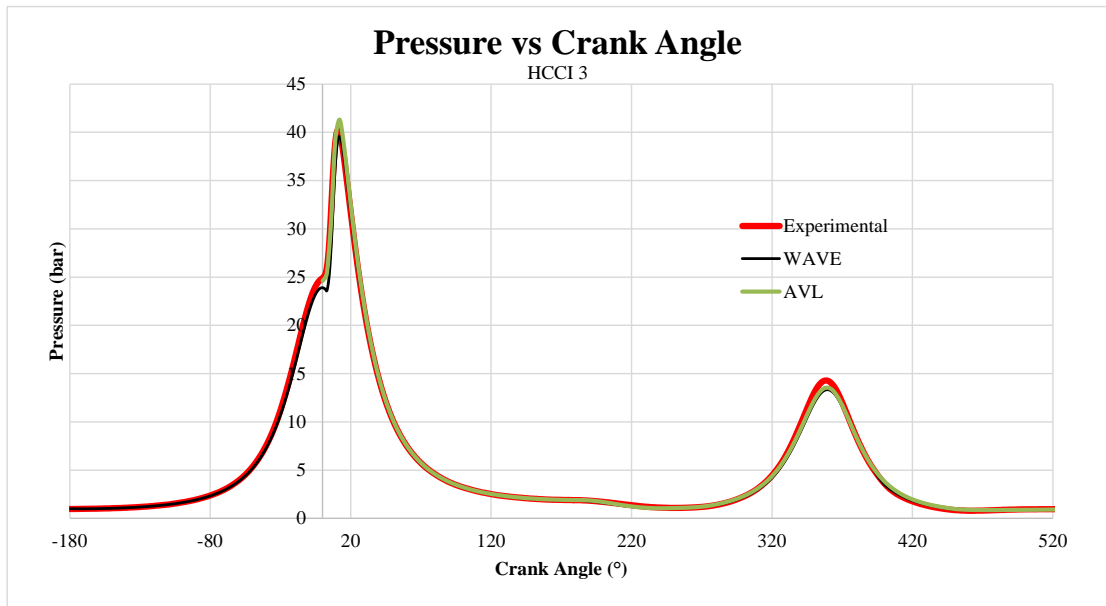
Figure 5-14 Cylinder Pressure HCCI 3 (AVL-WAVE-Experimental)
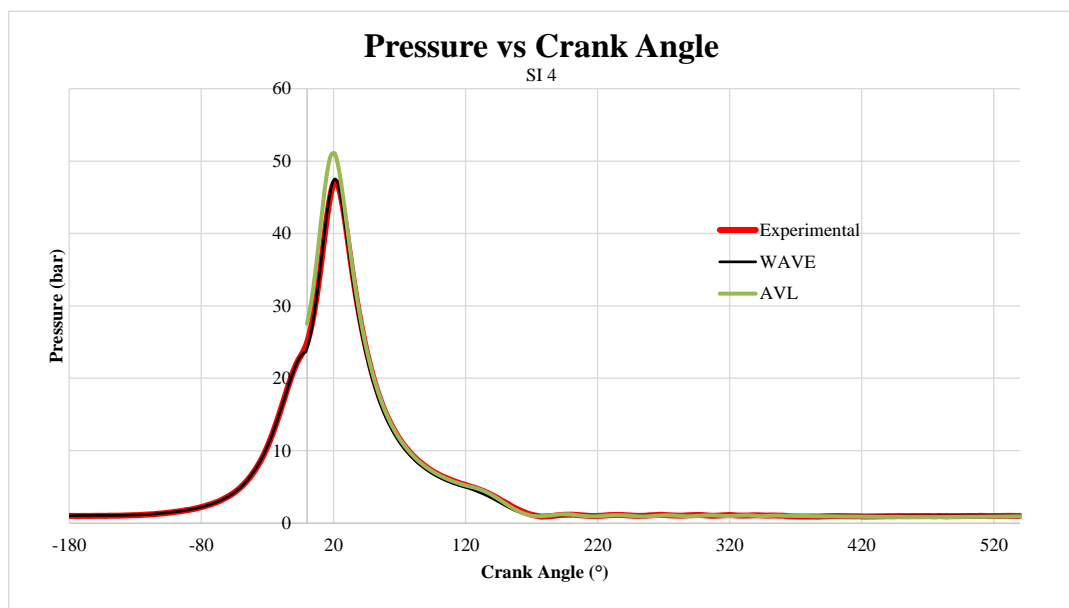
Figure 5-15 Cylinder Pressure SI 4 (AVL-WAVE-Experimental)
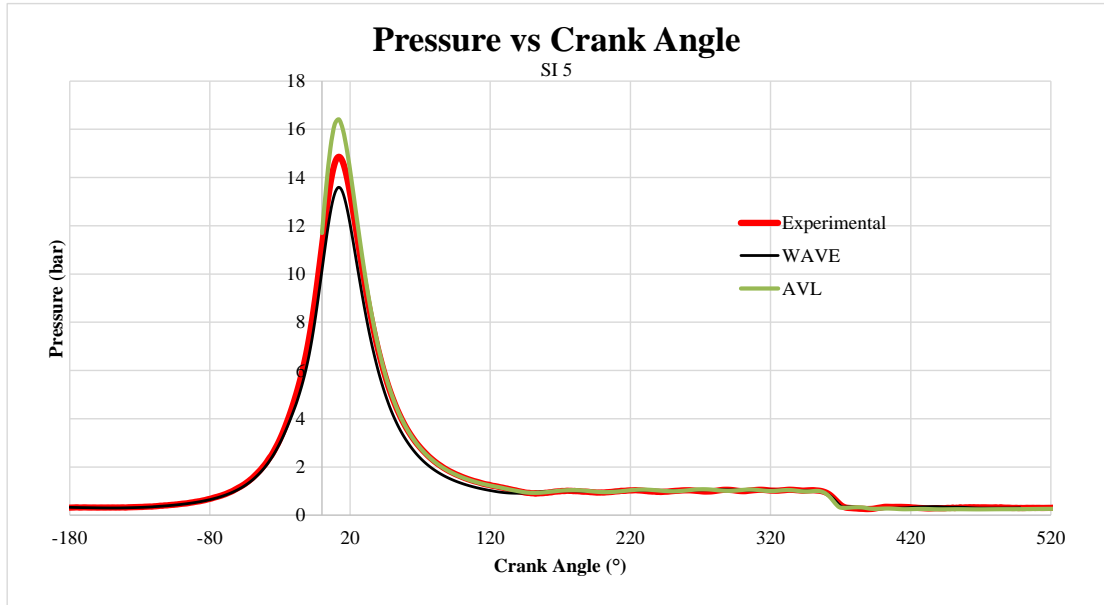
Figure 5-16 Cylinder Pressure SI 5 (AVL-WAVE-Experimental)
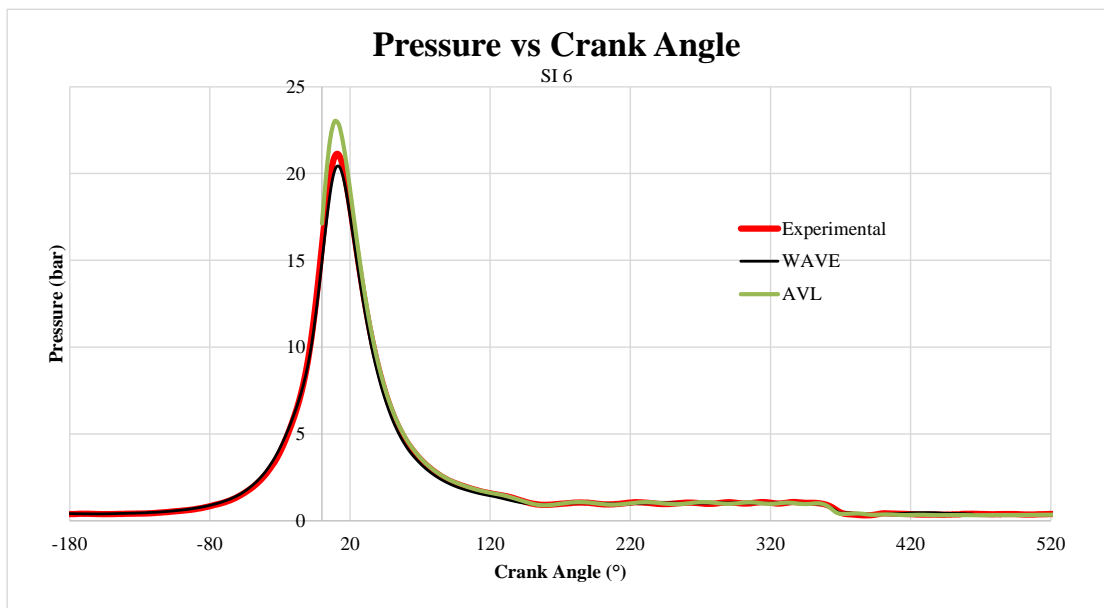
Figure 5-17 Cylinder Pressure SI 6 (AVL-WAVE-Experimental)
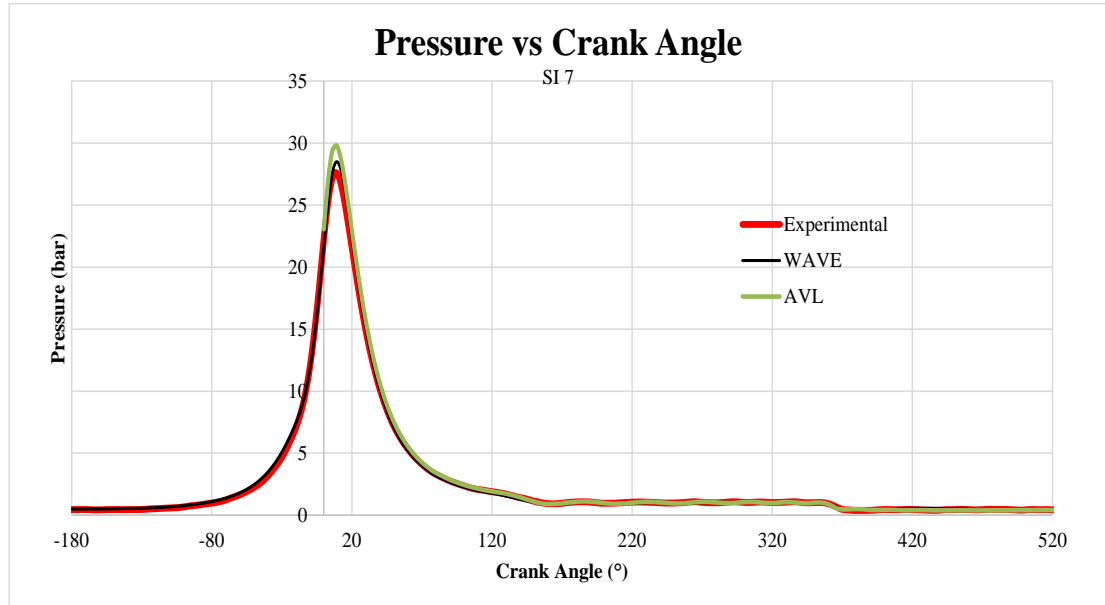
Figure 5-18 Cylinder Pressure SI 7 (AVL-WAVE-Experimental)

Finally, all the simulation and experimental results were gathered in one table to investigate the errors and accuracy of the prepared models. Table 5.5 is a comprehensive summary of experimental and simulation results which indicates the very beneficial and small errors that were gained from the simulation.

Table 5-3 Summary of Experimental and Modelling Results (a)

Condition	Case	Type	IMEP (bar)	Pmax (bar)	Pmax CAD (°)	Pmax CAD (°)
HCCI	1	Experiment	1.81	29.8	371	11
		AVL BOOST	1.8	31.75	370.46	10.46
		Ricardo WAVE	2.19	29.9	370.93	10.93
		Error AVL	-0.55%	6.54%	-0.15%	-4.91%
		Error WAVE	20.77%	0.34%	-0.02%	-0.64%
HCCI	2	Experiment	2.8	38.3	369.5	9.5
		AVL BOOST	2.8	40.74	368.79	8.79
		Ricardo WAVE	3.056	38.33	369.518	9.518
		Error AVL	0.00%	6.37%	-0.19%	-7.47%
		Error WAVE	9.14%	0.08%	0.00%	0.19%
HCCI	3	Experiment	3.48	40.2	372	12
		AVL BOOST	3.48	41.41	371.42	11.42
		Ricardo WAVE	3.75	39.72	371.97	11.79
		Error AVL	0.00%	3.01%	-0.16%	-4.83%
		Error WAVE	7.76%	-1.19%	-0.01%	-1.75%

Table 5-4 Summary of Experimental and Modelling Results (b)

Condition	Case	Type	IMEP (bar)	Pmax (bar)	Pmax CAD (°)	Pmax CAD (°)
SI	4	Experiment	10.04	47.2	382	22
		AVL BOOST	10.03	51.24	379.97	19.97
		Ricardo WAVE	9.586	47.54	381.31	21.31
		Error AVL	-0.10%	8.56%	-0.53%	-9.23%
		Error WAVE	-4.52%	0.72%	-0.18%	-3.14%
SI	5	Experiment	1.73	14.9	372.5	12.5
		AVL BOOST	1.73	16.43	371.17	11.17
		Ricardo WAVE	2.01	13.59	372	12
		Error AVL	0.00%	10.27%	-0.36%	-10.64%
		Error WAVE	16.18%	-8.79%	-0.13%	-4.00%
SI	6	Experiment	2.58	21.1	371.5	11.5
		AVL BOOST	2.58	23.06	370.15	1.15
		Ricardo WAVE	2.83	20.44	371.38	11.38
		Error AVL	0.00%	9.29%	-0.36%	-90.00%
		Error WAVE	10%	-3%	0%	-1%
SI	7	Experiment	3.25	27.6	369.5	9.5
		AVL BOOST	3.24	29.86	368.12	8.12
		Ricardo WAVE	3.52	28.49	369.30	9.30
		Error AVL	-0.31%	8.19%	-0.37%	-14.53%
		Error WAVE	8.18%	3.22%	-0.06%	-2.15%

5.9.2 Emission Improvements

Some relatively easy ways in AVL BOOST to reduce the emissions from the SI engine are to increase the valve overlap between the intake and exhaust valves and increase λ (excess air). For the HCCI engine, the inlet and exhaust valve timings were advanced and retarded by 3° respectively. Case 3 and Case 7 were chosen as the models were the closest to the experimental results.

NO_X and soot emissions are harmful to health and are known to cause long lasting respiratory issues. The NO_X emissions are a prime target and need to be reduced as much as possible. The formulation of NO_X occurs from three main factors, although most importantly from high combustion temperatures [23, 24].

Internal EGR is the trapping of residual gases within the cylinder through the use of valve overlap. Operating a retarded, standard and advanced IVO can affect the amount of cylinder residual gases, which can directly affect NO_X and soot emissions.

In order to reduce emissions, the associated effects of internal EGR were investigated. Since the prototype engine operated on a variable valve timing system (VVT), the manipulation of the intake valve opening was investigated within the permissible range. Changing the IVO was carried out for Cases 3 and 7, whilst maintaining a constant EVC time (Tables 5.6 and 5.7). To validate the emissions' model, the simulation NOx output was adjusted using the 'NOx kinetic multiplier' which was validated according to the experimental results at the initial valve timings. The NOx and soot were then recorded for each change in IVO. It must be noted that no validation for soot was conducted. From changing the IVO, only a negligible

change on IMEP and Pmax, 0.24 bar and 1.85 bar respectively (Tables 5.6 and 5.7) was found.

Table 5-5 HCCI Valve Timing and IMEP and Emission Improvements

		IVO (° bTDC)	EVC (° aTD)	IMEP (bar)	Internal EGR	Pmax (bar)	NOx (ppm)	NOx (g/kWh)	Soot (g/kWh)
Experiment		*-75*	*-75*	*3.48*	*-*	*40.2*	*66*	*0.36*	*-*
Improvements-HCCI 3	AVL- Emission	-55	-75	3.13	0.48	38.12	31.24	0.17	0.06
		-65	-75	3.42	0.46	40.65	57.49	0.31	0.05
		-75	*-75*	*3.47*	*0.45*	*41.10*	*64.51*	*0.35*	*0.05*
		-85	-75	3.42	0.45	40.85	63.91	0.34	0.05
		-95	-75	3.26	0.46	39.17	53.07	0.29	0.05
		-100	-75	3.15	0.47	38.91	45.95	0.28	0.05
HCCI 3	Wave- Emission-	WAVE prediction without any change					*396.4*		
		IVO+3°, EVO-3°					318.4		

Table 5-6 SI Valve Timing and IMEP and Emission Improvements

		IVO (° bTDC)	EVC (° aTD)	IMEP (bar)	Internal EGR	Pmax (bar)	NOx (ppm)	NOx (g/kWh)	Soot (g/kWh)
Experiment		*10*	*10*	*3.25*	*-*	*27.6*	*2656*	*9.03*	*-*
SI 7	AVL- Emission Improvements-	-20	10	3.3	0.09	28.24	2397	14.43	16.95
		-10	10	3.29	0.09	28.41	3029	14.97	17.05
		0	10	3.26	0.09	28.45	3086	15.41	17.17
		10	*10*	*3.26*	*0.12*	*28.91*	*2661*	*13.28*	*17.67*
		20	10	3.31	0.17	30.04	1677	8.21	18.41
		25	10	3.35	0.021	30.08	1178	5.96	18.63
SI 7	Wave- Emission-	WAVE prediction without any change					*3187*		
		By increasing valve overlap					2258		
		By increasing the λ by 0.02					2539		

From retarding the IVO, the amount of EGR is much greater from advancing it. Retarding the IVO increases the positive valve overlap, resulting in more residual gases; this is caused by the back flow of the exhaust originating from the pressure difference in the inlet/exhaust valve opening. The result is exhaust gas displacing fresh air entering the cylinder.

5.10 Conclusion

An engine model of a four-stroke compression ignition engine was developed and applied to study the engine's performance and emission characteristics with both

model and experimental conditions. The engine model was calibrated and then the pressure diagram and IMEP at these operating conditions were compared between the simulation and the experiments. In addition, some emission improvements were also applied in the model.

In addition, the mass fraction burned and heat release data have been successfully calculated. The experimental engine was successfully modelled in Ricardo WAVE and has been validated by comparing it to the experimental values. The IMEP, Pmax crank angle at Pmax all agree with the experimental results with an average error of 5%. A model was also created of a single case in AVL BOOST, and was calibrated, aligning pressure traces and matching the IMEP. In the future, for a more accurate model, more data from the engine such as geometry and temperatures could be used.

The main errors occurred for the peak pressure of the engine. This could be due to experimental condition differences, minute fuel variances, ambient temperatures and turbulent flows of gases into the cylinder and the flame propagation characteristics. Nonetheless, the HCCI and SI offer moderately accurate results which can be used to conduct emissions' tests.

In conclusion, the validation of an SI and HCCI engine has proven successful. The results produced are accurate and can be used to conduct further engine analysis. Evidently, HCCI engines are more optimised than SI engines at low loads, through producing lower emissions and permitting leaner AFR ratios. However, the combustion unpredictability need for variable valve timing and poor high load operation prevent the widespread application of the technology.

Poor results for the CI engine simulation have limited the analysis of the results, highlighting the limitations of AVL BOOST.

The NOx emissions can be significantly improved with only a low effect on performance by utilizing EGR in SI engines; however, it is important that soot is also managed. Improvements to HCCI emissions are not recommended and can be considered negligible due to their already low emission output.

Given the complexity of engines and the vast amount of trade-off, improving engines in certain aspects will have an opposite effect in others. This limits how much an engine can be improved before another aspect will become a hindrance.

Chapter 6 – Investigation into the Effect of Bore to Stroke Ratio on the Performance of a Single Cylinder Two-stroke Opposed Piston Engine

Most of this chapter was published in the PTNSS journal by the author of this thesis [22].

This chapter investigates opposed piston (OP) engines' promising fuel efficiency which has attracted the interest of the automotive industry in recent years. The opposed piston two-stroke (OP2S) engine technology heightens this fuel efficiency benefit and offers advances in structure, power density and thermal efficiency, whilst sustaining its lower cost and weight. Today, thermodynamic modelling remains an indispensable and cost-effective route in the development and optimisation of internal combustion engines (ICEs). To achieve this goal, the OP2S engine is simulated and validated against experimental results in AVL Boost™, which is hailed as one of the most reliable and advanced engine simulation tools. Detailed analyses of the piston dynamics, heat release, scavenging and heat transfers are highlighted in discrete sections of this paper. Having compared distinct heat release models, the Wiebe 2-Zone model emerged efficacious in replicating the heat release characteristics of the PAMAR™ engine. In comparing the numerical and experimental results, the simulation revealed minimal differences in peak pressure, peak temperature and maximum pressure raise rate, under ±2.5% differences for indicated power, IMEP, indicated thermal efficiency (ITE) and ISFC. Subsequently, the confidence taken from the validated numerical model is then deployed to investigate the effect of stroke-to-bore (S/B) ratio on OP2S performance. Three combinations of S/B ratios (0.5, 1.25, and 1.69) with identical swept volume are analysed in this study. Utilisation of the validated model ensured the standardisation of the intake, exhaust and the combustion systems in order to isolate the effects of the S/B ratio. Results indicate that heat losses decrease with increasing S/B ratio

because of the reduced surface area to volume in the cylinder. Consequently, an improvement in ITE and mechanical efficiency is observed with reduced ISFC for higher B/S ratios. A tendency of an upsurge in combustion efficiency is also evident for higher B/S ratios, due to reduced heat transfer near the minimum volume of the combustion chamber.

6.1 Introduction

The automotive industry has faced unprecedented challenges due to its high energy consumption and pollutant emissions over the past few decades. With soaring demand for high-efficiency and emissions-compliant powertrains for ordinary and industrial applications, substantiation of radical advances in reciprocating engine technology has proved indispensable [14, 25].

Superior thermodynamic properties and the improvement of designs that have surpassed the impediments of previous implementations are the pivotal factors that have encouraged the renaissance of OP engines. The fundamental thermal efficiency of the OP engine, besides its low emissions, compact packaging and low manufacturing costs comparative to four-stroke engines, make it a substantial candidate for future commercial and passenger vehicles [12, 15].

In addition, modern computational tools, fuel system advancements (high pressure common rail) and the electronic control technology of ICEs have paved the way for successful modernisation of OP engines [26].

6.2 Aims and Objectives

The main aim of this chapter is to gain a comprehensive understanding of the software AVL BOOSTt and create a 1D thermodynamic model of the PAMAR™ OP2S engine. A detailed numerical simulation of the 1.00 l single cylinder research engine is executed and validated against existing experimental data. A distinct predictive Vibe combustion model in AVL BOOST was investigated and then the effect of the bore to stroke ratio on the wall heat losses of the OP2S engine's efficiency and fuel consumption were studied.

6.3 Opposed Piston Engine Numerical Modelling in AVL BOOST
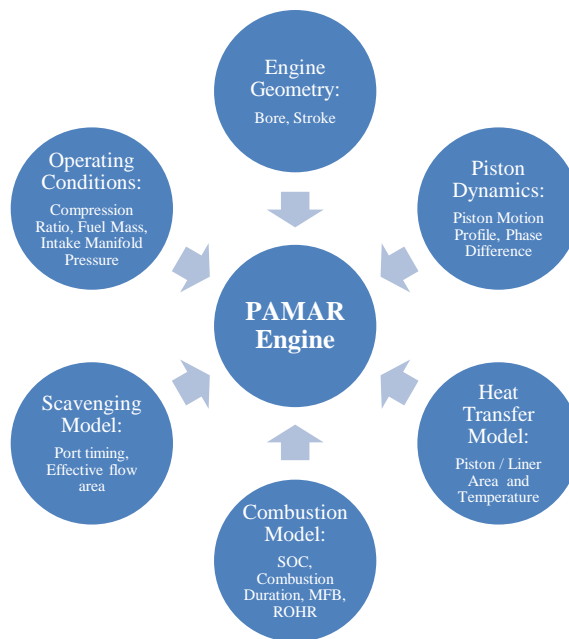
Figure 6-1 Numerical Methodology

Nowadays, thermodynamic modelling has become an integral process in the development and optimisation of ICEs [27]. It is a broad and fertile research area, considering the variety of analytical techniques present. As a result, laboratories and

automotive stakeholders have produced their own thermodynamic models with a degree of complexity, scope and ease of use. Although, most of the processes in the engine are 3D, often 1D simulations are deployed to compromise for complexity and time constraints [28]. When it comes to numerical modelling of ICEs, there are three major 1D engine simulation computer programs, namely GT Power, AVL BOOST and Ricardo WAVE. Unfortunately, none of them has a built-in module capable of simulating an opposed piston (OP) engine. However, AVL BOOST is the beneficial due its compatibility of defining the relative piston motion profile, thus enabling the modelling of the OP configuration [14]. Furthermore, it provides advanced options in terms of design, cycle simulation and heat release models, compared to other industrial modelling platforms. Although numerous OP2S concepts have been universally modelled and examined by researchers in the recent past, only a limited number of journals have exposed experimental data from fully developed engines. The prime focus has been vastly restricted to basic engine performance, as comprehensive analysis of intricate engine operations (in-cylinder gas motion/mixture formation) proves to be challenging [8]. As mentioned previously, Diesel RK is the only known 0D simulation software that has built in features to model the OP configuration. Unlike AVL BOOST, its degree of flexibility in widespread modelling of an engine is limited. Simulating a flawless model of an OP engine proved to be quite challenging at the initial stages of this project. Finally, three simplified models were addressed as shown in the figures below.
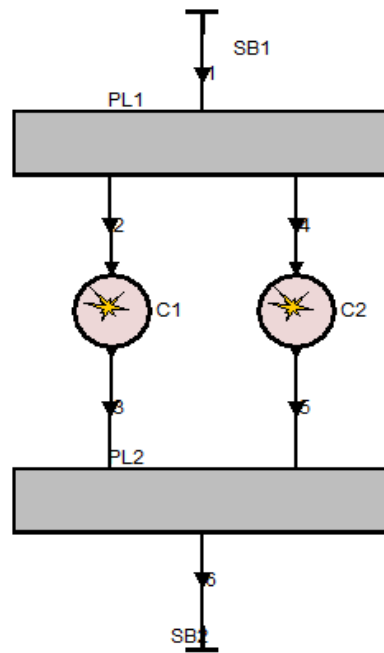
Figure 6-2 Conventional Two-Cylinder Model
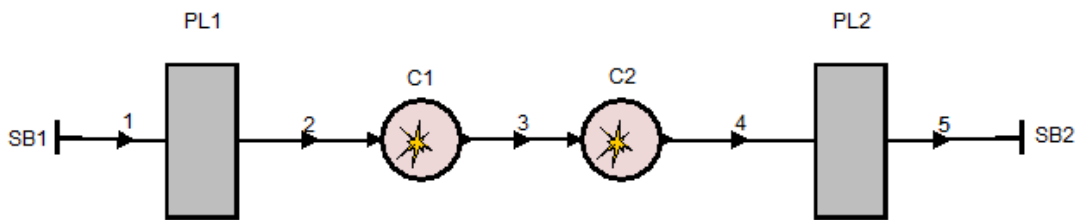
Figure 6-3 Two-Cylinder Model Coupled via Pipe Attachment
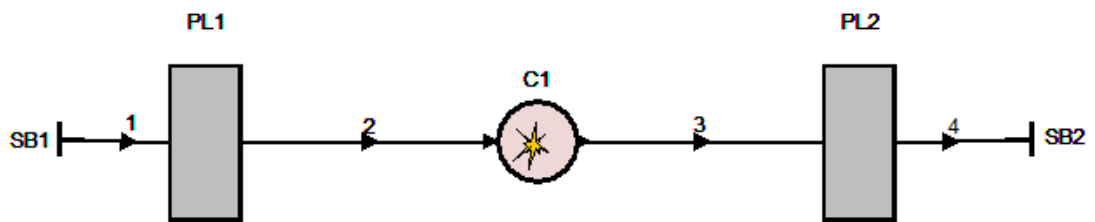
Figure 6-4 Single-Cylinder Model

Even though all three models proved successful in simulating an OP configuration, the first two layouts were problematic in a thermodynamic sense. After numerous iterations and fine-tuning, layout 3 revealed the most accurate representation of an OP2S engine.

The first OP engine layout was proposed as such to simulate the intake and exhaust piston motion separately; hence the two-cylinder arrangement. Although, this layout produced results with an acceptable range of uncertainty, the principle theory of two pistons operating in a single cylinder is contradicted. Additionally, due to the two-cylinder layout, two sets of intake and exhaust ports were defined, as opposed to a single set of intake and exhaust ports in a conventional OP engine. Consequently, a substantial discrepancy in cylinder pressure was observed.

Subsequently, the second OP layout was suggested to eliminate such inconsistencies in in-cylinder pressure by attaching both cylinders through a pipe. Ideally, the pipe attachment between the cylinders must be open throughout the two-stroke cycle to generate a unified combustion chamber. Unfortunately, AVL BOOST doesn't tolerate such open-ended connection during the combustion phase, forcing the pipe connection between the cylinders to be mandatorily closed. Progressing to the thermodynamic analysis of this layout, divergence in the wall heat flow and performance parameters (IMEP, HRR, peak pressure and temperature) was apparent.

6.3.1 Engine Cycle Simulation

AVL BOOST version 2014.1 is used for this modelling project. The main tool used in the software was the *Workspace* (the graphical user interface), which is composed of predefined elements that represent components of an ICE. The 1D

engine model is built within the workspace, selecting various elements from the element tree and is joined by pipe attachments to their desired connectors.

The numerical model created to represent the PAMAR single cylinder OP2S engine is shown in Figure 6.6. Figure 6.6 displays a schematic of the input data needed to implement a 1D simulation of OP2S in AVL BOOST. Cylinder geometry, port timings, operating and initial conditions are identical to what exists in the actual engine. Piston motion, heat release, heat transfer and scavenging models are aligned accordingly to reproduce the heat release characteristics of the PAMAR engine and are discussed inclusively in the following sections. Factors that influence in-cylinder combustion characteristics like the piston bowl shape, injector technology, rail pressure and EGR capability are not reflected here as these are beyond the scope of this chapter.
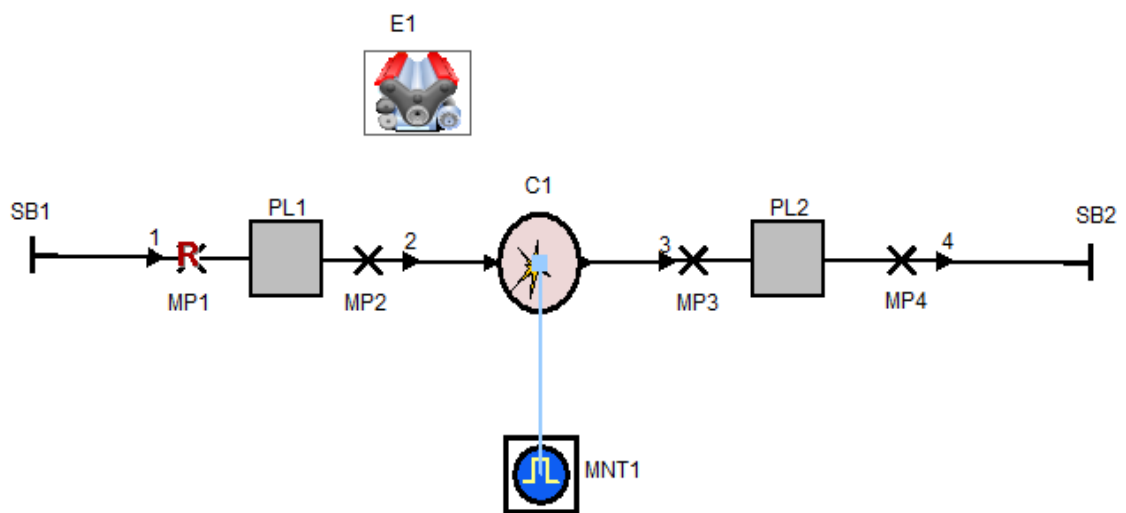
Figure 6-5 AVL Model

6.3.2 Piston Dynamic Model

Due to the presence of phase difference in the piston motion, both pistons do not arrive at their respective IDCs in harmony. Given the phase differences φ, the piston displacements are calculated as described in [25].

$$X_{in} = \left(1 - \cos\left(\alpha - \frac{\varphi}{2}\right) + \frac{1}{2}\lambda\,sin^2\left(\alpha - \frac{\varphi}{2}\right)\right), \qquad \textbf{Eq 6.1}$$

$$X_{ex} = r\left(1 - \cos\left(\alpha + \frac{\varphi}{2}\right) + \frac{1}{2}\lambda\,sin^2\left(\alpha + \frac{\varphi}{2}\right)\right), \qquad \textbf{Eq 6.2}$$

where:

X_{in}: Displacement of the intake piston

X_{ex}: Displacement of the exhaust piston

r: Crank radius

α: Equivalent crank angle

φ: Phase differences

$\lambda = \frac{r}{l}$: Ratio of crank radius to connecting rod

l: Length of the connecting rod

Intake and exhaust pistons move towards each other face-to-face. However, the optional user defined piston motion in AVL BOOST only allows the user to input a relative position of the piston motion profile. The connecting rod length of the engine is not specified in Naik et al. [26]. It is assumed that the connecting rod length is much greater than the crank radius. As $l \ggg r$, $\lambda\lambda$ tends to an infinitesimal

value, causing the latter part of the piston motion equation to become insignificant [16]. The relative displacement of the piston is indicated by the following equation:

$$X_{relative} = r\left(1 - \cos\left(\alpha - \frac{\varphi}{2}\right)\right) + \left(1 - \cos\left(\alpha + \frac{\varphi}{2}\right)\right) \quad \textbf{Eq 6.3}$$

Ma et al. [25] demonstrates that with an increasing piston motion difference, from 0ºCAD to 18ºCAD, the delivery ratio and scavenging efficiency increases progressively. However, the trapping efficiency increases initially and then declines after it achieves optimum efficiency at 15ºCA, so it does the indicated work. Henceforth, 15º is assumed for the phase difference in our simulation. The phase difference also affects the maximum and minimum value of the cylinder volume [25]. As the phase difference increases, the minimum distance between the pistons at IDC increases and the maximum distance at ODC decreases. Consequently, the compression ratio (CR) is adversely affected.

6.4 Effect of Bore to Stroke Ratio on OP2S Engine Performance

The inquiry that this part of the chapter attempts to answer is how do changes in the bore to stroke (B/S) ratio of an OP2S engine influence efficiency, fuel consumption and wall heat losses. The analysis was carried out on nine combinations of bore and stroke to be contrived to yield a common swept volume of one litre with B/S ratios as follows in Table 6.2.

Table 6-1 Specification for Bore to Stroke Ratio Investigation

Engine Specification								
Bore to Stroke Ratio	0.25	0.5	0.75	1	1.25	1.35	1.69	1.89	2.4
Bore (mm)	68.5	86	99	108.5	117	120	129	134	145
Stroke (mm)	274	172	132	108.5	93.6	88.42	76.5	71	60.6
Bore Surface Area (mm^2)	3685.28	5808.8	7697.69	9245.9	10751.32	11309.73	13069.81	14102.61	16513
Clearance height (mm)	19.29	12.24	9.24	7.69	6.61	6.29	5.44	5.04	4.30
2 x Piston Head Linear Area @ TDC	7370.57	11617	15395.37	18492	21503	22619.4	26139.62	28205.22	33026
	4152.21	3307.2	2873	2621.4	2431	2370.22	2204.86	2122.58	1962

In order to isolate the effect of the B/S ratio, the simulations were executed with a similar heat release rate (HRR) between the combinations. This is achieved by adapting the OP2S numerical model validated in the previous section. By this means, the intake, exhaust and combustion systems are standardised. Thus, the effects of the B/S ratio investigated are independent of the combustion system itself. Scavenging characteristics, heat transfer model, effective flow area and other operating conditions of the validated model were kept the same. A mutual piston motion profile is deployed across the B/S combinations to ensure the rate of change of volume in the cylinder is conserved Sandu et al. [29]. The assumption of flat piston head is incorporated in the analysis. The tabulated results below show negligible

differences in peak cylinder pressure, temperature and MPRR; ensuring that heat release characteristics for the combination of B/S ratios remain the same.

6.5 Results and Discussion

Results from the modelling of the engine are presented in below sections.

6.5.1 Indicated and Brake Mean Effective Pressure

Results of the IMEP from Figures 6.7 and 6.8 indicate that increasing the B/S ratio slightly increases the mean effective pressure and it has the same trend as the BMEP.
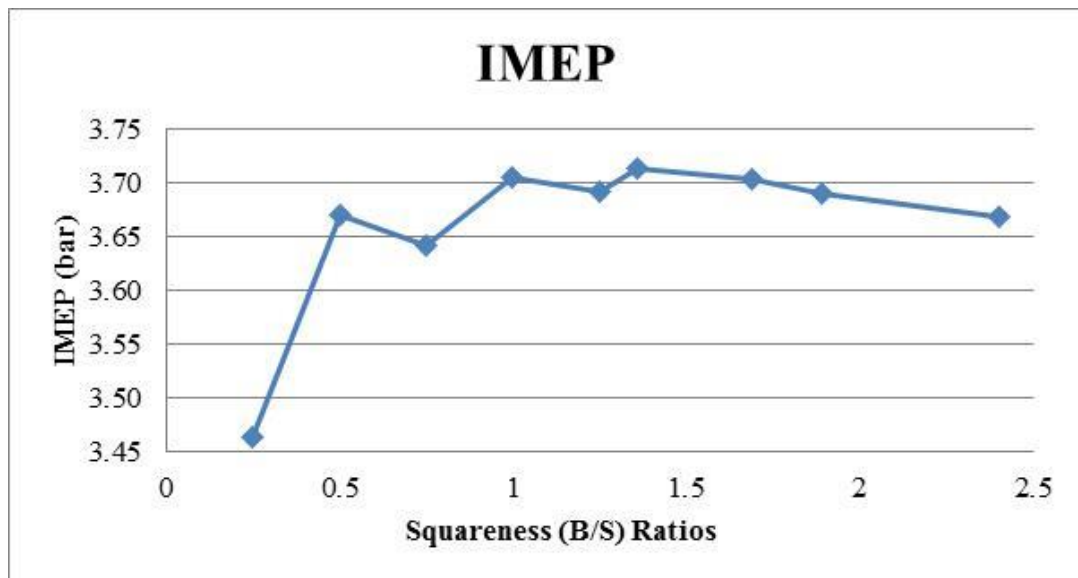
Figure 6-6 Effect of B/S Ratio on IMEP
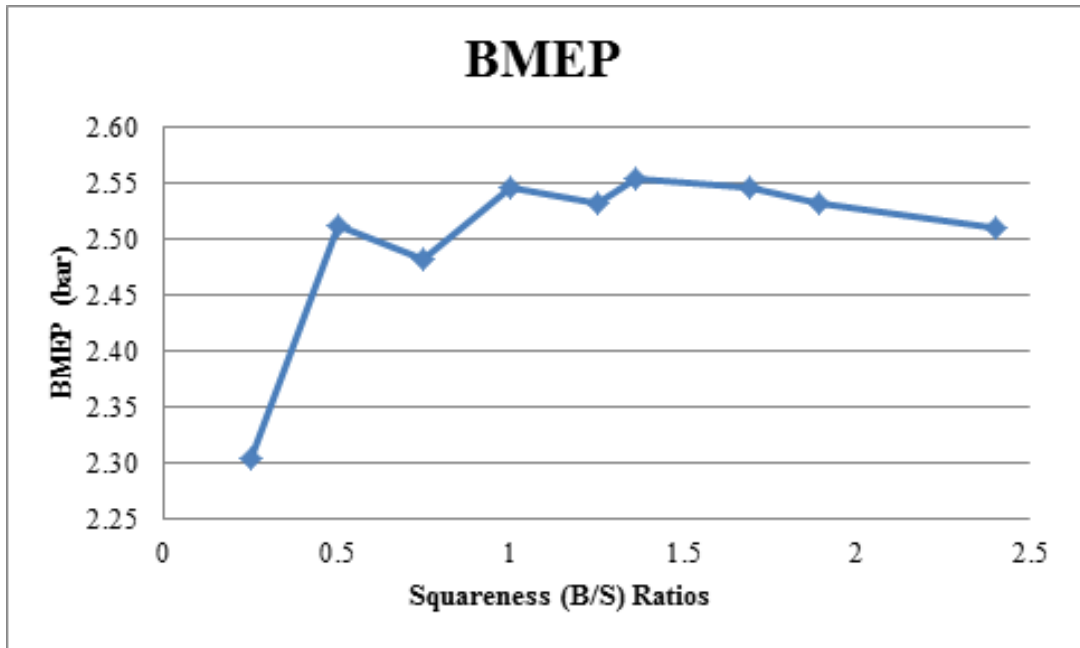
Figure 6-7 Effect of B/S Ratio on BMEP

6.5.2 Fuel Consumption

Indicated specific fuel consumption (ISFC) will increase by improving the bore to stroke ratio from 0.25 to 1; in contrast, by increasing the ratio, fuel consumption increases. Brake specific fuel consumption has the same trend as ISCF; both are shown in Figures 6.9 and 6.10.
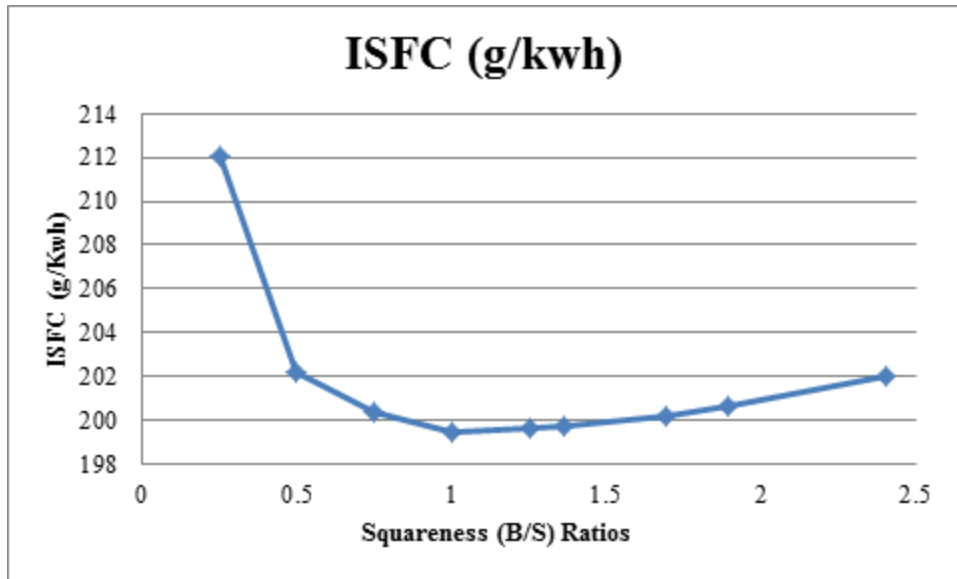
Figure 6-8 Effect of B/S Ratio on ISCF
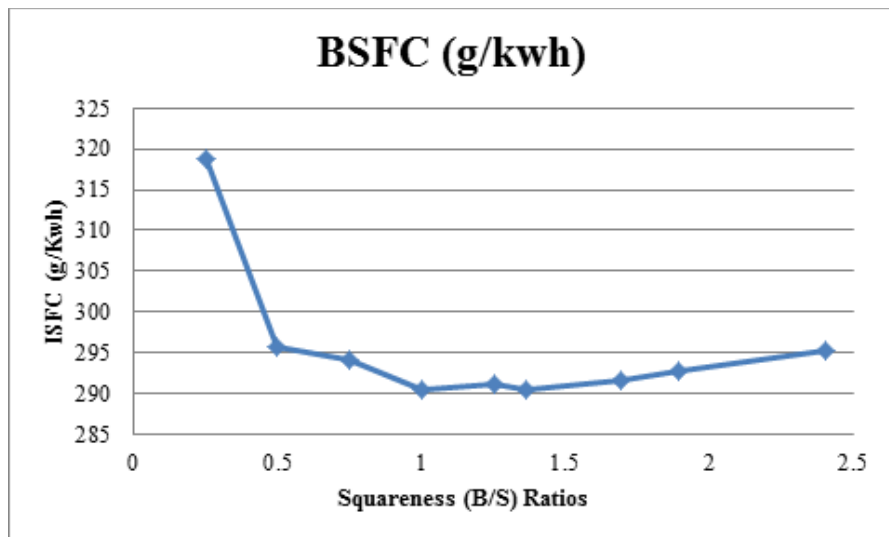
Figure 6-9 Effect of B/S Ratio on BSCF

6.5.3 Total Wall Heat Loss

Total wall heat flow defines heat rejected to the entire surface of the combustion chamber (piston and liner). As seen in Figure 6.11, in-cylinder heat losses are largest for the highest B/S ratio. A general trend of increase in heat loss is evident with increasing bore size (i.e. increasing B/S) as the piston area available to dissipate the

heat is reduced. The decrease in combustion chamber surface area to volume ratio with increasing B/S is seen as the predominant factor in such a trend [25]. With different combinations of B/S, similar temperature expansion occurs over a higher surface area for higher B/S ratios, hence the reduced heat loss [30, 31]. Wall heat losses increase with the engine cycle progressing into the expansion stroke, as burnt gasses are exposed to a greater surface area. It is apparent that maximum heat loss occurs at the very end of the combustion process. This is an indication of enhanced combustion efficiency, attributed towards the OP configuration. It is also to be noted from Figure 6.11 that the peak is at the minimum volume of the combustion chamber.
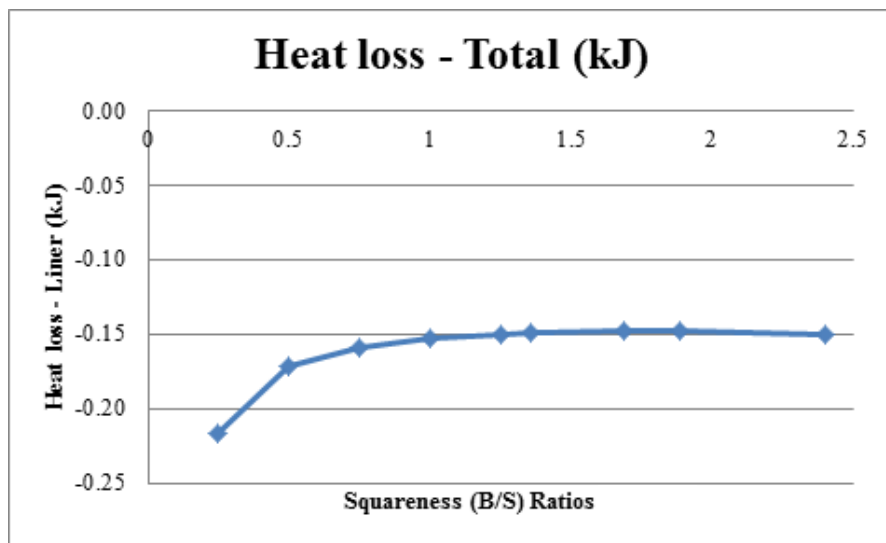
Figure 6-10 Effect of B/S Ratio on Wall Heat Loss

6.5.4 Efficiency

The decrease in heat transfer reduces the heat rejected to the coolant, consequently leading to an increase in indicated thermal efficiency (ITE), as illustrated in Figure 6.12. The change in ITE gets progressively better with increasing the S/B ratio overall; the trend is non-linear. There is a steep increase in

ITE from B/S ratio 0.5 to 1, which is shown in Figure 6.12. Mechanical Efficiency

has almost the same trend as the indicated thermal efficiency which is depicted in

Figure 6.13.
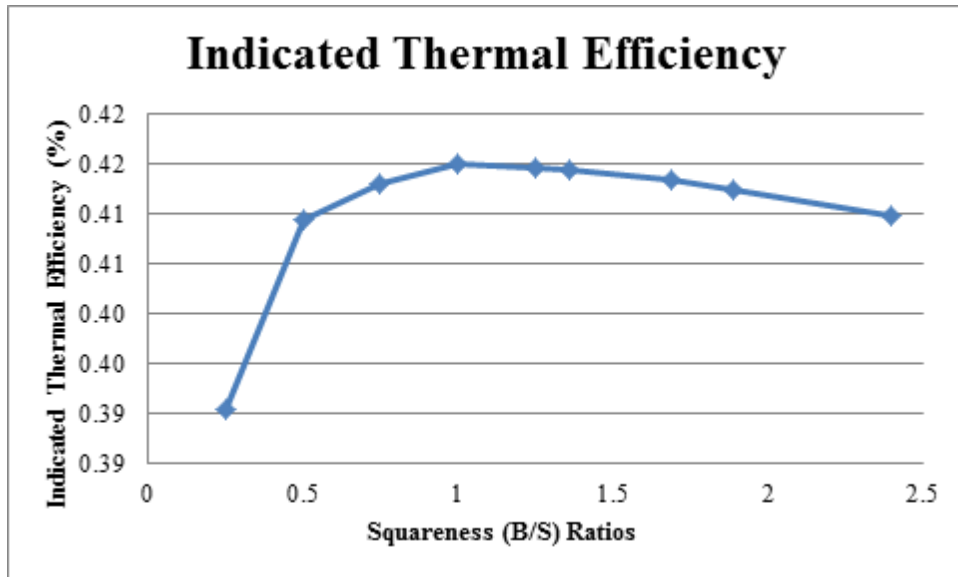
Figure 6-11 Effect of B/S Ratio on Indicated Thermal Efficiency
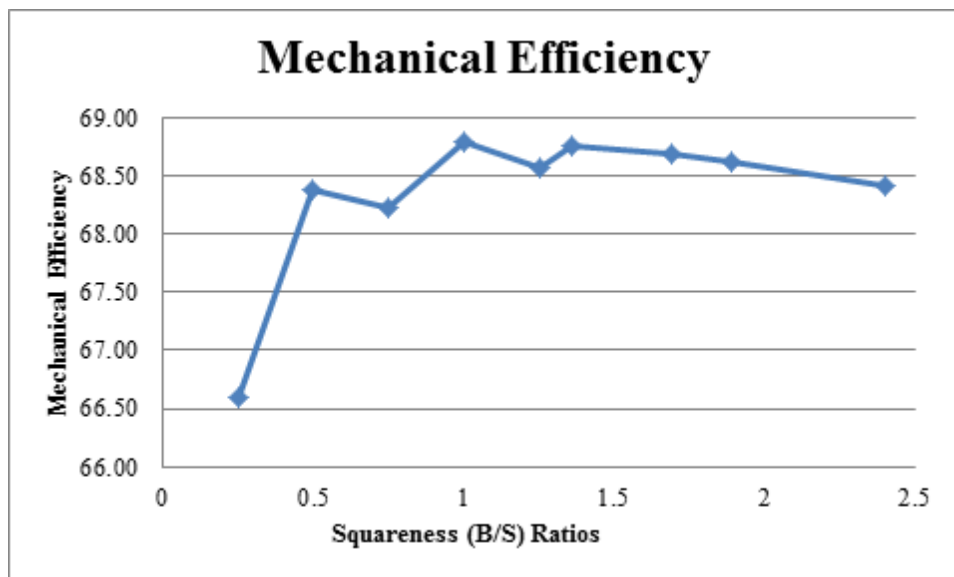
Figure 6-12 Effect of B/S Ratio on Mechanical Efficiency

6.6 Conclusion

A brief history of the dawn of OP engines and their enduring research progress in the 21st century has been described. A comprehensive 1D thermodynamic modelling of the PAMAR™ single cylinder engine was performed in AVL BOOST to demonstrate its fundamental engine performance. The Wiebe, Wiebe 2-Zone and Double Wiebe heat release models were independently analysed. When it comes to compression ignition like combustion, Double Wiebe is the obvious choice in AVL BOOST. However, a lack of information on fuel allotment produced unreliable results. The Wiebe 2-Zone model unveiled its robustness over Wiebe and Double Wiebe models, with its utilisation to validate the OP2S engine. With great confidence taken from the validation, nine different B/S combinations of the OP2S engine for the same swept volume were investigated. The main conclusions of this analysis were that the heat losses increase with increasing B/S ratio; due to the lower surface area to volume exposed; an increase in ITE and mechanical efficiency was observed with increasing B/S ratios; and improvement in fuel consumption is evident with increasing B/S ratio. Higher B/S ratio is desirable for applications that require better fuel efficiency.

Chapter 7 – Evaluation of the Effect of Variable Compression Ratios' Performance on Opposed Piston 2-stroke Engine

This chapter was mostly published in one issue of the PTNSS journal [32].

In the course of recent decades, the automotive industry has confronted exceptional difficulties and challenges due to its pollutant emissions and high-energy consumption. As a result of this, a substantiation of radical advances in responding motor innovation has been demonstrated as essential. The opposed piston two-stroke engine (OP2S) was first developed in the late 1800s. A keen and rapid development was noted in the first half of the 20th century across many countries for wide range of applications; and its promising fuel efficiency attracted the interest of the automotive industry. Unfortunately, severe regulations on emissions led to a discontinuance of OP2S engines despite their high-efficiency.

The aim of this chapter is to model and simulate a simple single-cylinder two-stroke opposed piston engine and investigate the effect of variable compression ratio (VCR) on an OP2S engine's performance, using the software programme AVL BOOST. This is fully integrated IC engine simulation software; henceforth, it was ideal to use AVL BOOST to model, simulate and analyse the performance of a two-stroke opposed piston engine by changing desired parameters.

In order to meet this aim, the experimental results from a unique engine are used to make a comparison with the results obtained from the AVL BOOST model. A validation of this comparison will be produced looking at the six different compression ratios ranging from 12 to 20, with two different engine speeds– 420 rpm and 1500 rpm.

A comparison between the two engine speeds with increasing combinations of compression ratios revealed the following for the 1500 rpm simulation: higher peak

pressure; higher peak temperature; reduction in heat loss; and higher mechanical efficiency. Detailed analyses of these parameters are highlighted in discrete sections of this chapter.

7.1 Introduction

The Achates Power Opposed-Piston Two-Stroke Engine: Performance and Emissions Results in a Medium-Duty Application [33] states that, "Historically, all types of engines have faced a number of technical challenges related to emissions, fuel efficiency, cost and durability". An asymmetric motion of pistons means that the opposed piston (OP) configuration acquires an exceptional engine balance.

According to the book, Opposed Piston Engines: Evolution, Use, and Future Applications [7], "OP engines evolved because of their ease of manufacture, excellent balance, and competitive performance and fuel efficiency relative to comparable four-stroke engines With the progressive development of OP engines other significant advantages also emerged Among these advantages were cutting-edge specific output, high specific torque, very high power density, and very high power-to-bulk ratio." The fundamental thermal efficiency of an OP engine as well as its low emissions, compactness and low manufacturing costs make it a substantial candidate for future commercial and passenger vehicles.

The OP2S engines are capable of very high efficiency, low weight and a compact envelope. These engines are being developed by a team at Warsaw University of Technology (WUT) and we have cooperated with this team on thermodynamic modelling of these engines in AVL Boost. The engine is a 100 kW range extender

duty in vehicles for the purpose of quick recharging and/or backup power when batteries run flat.

Most recently, WUT is developing a new type of barrel engine called PAMAR-4 under a Polish-Norwegian research programme. This is iteration is from a successor of PAMAR-3, which was a 3.0 l, 340 kw engine built for the purposes of aviation. PAMAR 3 was a huge success mainly due to an eight-cylinder barrel engine. Counter-rotating cylinder groups and a crankshaft provide cancellation of torque reactions and gyroscopic forces during engine speed fluctuations and vehicle manoeuvres. Some of the advantages of a barrel engine are as follows: simple technology; less parts required, hence low weight; axial symmetry; low vibration level; and high-power concentration. PAMAR-3 accomplished a test bench efficiency of 44% and has successfully functioned on LPG, propane, alcohol, CNG, gasoline and diesel fuels. One of the many reasons for the great output of the PAMAR-3 engine was due to an OP2S engine which meant unnecessary strokes were eliminated; uni flow scavenging; and no valve train. In addition, the elimination of a crankshaft reduced piston side thrust. All of these factors led to an increased ME, henceforth increased engine efficiency. Another reason for the great output of the PAMAR-3 engine is due to its axial symmetry of its cooling system–keeping a constant thermal condition in all cylinders and inlet and exhaust axial symmetry keeping a constant volumetric efficiency and equivalence ratio in all cylinders. Consequently, equal work of the cylinders and thus homogeneous charge compression ignition (HCCI) at the whole range of loads. The manufacturing cost of the PAMAR-3 engine was reduced by an incredible 40%. Opaliński et al. [16] refers

to a comparison of the gas-dynamics of this engine, which has been modelled and quantified using Ricardo WAVE (1D) and ANSYS Fluent (3D CFD).

7.2 Aims and Objectives

The overall aim of this project is to model and simulate a simple single-cylinder two-stroke opposed piston engine and investigate the effect of a variable compression ratio (VCR) on the OP2S engine's performance, using the software programme AVL BOOST. In addition, the effect of the variable compression ratio (VCR) was analysed for two engine speeds 420 rpm and 1500 rpm.

In order to meet this aim, the experimental results from the PAMAR series engine will be used to make a comparison with the AVL BOOST model. A validation of this comparison will be produced looking at the following parameters: IMEP (indicated mean effective pressure); peak pressure; peak temperature; ISFC (indicated specific fuel consumption); BSFC (brake specific fuel consumption); volumetric efficiency; and mechanical efficiency.

7.3 Overview of PAMAR Engine

A research team at WUT in Poland has been developing a modern car engine, called the PAMAR, under the management of Dr. Pawel Mazuro. Having collaborated with the research team, some experimental data from the PAMAR series engine were obtained and used for the modelling process of the investigation in this chapter.

The PAMAR engine is equipped with a uniflow scavenging system with an injector on its cylinder liner. Gas ports are positioned on either end of the cylinder;

intake ports to deliver fresh charge into the cylinder from one side, and exhaust ports on the other side to get rid of the burnt gas as well as residuals. The piston motion controls the opening and closing of these ports. Two pistons are deployed at opposite ends of the cylinder liner, intake and exhaust pistons, respective to their effective control of port opening and closing during the scavenging process. A combustion chamber is formed at inner dead centre (IDC), i.e. at the point of minimum distance between the pistons. Outer dead centre (ODC) is defined when the distance between two pistons is at a maximum.

7.4 Opposed Piston Two-stroke Engine Working Cycle

A completion of the OP2S cycle is indicated by every crankshaft revolution. The compression stroke begins at ODC, i.e. when the pistons entirely cover the intake and exhaust ports, and ends once the piston reaches IDC. At the end of the compression stroke, fuel is injected at high pressure, just before the pistons reach IDC. Subsequently, fuel is atomised, evaporated and burned in the high-pressure, high-temperature environment produced by the in-cylinder air which is then followed by the expansion stroke.

The expansion stroke is induced due to the prompt increase in pressure and temperature as a result of fuel combustion, causing the pistons to move from IDC to ODC. Near the end of the expansion stroke, exhaust ports are open to allow burnt gases to discharge with the aid of residual gas pressure. Moments later, the intake ports are opened, allowing the fresh charge to enter the cylinder and driving the exhaust gas out of the cylinder, simultaneously. At this instant, the in-cylinder pressure is lower than atmospheric pressure.

The scavenging process is vital as it comprises of both forcing the exhaust gas out of and admitting fresh charge into the cylinder. Intake and exhaust ports remain open at the start of the compression stroke; therefore, the scavenging process begins from the instant the ports are uncovered during the expansion stroke, and continues until they are completely closed again.

7.5 Methodology of AVL BOOST Modelling

AVL BOOST™ is fully integrated IC engine simulation software. It delivers advanced models enabling accurate prediction of engine performance, tailpipe emissions and acoustics. The flexible AVL BOOST™ 3D-approach to simulate linear acoustics delivers highly accurate solutions even in high frequency ranges. AVL BOOST™ offers proven methodologies, combined with know-how, skills and experience embedded in an easy-to-use, functional and powerful software solution.

Some of the advantages of using AVL BOOST are as follows: easy and fast model set-up, shortest simulation times ideal for integration in both concept and detailed design phase; empirical and physical models for speed and accuracy; reliable and accurate simulation of steady and transient engine performance parameters; and excellent software and engineering support. The interactive pre-processor in BOOST facilitates the user to model a one-dimensional engine test bench set-up using predefined elements provided in the AVL Workspace Graphical User Interface.

Henceforth, it was ideal to use AVL BOOST to model, simulate and analyse the performance of a two-stroke opposed piston engine by changing desired parameters.

The purpose of the project was to model an OP2S engine in AVL BOOST and investigate the effect of variable compression ratio to enhance engine performance.

7.5.1 Numerical Modelling of Engines

There are three major 1D engine simulation computer programs when it comes to numerical modelling of ICEs, namely GT-POWER, Ricardo WAVE, and AVL BOOST. Unfortunately, since OP engines are unique, none of them has a built-in module capable of simulating an OP engine. AVL BOOST is the favourite of the above-mentioned, due to its compatibility of defining a relative piston motion profile, thus enabling the modelling of the OP configuration. In addition, AVL BOOST provides the option of advanced engine simulations in terms of cycle simulation, design and predictive combustion models, in comparison to other industrial modelling platforms.

7.5.2 Opposed Piston Configuration in AVL BOOST

As mentioned previously, AVL BOOST has no built-in module capable of simulating an OP engine. Thus, simulating a flawless model of an OP engine proved challenging at the initial stages of this project and some difficulties were encountered during the process of modelling. So, a simple single-cylinder two-stroke opposed piston engine shown in Figure 7.1 was modelled.
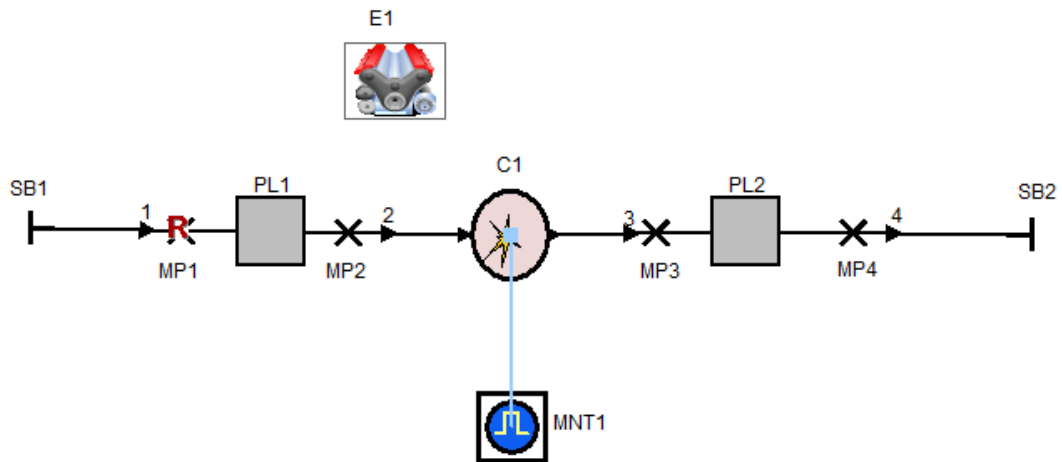
Figure 7-1 AVL Model

7.5.3 Engine Cycle Simulation

The main tool used in AVL BOOST software is Workspace (graphical user interface), which is composed of predefined elements that represent components of the ICE. The 1D engine model is built within the workspace by selecting various elements from the element tree. They are joined by pipe attachments to their desired connectors. Table 7.1 list all the elements, as well as the quantity, used to create an OP configuration in AVL BOOST.

Table 7-1 Elements Used to Create OP Configuration in AVL BOOST

Element	Symbol	Quantity
Engine	E	1
System Boundary	SB	2
Measuring Point	MP	4
Monitor	MNT	1
Plenum	PL	2
Cylinder	C	1
Pipe	-	4

Since an OP is a unique engine, a cylinder with a plenum on either side of the cylinder was modelled to create an OP configuration in AVL BOOST. The screenshot of the model in AVL BOOST is represented in Figure 7.1.

7.6 Constraints Defined in AVL BOOST

Having designed the model in AVL BOOST, the data collected from the PAMAR series engine were then entered into the computer software.

Certain constraints, such as crank radius, con-rod length, bore and stroke were collected from the PAMAR. These values are listed in Table 7.2. Using these constraints, other parameters such as squareness, bore surface area and swept volume were calculated, which are also presented in Table 7.2. Although a piston stroke length of 150 mm was required, the con-rod length was defined as 300 mm (twice the stroke) in order for the software to assume it is an OP engine.

Table 7-2 Engine Geometry in AVL BOOST

Defined Parameters	
Crank Radius	75 mm
Con-rod Length	300 mm
Bore	55 mm
Stroke	150 mm
Bore Surface Area	2376 mm^2
Swept Volume	356374 mm^3

7.6.1 Phase Difference

Phase difference was a vital variable in this investigation. It affects the minimum and maximum value of the cylinder volume. As the phase difference increases, the minimum distance between the pistons at IDC increases, thus reducing the maximum distance at ODC. Consequently, *compression ratio* is adversely affected.

According to Fukang Ma et al. [25], with increasing piston motion difference, from 0° to 18°, delivery ratio and scavenging efficiency increases progressively throughout. On the other hand, trapping efficiency initially increases and then decreases after it achieves optimum efficiency at 15° and so does the indicated work. As a result, 15° was decided upon as the phase difference. The intake port and exhaust port dimensions were collected from the PAMAR series engine and are listed in Table 7.3.

Table 7-3 PAMAR Engine Intake and Exhaust Ports' Specification

	Intake Port	Exhaust Port
Height (mm)	20	2.5
Width (mm)	6.4	6.4
Number of holes	24	18
Maximum Flow Area (mm^2)	3072	2880
Phase Difference (°)	0	15

7.6.2 Piston Dynamic Model

Since AVL BOOST has no built-in module capable of simulating an OP engine, the piston motion was user defined. Due to a phase difference in piston motion on both pistons, the two pistons are out of alignment, thus non-harmonic (i.e. do not reach IDC in harmony). Having decided upon a value for the phase difference (φ), the piston displacements were calculated using the following equations [25]:

$$X_{in} = \left(1 - \cos\left(\alpha - \frac{\varphi}{2}\right) + \frac{1}{2}\lambda \sin^2\left(\alpha - \frac{\varphi}{2}\right)\right) \qquad \textbf{Eq 7.1}$$

$$X_{ex} = r\left(1 - \cos\left(\alpha + \frac{\varphi}{2}\right) + \frac{1}{2}\lambda \sin^2\left(\alpha + \frac{\varphi}{2}\right)\right) \qquad \textbf{Eq 7.2}$$

Where:

X_{in}: Displacement of the intake piston (mm)

X_{ex}: Displacement of the exhaust piston (mm)

r: Crank radius (mm)

α: Equivalent crank angle (degree)

φ: Phase difference (degree)

$\lambda = \frac{r}{l}$: Ratio of crank radius to connecting rod

l: Length of the connecting rod (mm)

Intake and exhaust pistons move towards each other face-to-face. One of the limitations observed whilst modelling an OP engine is that the option *user defined piston motion* in AVL BOOST only allows inputting a relative position of the piston profile. Relative displacement is obtained by simply adding the displacements of each piston. This approach conserves the volume change rate of the engine, therefore avoiding possible discrepancies of work done in the thermodynamic cycle. The relative displacement of the piston was determined by the following equation [25]:

$$X_{relative} = r\left(1 - \cos\left(\alpha - \frac{\varphi}{2}\right)\right) + \left(1 - \cos\left(\alpha + \frac{\varphi}{2}\right)\right) \quad \textbf{Eq 7.3}$$
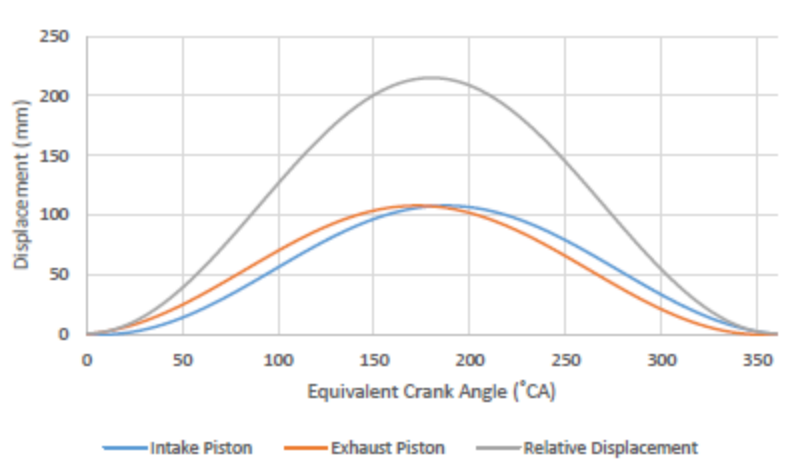
Figure 7-2 Piston Motion Profile

From the graph, it is evident that the compression and expansion stroke of this OP2S engine is asymmetric about the IDC. The exhaust piston leads from 0˚CA to 180˚CA and the intake piston leads from 180˚CA to 360˚CA relative to each other.

7.6.3 Heat Release Rate

The effect of variable compression ratio on the OP2S engine's performance was analysed. To investigate this effect, six different values for the compression ratio were selected ranging from 12 to 20. Using the compression ratios, clearance volume and clearance height were calculated, which are presented in Table 7.4.

Table 7-4 Variation of the Model

Compression Ratio	12	13.5	15	16.5	18	19.5
Clearance Volume (mm^3)	32398	28510	25455	22992	20963	19263
Clearance Height (mm)	13.64	12.00	10.71	9.70	8.82	8.11

The heat release rate was calculated in Microsoft Excel using pressure obtained from experimental data of the PAMAR series engine and volume using the parameters in Table 7.2. The pressure and volume were obtained for one cycle (360°) with an increment of 0.5°. Pressure and volume against crank angle degree (CAD) are illustrated in Figures 7.3 and 7.4 respectively.
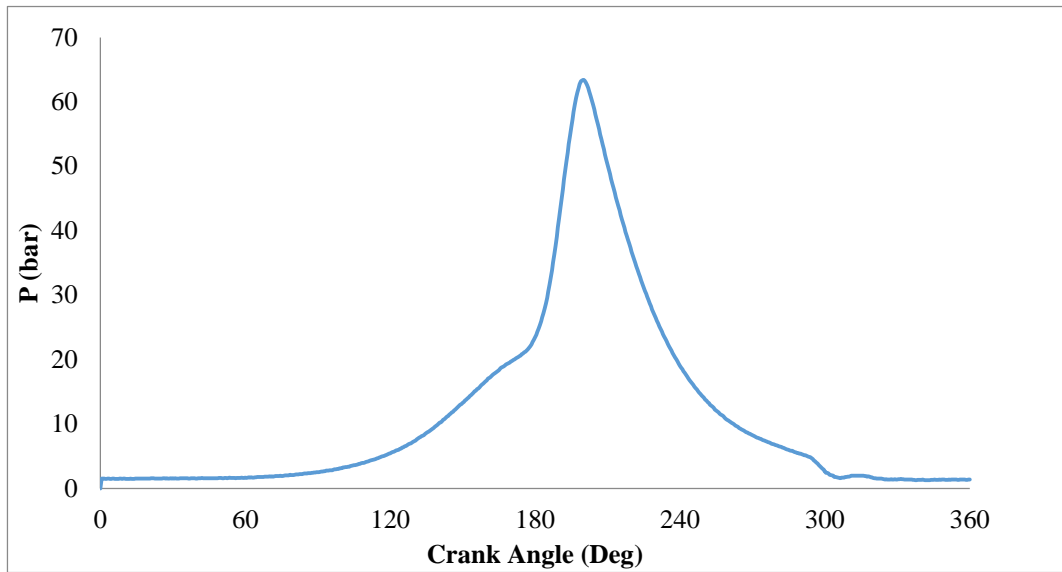
Figure 7-3 Pressure Profile versus Crank Angle
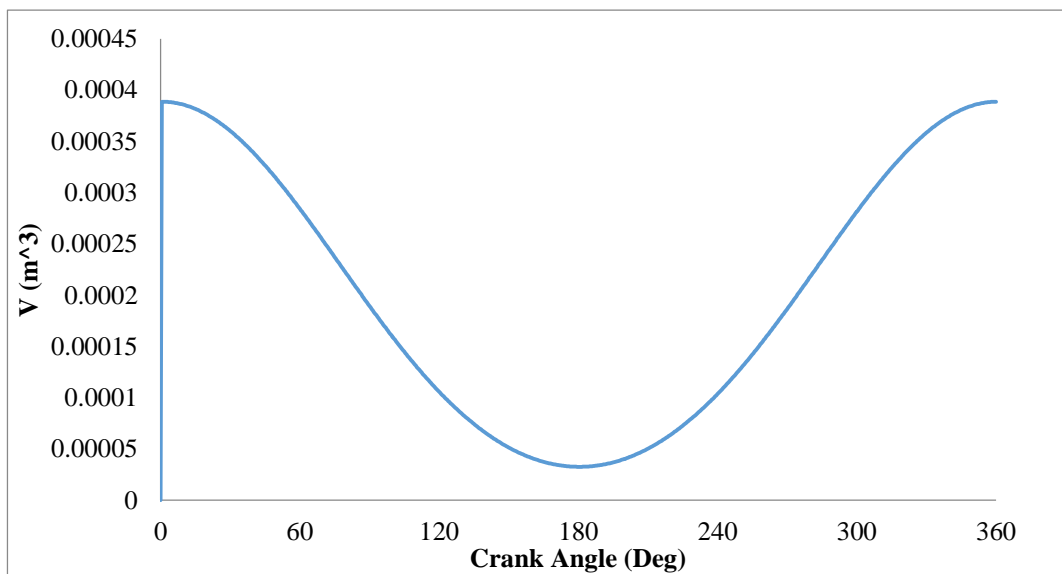
Figure 7-4 Cylinder Volume versus Crank Angle

The change in cylinder volume with respect to CAD was calculated using Equation 7.4 [1, 5]:

$$V = A\big((1 - \cos(\varphi)) + \lambda 4(1 - \cos(2\varphi))\big), \qquad \textbf{Eq 7.4}$$

where:

A: Bore area (mm^2)

r: Crank radius (mm)

φ: Crank angle (degree)

$\lambda = \frac{r}{l}$: Ratio of crank radius to connecting rod

A pressure versus volume diagram was plotted to visualise the changes in pressure with respect to volume in an opposed piston system (Figure 7.5). The graph also represents the amount of energy expended or received by the system as work, which can be determined by integrating the equation of the graph (i.e. area under the curve).
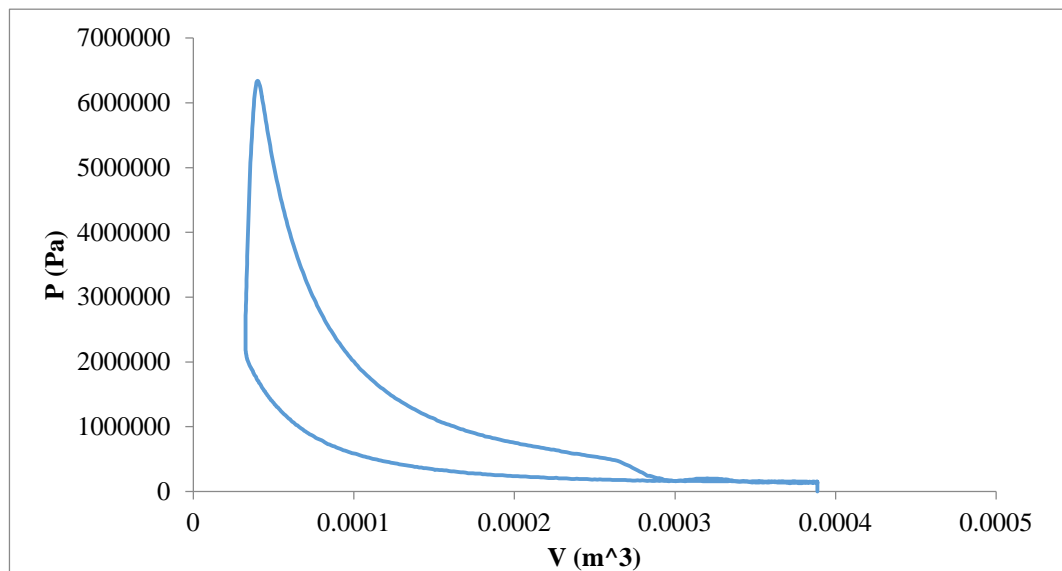
Figure 7-5 Pressure versus Volume

Figures 7.5 and 7.6 show pressure-volume data on both a linear pV and a LogP versus LogV diagram. In Figure 7.6, the compression process is a straight line of slope 1.32; and the expansion stroke following combustion is essentially linear with slope 1.36. Since both the compression of the unburned mixture prior to combustion and the expansion of the burned gases following the end of combustion are close to adiabatic isentropic process (for which PV^k = constant) the observed behaviour is as expected [1]. More extensive studies [34, 35] show that the compression and expansion process are well fitted by a polytrophic relation:

LogP versus LogV plots can be used to check the quality of cylinder pressure data [1]. Furthermore, LogP versus LogV plots approximately define the start and end of combustion, but do not provide a mass fraction burned profile.

For the compression and expansion processes the polytrophic index is 1.3 (± 0.05) for conventional fuels [1]. Thus, a polytrophic exponent value of 1.34 was assumed.
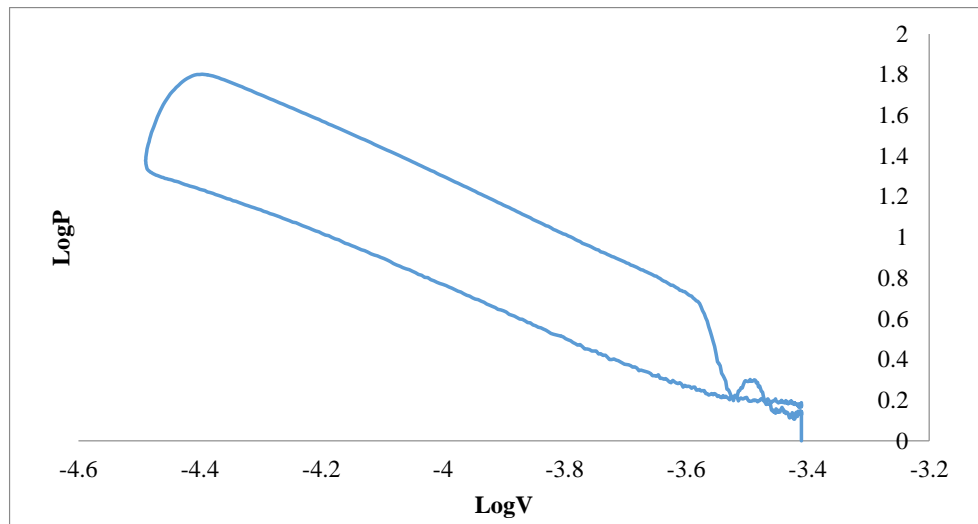
Figure 7-6 LogP versus LogV Profile

Heat release calculations are an approach to acquire information about combustion processes. Heat release analysis is performed based on cylinder gas pressure (CGP) data. The most widely used was developed by Krieger and Borman [36]. Using the cylinder pressure (P), cylinder volume (V) and polytrophic index (k), the heat release rate (HRR) was calculated with ease using Equation 7.5 [1, 37].

$$\frac{dQ_n}{d\theta} = \frac{\bar{k}}{k-1} P \frac{dV}{d\theta} + \frac{1}{k-1} V \frac{dP}{d\theta} \qquad \textbf{Eq 7.5}$$

Rate of heat release is the difference between heat released by the combustion of fuel and heat transfer from the cylinder to its walls. The calculation procedure of HRR enables the engineer to predict the amount of heat released from combustion to produce a pressure variation.

The piston and cylinder head shapes and valve geometry influence the turbulence level in the engine and therefore the rate of heat release during combustion [38].

The oscillation on either side of the peak illustrates a large amount of noise generated from the collision of the piston and cylinder wall. This is known as piston slap. The piston rocks in the cylinder due to excessive side clearance. This causes pre-ignition in spark knock which means that the combustion in the cylinder happens before the piston reaches IDC, hence knocking or rattling. By calculation of the desired values and specifying the range for the compression ratio, the simulation was set to run at two engine speeds, 420 rpm and 1500 rpm, to make a comparison. The heat release rate is shown in Figure 7.7. which then smoothens to show the maximum heat release rate in Figure 7.8.
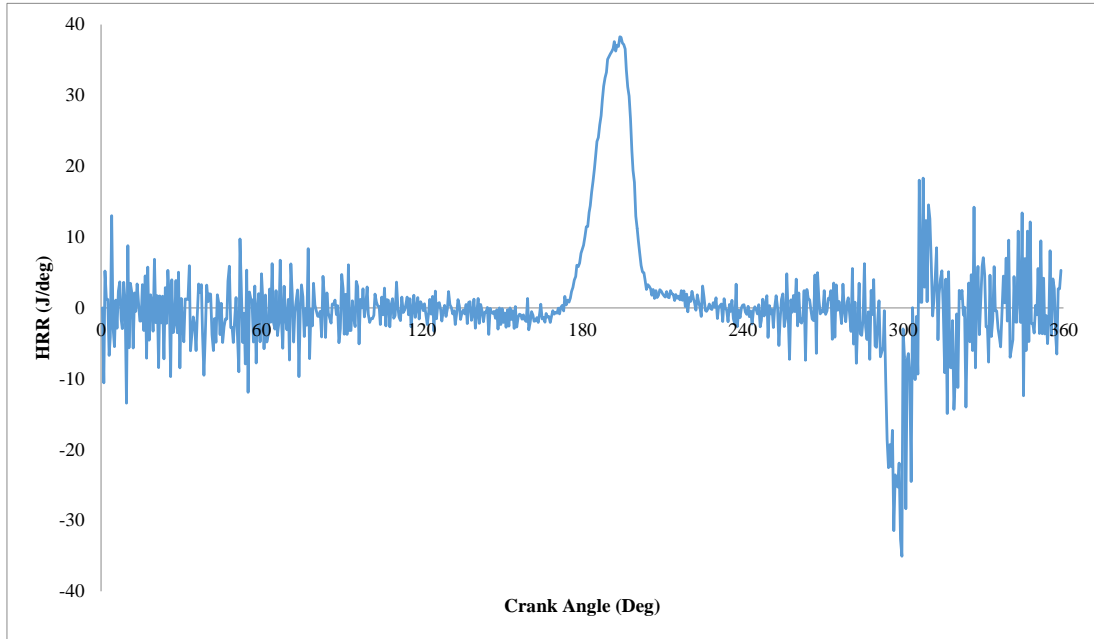
Figure 7-7 Heat Release Rate versus Crank Angle
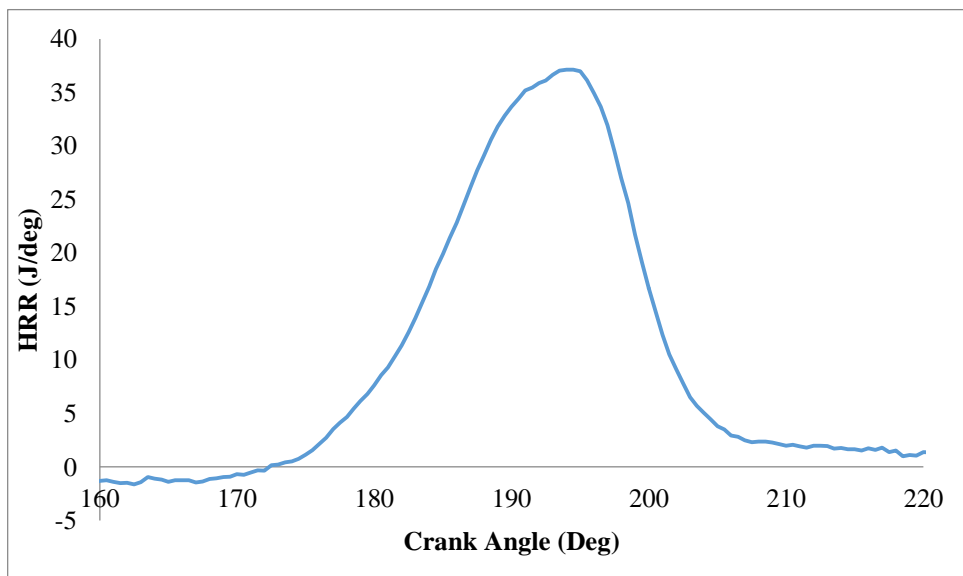
Figure 7-8 Maximum Heat Release Rate

7.7 Effect of Variable Compression Ratio

The VCR is a technology that allows adjusting the compression ratio of an engine while it is in operation to increase fuel efficiency under varying loads. Thus, a VCR mode allows for the volume passing the piston at IDC to be changed. For automotive use, this is achieved dynamically in response to the load and driving demands. The VCR is a cost-effective method of achieving increased fuel economy, reduced carbon dioxide emissions of about 30-40% in comparison to conventional motors.

The effect of variable compression ratio at two different engine speeds 420 rpm (simulation 1) and 1500 rpm (simulation 2) was investigated and discussed in this section. To do so, the following parameters were analysed: IMEP; peak pressure; peak temperature; ISFC; BSFC; volumetric efficiency; and mechanical efficiency. The results obtained from AVL BOOST are summarized in a Table.7.5 and 7.6.

Some parameters either remained constant with increasing CR or didn't show a trend. This suggests that these parameters were independent of CR. Thus, graphs of each parameter mentioned against compression ratio were plotted for both simulations of the models to visualise the values in Table 7.5 and Table 7.6 clearly.

Table 7-5 Summary of Results for Engine Speed 420 rpm

Parameters	Compression Ratio					
	12	13.5	15	16.5	18	19.5
Peak Pressure (MPa)	5.02209	5.36196	5.67318	5.95697	6.21475	6.44725
Peak Temperature (K)	2490.22	2493.29	2496.08	2499.01	2500.41	2501.73
IMEP (Bar)	7.84179	7.85847	7.85967	7.84786	7.82716	7.79981
BMEP (Pa)	684179	685847	685967	684786	682716	678881
ISFC (kg/Ws) e-008	7.3713	7.3557	7.3546	7.3656	7.3851	7.4110
BSFC(kg/Ws) e-008	8.4487	8.4282	8.4267	8.4412	8.4668	8.5009
Indicated Efficiency (%)	31.1864	31.2527	31.2575	31.2105	31.1282	31.0194
Pressure @SOC (Pa)	2.38144	2.67484	2.95111	3.22056	3.48481	3.73191
Temperature @SOC (K)	903.942	927.435	948.214	966.715	983.771	997.751
Volumetric Efficiency (%)	88.0563	86.811	85.7698	84.9614	84.2933	83.7365
Delivery Ratio	91.5004	91.5061	91.5108	91.5156	91.5208	91.526
Heat Loss-Piston (kJ)	0.0183031	0.0183128	0.0183113	0.0183125	0.0183145	0.0183136
Heat Loss-Liner (kJ)	0.105667	0.105763	0.105747	0.105758	0.105778	0.105768
Heat Loss-Total (kJ)	0.123945	0.12405	0.124032	0.124044	0.124066	0.124055
Indicated Power (kW)	1.96	1.96	1.96	1.96	1.96	1.96
Friction Power (kW)	0.25	0.25	0.25	0.25	0.25	0.25
Brake Power (kW)	1.71	1.71	1.71	1.71	1.71	1.71
Mechanical Efficiency (%)	87.244897	87.24489	87.24489	87.24489	87.24489	87.24489

Table 7-6 Summary of Results for Engine Speed 1500 rpm

Parameters	Compression Ratio					
	12	13.5	15	16.5	18	19.5
Peak Pressure (MPa)	5.10922	5.48479	5.81518	6.12601	6.41423	6.68478
Peak Temperature (K)	2560.58	2570.6	2576.03	2582.04	2585.18	2588.01
IMEP (Bar)	9.26046	9.41214	9.51718	9.62099	9.695	9.76128
BMEP (Pa)	810046	825214	835718	846099	853500	860128
ISFC (kg/Ws) e-008	6.2421	6.1415	6.0737	6.0082	5.9623	5.9218
BSFC(kg/Ws) e-008	7.1359	7.0048	6.9167	6.8319	6.7726	6.7204
Indicated Efficiency (%)	36.8284	37.4316	37.8493	38.2622	38.5565	38.8201
Pressure @SOC (Pa)	2.36844	2.66704	2.95881	3.24454	3.52245	3.79302
Temperature @SOC (K)	898.031	928.395	945.961	966.209	984.407	1000.98
Volumetric Efficiency (%)	85.5234	84.2658	83.2687	82.4669	81.8034	81.2466
Delivery Ratio	26.6925	26.6928	26.6935	26.6939	26.6945	26.6949
Heat Loss-Piston (kJ)	0.014174	0.0141737	0.0141734	0.0141731	0.0141729	0.0141727
Heat Loss-Liner (kJ)	0.0799471	0.0799402	0.0799343	0.0799293	0.0799251	0.0799215
Heat Loss-Total (kJ)	0.0940821	0.0940792	0.0940763	0.094074	0.0940719	0.0940707
Indicated Power (kW)	8.25	8.39	8.48	8.57	8.64	8.7
Friction Power (kW)	1.03	1.03	1.03	1.03	1.03	1.03
Brake Power (kW)	7.22	7.35	7.45	7.54	7.61	7.68
Mechanical Efficiency (%)	87.51515152	87.604290	87.853773	87.98133022	88.0787037	88.27586207

7.7.1 Indicated Mean Effective Pressure

The IMEP is the ratio of indicated work to swept volume. It is a fictitious constant pressure that would produce the same amount of work per cycle if it acted on the piston during the power stroke.
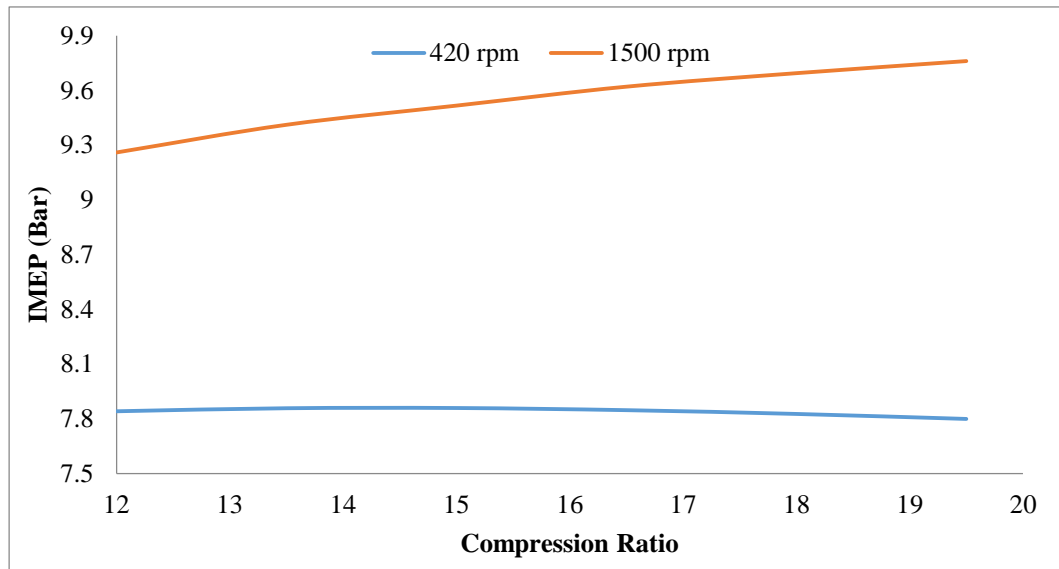
Figure 7-9 Effect of VCR on IMEP at Different Engine Speeds

The general trend is that a higher IMEP is achieved with increasing engine speed. In simulation 1, the IMEP remains approximately around 780000 Pa; whereas in simulation 2, when the engine speed was increased from 420 rpm to 1500 rpm, the IMEP starts to increase from 926046 Pa to 976128 Pa, with increasing CR. The IMEP is higher when the engine speed is set at 1500 rpm.

7.7.2 Peak Pressure

The purpose of an engine is to generate internal pressure which can be used to do work. Therefore, high pressures are desirable. However, excessively high and erratic pressures are a source of potential damage and should be avoided.

Cylinder pressure is the pressure in the engine cylinder during the two strokes of engine operation. Cylinder pressure is constantly changing inside the cylinder for both strokes. There are certain characteristics of this pressure which can be analysed, for example peak (maximum) cylinder pressure near the IDC.

During the combustion stroke, the air/fuel mixture is ignited, creating very high cylinder pressure which rise very quickly (also known as the peak pressure). This is where the engine's power comes from, as it forces the piston down. As the piston moves towards the ODC, the cylinder volume increases which reduces the cylinder pressure. When the piston reaches the ODC there will be a significant amount of reduction in cylinder pressure.

Peak pressures that occur during combustion are much higher and are more difficult to obtain by calculation. Thus, AVL BOOST was used to determine the peak pressure for each CR. Figure 7.10 indicates the change in peak pressure with increasing CR.
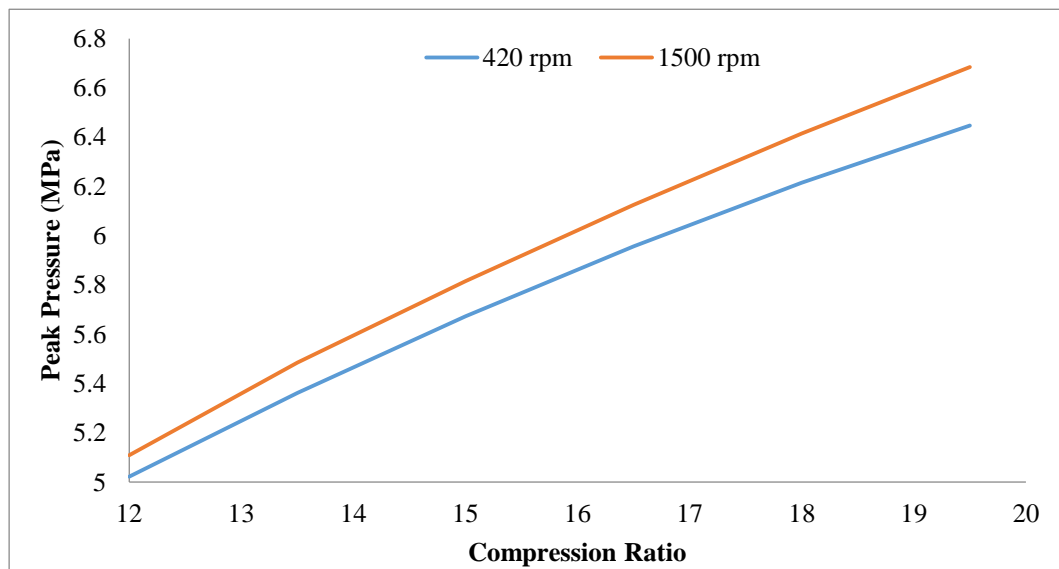
Figure 7-10 Effect of VCR on Peak Pressure at Different Engine Speeds

For the 420 rpm simulation, at a compression ratio of 12 and 19.5, the peak pressures were 5.02 MPa and 6.45 MPa, respectively. As for the 1500 rpm simulation, at a compression ratio of 12 and 19.5 the peak pressures were 5.11 MPa and 6.68 MPa, respectively.

The general trend is that peak pressure increases with increasing CR. Since compression ratio is equal to the ratio of volume at the ODC and volume at the IDC, compression ratio is inversely proportional to the volume at the IDC. Thus, a higher CR means a reduction in volume at the IDC. A reduction in volume at the IDC means that the piston can do more work and compress the air/fuel ratio further, hence increasing the cylinder pressure at the IDC (i.e. peak pressure). Thus, an increase in CR means an increase in peak pressure.

A more observed trend that can be obtained from Figure 7.10 is that a higher engine speed results in a higher peak pressure. At 420 rpm and 1500 rpm, the maximum peak pressures obtained were 6.45 MPa and 6.68 MPa (at a CR of 19.5), respectively. As the engine speed increases, the mixture in the combustion chamber must be ignited earlier as there is less time between spark and optimum peak pressure angle. In case the mixture density is changed due to higher compression ratio or boost, the spark has to be ignited later to achieve the same optimal point.

Figures 7.11 to 7.22 indicate pressure against CAD for different compression ratios at different speeds of 420 rpm and 1500 rpm.
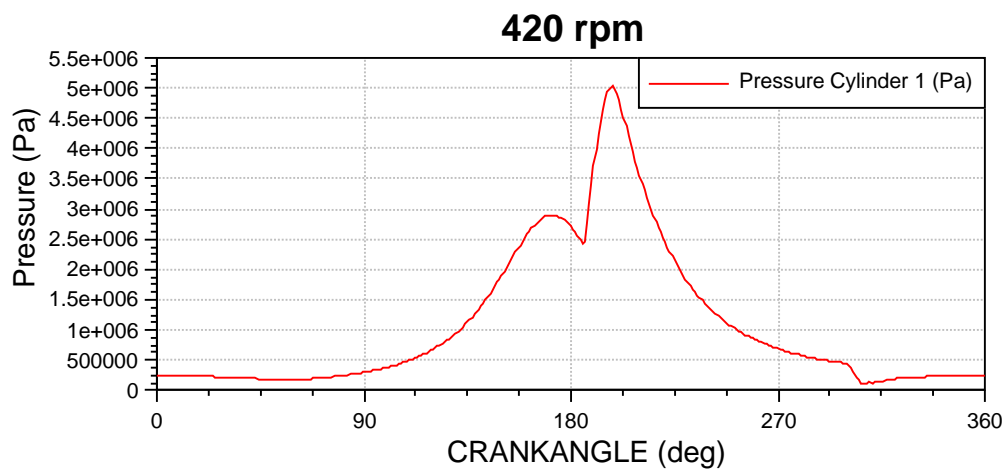
Figure 7-11 Effect of VCR Case 1 on Cylinder Pressure Profiles at a Speed of 420 rpm
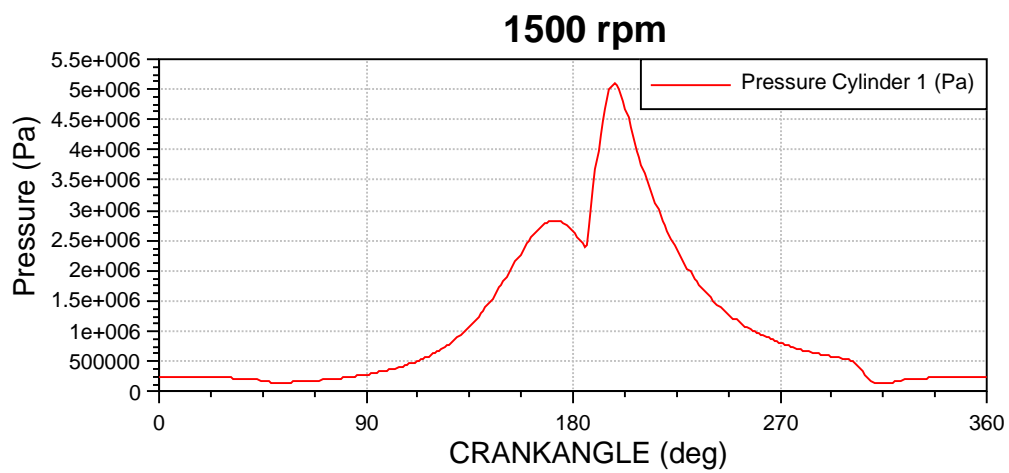
Figure 7-12 Effect of VCR Case 1 on Cylinder Pressure Profiles at a Speed of 1500 rpm
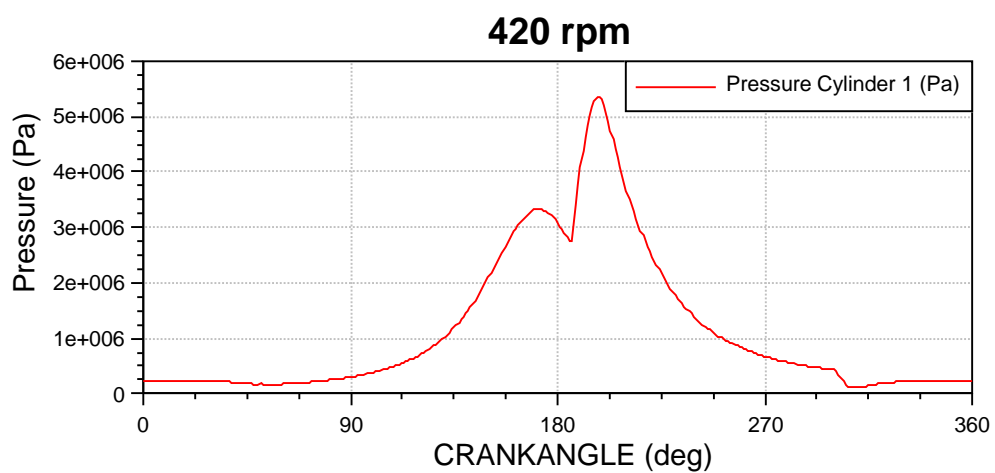
Figure 7-13 Effect of VCR Case 2 on Cylinder Pressure Profiles at a Speed of 420 rpm
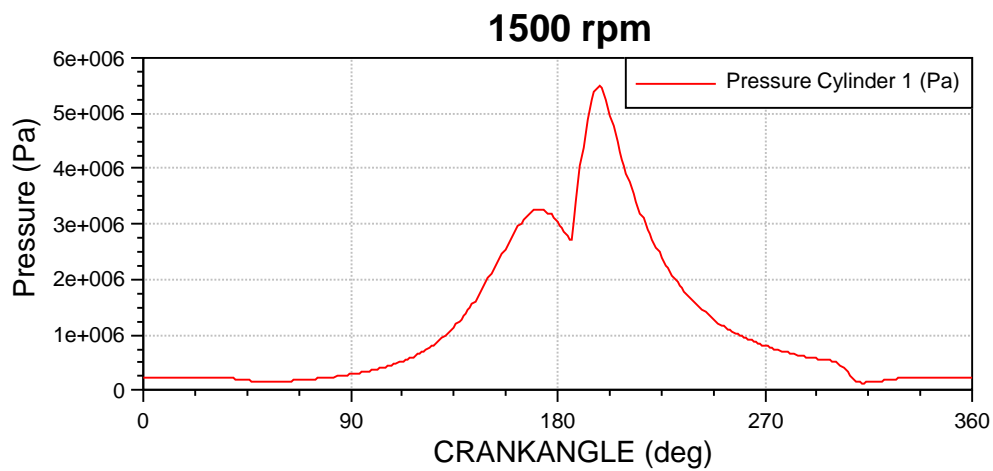
Figure 7-14 Effect of VCR Case 2 on Cylinder Pressure Profiles at a Speed of 1500 rpm
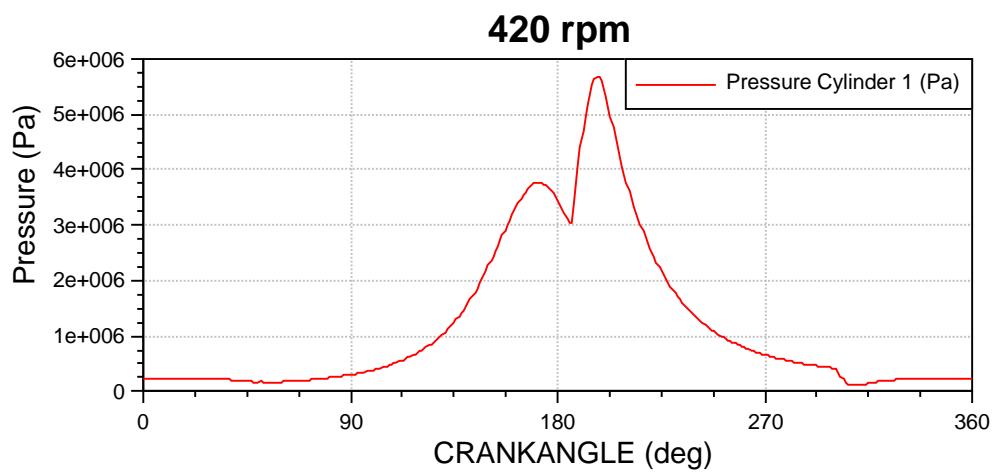
Figure 7-15 Effect of VCR Case 3 on Cylinder Pressure Profiles at a Speed of 420 rpm
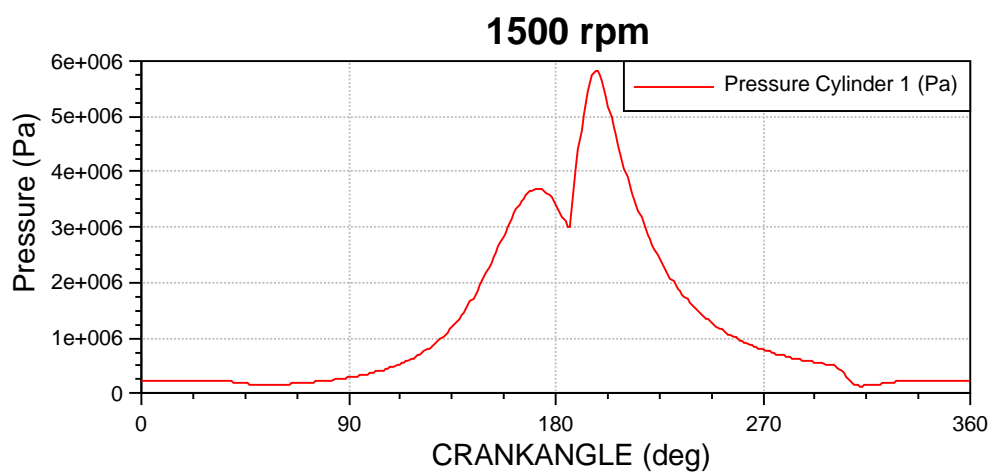
Figure 7-16 Effect of VCR Case 3 on Cylinder Pressure Profiles at a Speed of 1500 rpm
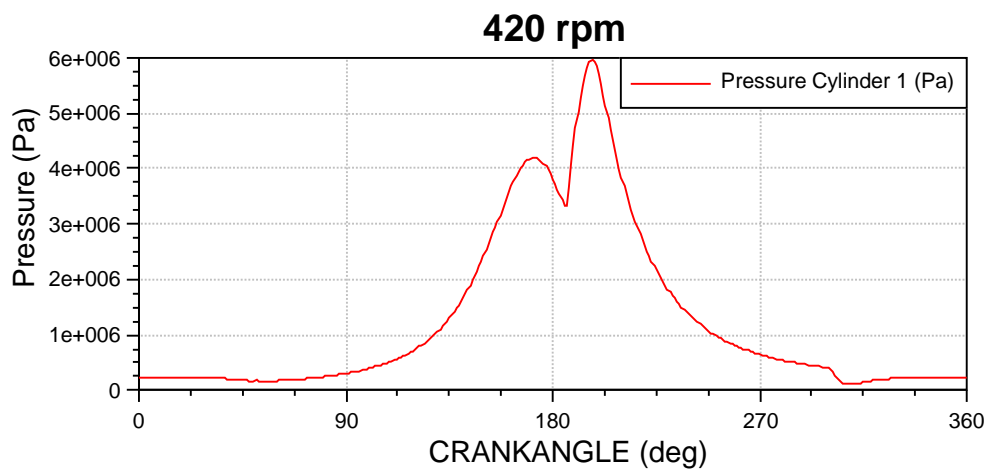
Figure 7-17 Effect of VCR Case 4 on Cylinder Pressure Profiles at a Speed of 420 rpm
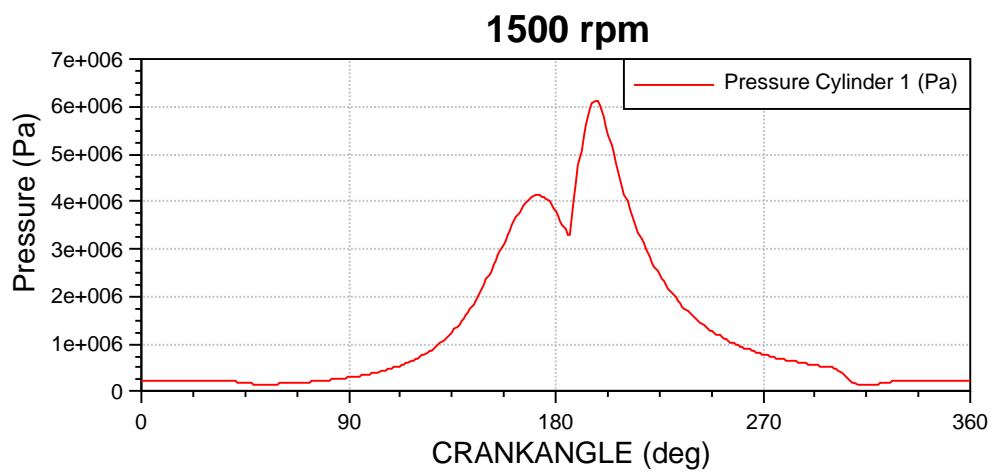
Figure 7-18 Effect of VCR Case 4 on Cylinder Pressure Profiles at a Speed of 1500 rpm
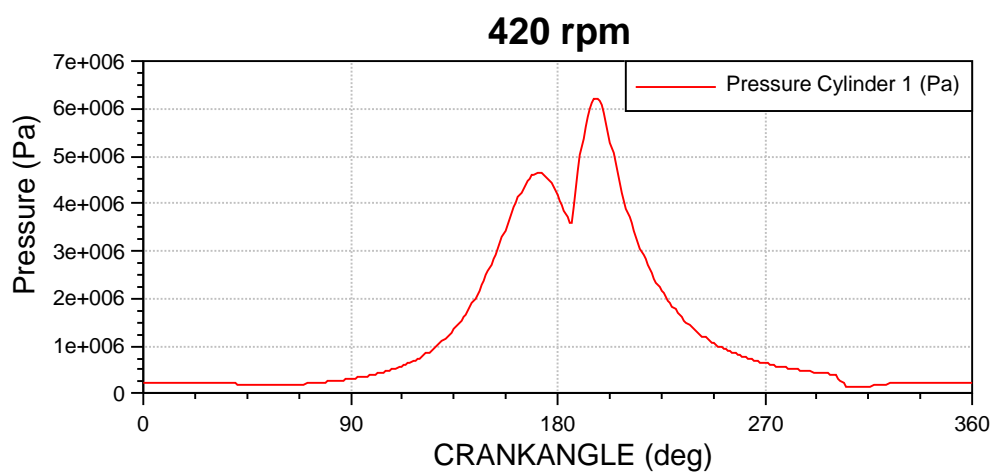
Figure 7-19 Effect of VCR Case 5 on Cylinder Pressure Profiles at a Speed of 420 rpm
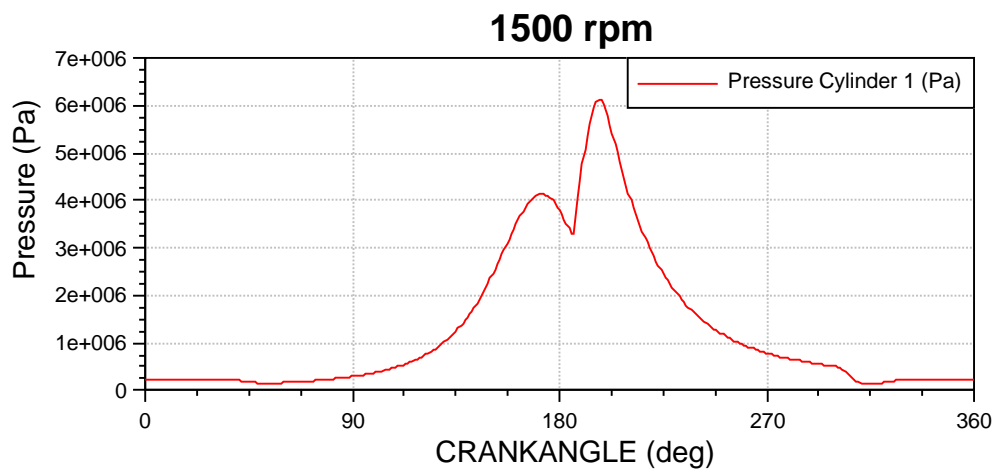
Figure 7-20 Effect of VCR Case 5 on Cylinder Pressure Profiles at a Speed of 1500 rpm
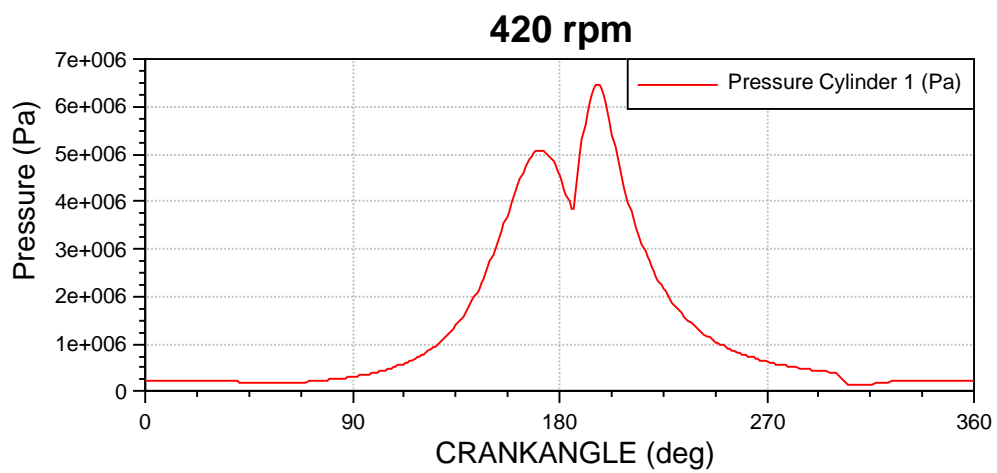
Figure 7-21 Effect of VCR Case 6 on Cylinder Pressure Profiles at a Speed of 420 rpm
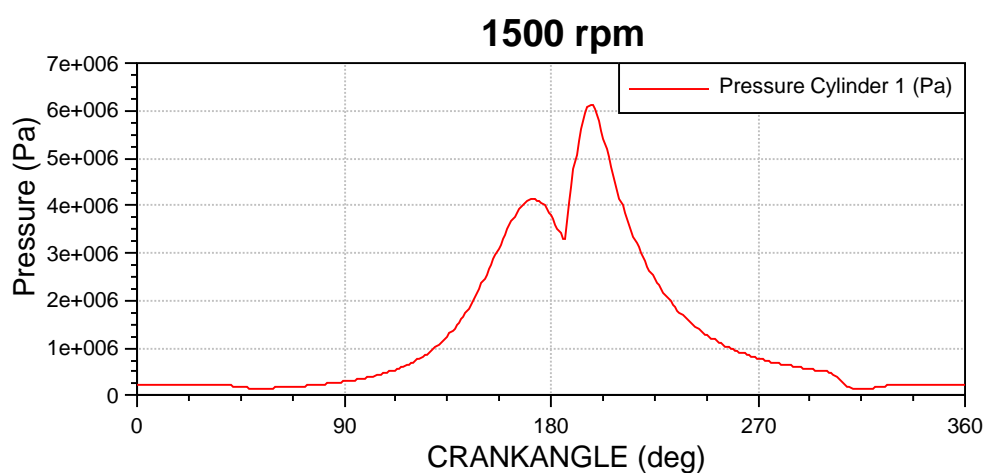
Figure 7-22 Effect of VCR Case 6 on Cylinder Pressure Profiles at a Speed of 1500 rpm

7.7.3 Peak Temperature

During the combustion process, the cylinder gas temperature reaches a high value (known as the peak temperature). The maximum temperature was recorded at the IDC. A considerable amount of heat is transferred to the walls of the combustion chamber. Thus, it is vital to provide proper cooling to its walls. Chemical and physical changes in the lubricating oil are possible due to the prevailing high temperature. Excessive cylinder wall temperatures will therefore cause a rise in the operating temperature of the piston head, which can affect the strength of the piston severely.
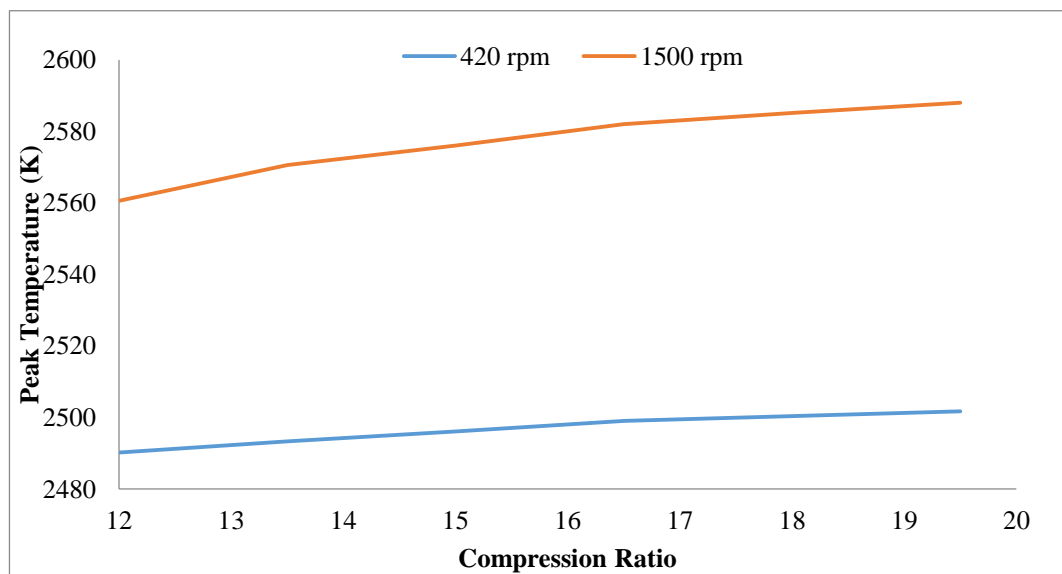
Figure 7-23 Effect of VCR on Peak Temperature at Different Engine Speeds

Figure 7.23 suggests that for both simulations, peak temperature increases with increasing CR. At an engine speed of 420 rpm peak temperature increases from 2490.22 K to 2501.73 K; and when the engine speed was set at 1500 rpm, peak temperature increases from 2560.58 K to 2588.01 K. This suggests that at low

engine speed, peak temperature increases with very small increments as the CR increases.

According to 'Internal Combustion Engines', Chapter 4, and page 242 [38]: 'Peak temperatures may range from 2400 to 2800 K'. Thus, the peak temperatures obtained from AVL BOOST are acceptable.

The compression due to piston motion and combustion in a confined volume leads to very high burned gas temperatures in reciprocating engines. The compression ratio determines the peak pressure and hence the peak temperature in the cycle. An increase in CR reduces clearance volume at the IDC. As a result, cylinder pressure increases as it compresses the air/fuel mixture further. Work done by the gas in the cylinder on the piston during the compression stroke heats the combustion products, thus increasing cylinder gas temperature. Therefore, increasing the CR causes an increase of peak temperature.

Nitrogen oxide (NOx) emissions result from the thermal fixation of atmospheric nitrogen, so control of these emissions can be achieved by reducing the peak flame temperatures. Therefore, in order to reduce lower peak temperature, the compression ratio must also be lower, thereby limiting NOx formation. On the other hand, the NOx, emission reductions achieved by reducing CR are smaller in comparison to those accumulated by retarding the spark. One other way of reducing peak temperature is by diluting the charge with cool combustion products. This process is known as exhaust gas recirculation (EGR). The benefits of cooling combustion products by dilution instead of excess air are as follows:

1) Dilution of the air/fuel mixture without the addition of excess O2 aids in NOx formation.

2) An increase in the specific heat of the gas due to the presence of H_2O and CO_2, reduces the temperature somewhat more than would the equivalent dilution with excess air.

Another way of reducing peak temperature is through exhaust gas recirculation or retarding the injection timing. Injection timing delays cause the heat release to occur late in the cycle, after some expansion work has occurred, thereby lowering the peak temperature.

7.7.4 Specific Fuel Consumption (SFC)

The efficiency of an internal combustion engine is generally reported in terms of the specific fuel consumption (SFC), the mass of fuel consumed per unit of energy output [38]. The SFC is a measure of how efficiently the fuel supplied to the engine is used to produce power.

In this section of the chapter, two types of SFC will be discussed. These are: indicated specific fuel consumption (ISFC) the ratio of the mass of the fuel to the indicated power; and brake specific fuel consumption (BSFC) the ratio of the mass of the fuel to the brake power. It is also convenient to present the specific fuel consumption in terms of the indicated work to eliminate the influences of parasitic losses and loads. Clearly a low value for SFC is desirable, since at a given power level less fuel will be consumed.
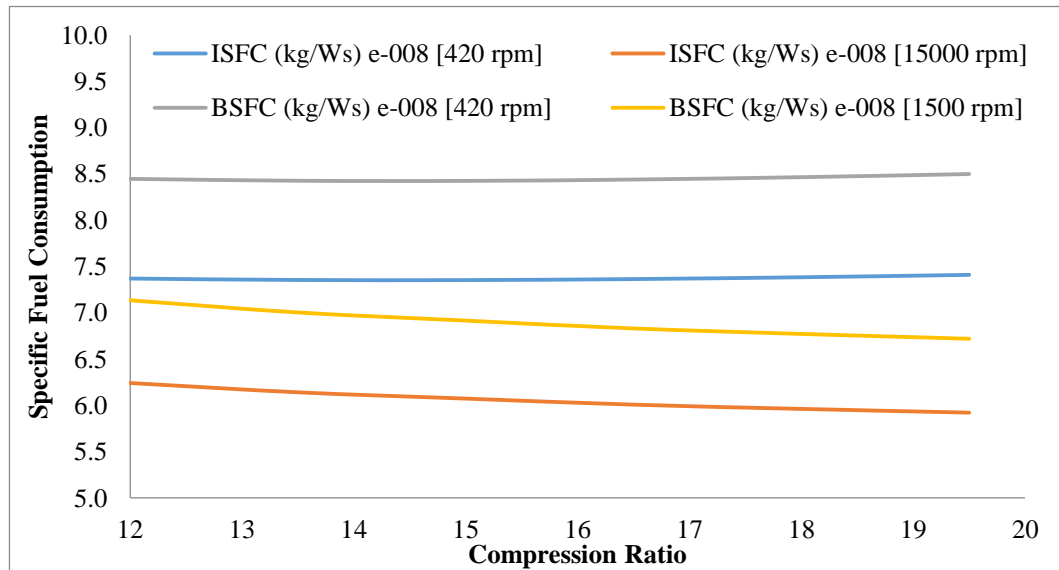
Figure 7-24 Effect of VCR on ISFC and BSFC at Different Engine Speeds

From Figure 7.24, Table 7.5 and Table 7.6 it can clearly understood that in simulation 1 the minimum ISFC and BSFC are obtained at a CR of 15, 7.35456 kg/Ws and 8.4267 kg/Ws respectively. At lower speeds, the BSFC increases due to the increased time for heat losses from the gas to the cylinder and piston wall.

In simulation 2, both the ISFC and BSFC decrease as the CR increases. A reduction of ISFC and BSFC of about 5.13% and 5.82% were obtained respectively. The BSFC reduced with increasing CR due to better combustion and lower heat losses where slight reduction of BSFC was observed at higher CR.

The SFC is effectively a measure of the engine's ability to convert the chemical energy to mechanical energy. Thus, a lower SFC is required for an engine to burn minimal fuel and produce maximum power output. This is achieved at a higher CR according to the results obtained in simulation 2 from AVL BOOST.

7.7.5 Engine Efficiency

Engine efficiency is becoming a more prominent factor in automobile manufacturers' decision making. It is the relationship between the total energy contained in the fuel and the amount of energy used to perform useful work. This makes engine efficiency one of the most vital factors to consider when modelling an internal combustion engine. Two efficiencies are discussed in this section of the chapter: volumetric and mechanical.

7.7.5.1. Volumetric Efficiency

The volumetric efficiency is probably one of the most variable efficiencies governing the performance of engines. Volumetric efficiency is the ratio of the actual volume of the air/fuel mixture drawn in during combustion to the swept volume. Volumetric efficiency determines how efficiently fuel is burnt; thus, affecting the power output because the amount of air drawn inside the cylinder is dependent on the volumetric efficiency of an engine. Figure 7.25 shows the volumetric efficiency trends with different compression ratios and engine speeds.
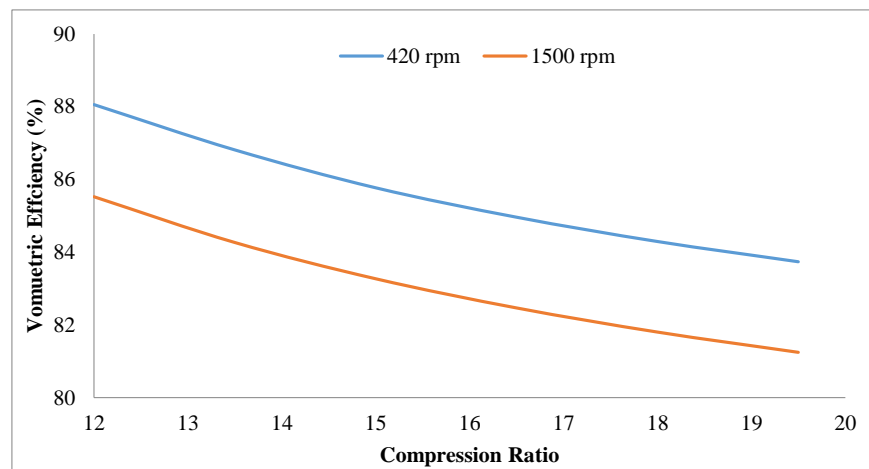
Figure 7-25 Effect of VCR on Volumetric Efficiency at Different Engine Speeds

The general trend is that volumetric efficiency decreases with increasing CR. When the engine speed was set at 420 rpm, the volumetric efficiency reduced from 88.1% to 83.7%. Similarly, the volumetric efficiency reduced from 85.5% to 81.2%, when the engine speed was set at 1500 rpm.

Typical values for Efficiency are in the range 75%-90%, and lower when the throttle is closed [38]. For both simulations, volumetric efficiency is within the typical range, thus the values obtained from AVL BOOST are acceptable. Basic calculations equations used are as follows [1]:

$$CR = \frac{Vs + Vc}{Vc} \qquad \textbf{Eq 7.6}$$

where:

Vs is swept volume [mm^3 or L]

Vc is clearance volume [mm^3 or L]

$$\eta V = \frac{Vair}{Vs} \qquad \textbf{Eq 7.7}$$

where:

ηV is volumetric efficiency

Vair is volume of air drawn into cylinder

$$Vs = \frac{Vair}{\eta V} = (CR \times Vc) - Vc \qquad \textbf{Eq 7.8}$$

Compression ratio is inversely proportional to volumetric efficiency, thus results obtained from AVL BOOST are acceptable.

The value of volumetric efficiency of a normal engine lies between 70 and 80%; and the values obtained from AVL BOOST lie between 80 and 90 percent, proving an OP engine is volumetrically more efficient in burning fuel.

One way of increasing the engine's volumetric efficiency in order to increase engine power would be forced induction. This can be achieved by using a turbo or super-charger. This draws in more air into the cylinder thus increasing volumetric efficiency.

Another method of increasing volumetric efficiency is induction ram. However, this only occurs at high speed and is due to the inertia of the high-speed air. In part intake valves are left open after the ODC to take advantage of this.

A third way of improving volumetric efficiency is intake tuning. The reflected pressure waves can be used to increase the air density at the inlet valve just prior to closing. This method is key to the success of naturally aspirated engines.

7.7.5.2. Mechanical Efficiency

The mechanical efficiency is how much of the power developed by the expanding of the gases in the cylinders is actually delivered as useful power.

Some of the power generated in the cylinder is used to overcome engine friction. The friction power (i.e. the power loss in the mechanical components of the engine due to friction) is defined as the difference between the indicated power and the brake power (i.e. difference between the moving parts and the energy taken to run

the auxiliary equipment such as the fuel pump, water pump, oil pump and alternator). Thus, the mechanical efficiency is defined as the ratio of brake power to indicated power.

Friction losses in the engine come from friction between moving parts (such as the piston rings on the cylinder walls), the power required to run the valve gear and the pumps, and the pumping losses.
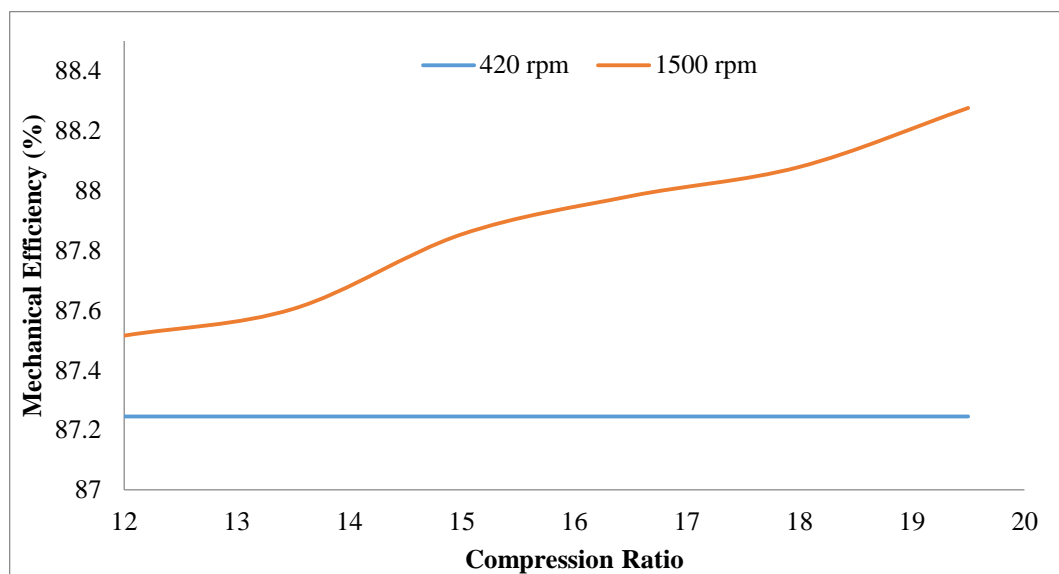
Figure 7-26 Effect of VCR on Mechanical Efficiency at Different Engine Speeds

For the 420 rpm simulation, an indicated power of 1.96 kW and a brake power of 1.71 kW was obtained; thus, a mechanical power of 87.2% was obtained from AVL BOOST for each CR. This suggests that at low engine speed the mechanical efficiency is independent of compression ratio.

Conversely, once the engine speed was set at 1500 rpm, the mechanical efficiency increases with respect to compression ratio, as do the indicated power and brake power. Therefore, a higher engine speed has an effect on mechanical efficiency.

7.8 Conclusion

This chapter discussed the effect of variable compression ratio on an OP2S engine's performance by modelling and simulating a simple single-cylinder two-stroke opposed piston engine in AVL BOOST. The aim was achieved by completing all the objectives. Results obtained from AVL BOOST indicate a general trend between the analysed parameters and the compression ratio.

In conclusion, the analysis of the results showed that some parameters, such as IMEP, peak pressure, peak temperature and volumetric efficiency, have an effect when increasing the compression ratio. Positive correlations were attained when analysing IMEP, peak pressure and peak temperature. On the other hand, volumetric efficiency decreased with increasing compression ratio.

In addition, certain parameters, such as SFC and mechanical efficiency, were only affected when the engine speed was set at 1500 rpm and remained constant at an engine speed of 420 rpm. One of the reasons as to why the results remained constant or had very little effect when increasing the compression ratio for simulation 1 is because perhaps 420 rpm was too low of an engine speed to analyse engine performance. In future, a higher value of engine speed will be used and more simulations will be carried out to make a better comparison.

Finally, it is recommended to use AVL BOOST to model and simulate an OP2S engine as it is easy and fast to set up the model and provide a reliable and accurate simulation of steady and transient engine performance parameters [32].

Chapter 8 - Summary,

Conclusion and

Recommendation for Future

Work

Finally, as conclusions, all the presented results in the main chapters are summarized here. In this thesis, detailed modelling studies have been done in order to investigate the possible effects of engine specification changes on engine efficiency. Experiments for Chapter 5 have been carried out at the University of Birmingham for seven different conditions; also for Chapters 6 and 7 experiments were completed in the Warsaw University of Technology. These experimental results have been used to validate and calibrate the simulations data and then find the optimum engine modification. After a review of the literature, the third chapter contains experimental set-ups which are used for experimental studies. The fourth chapter includes the modelling set-up in two software packages. The main findings of the research are summarized as follows:

8.1 Thermodynamic Simulation Comparison of AVL BOOST and Ricardo WAVE for HCCI and SI Engines' Optimisation

Here, engine models of a four-stroke compression ignition engine in seven different conditions were developed and applied to investigate the engine performance and emission characteristics with both model and experiment conditions. Using geometry data and experimental data from the engine test rig at the UoB allow to calculations of desired data. The engine models in AVL BOOST and Ricardo WAVE were calibrated and then the pressure diagram and IMEP at these operating conditions were compared between the simulation and experiments. In addition, some emission improvements were also applied in the model to study the effect of engine changes to possible emission improvements. Furthermore, the mass fraction burned and heat release data have been successfully calculated. The

experimental engine was successfully modelled in Ricardo WAVE and has been validated by comparing it to the experimental values. The IMEP and P_{max} Crank Angle at P_{max} all agree with the experimental results with an average error of 5%. A model was also created of a single case in AVL BOOST and was calibrated, aligning pressure traces and matching the IMEP. In the future, for a more accurate model, more data from the engine such as geometry and temperatures could be used.

The main errors occurred for peak pressure of the engine. This could be due to experimental condition differences, minute fuel variances, ambient temperatures and turbulent flows of gases into the cylinder and the flame propagation characteristics. Nonetheless, the HCCI and SI offer moderately accurate results which can be used to conduct emissions' tests.

In conclusion, the validation of an SI and HCCI engine has proven successful. The modelling is accurate and can be used to conduct further engine analysis. Evidently, HCCI engines are more optimised than SI engines at low loads, through producing lower emissions and permitting leaner AFR ratios. However, the combustion unpredictability, need for variable valve timing and poor high load operation, prevent the widespread application of the technology. Poor results for the CI engine simulation have limited the analysis of the results, highlighting the limitations of AVL BOOST.

NOx emissions can be significantly improved while little affecting performance by utilizing EGR in SI engines; however, it is important that soot is also managed. Improvements to HCCI emissions are not recommended and can be considered negligible due to their already low emission output. Given the complexity of engines

and the vast amount of trade-off, improving the engines in certain aspects will have an opposite effect in another. This limits how much an engine can be improved before another aspect will become a hindrance.

Both modelling packages yielded very useable results with accuracies typically around only 5% for all the results, which confirms the capabilities of both AVL and WAVE in modelling a single cylinder engine and predicting potential performance improvements. The inaccuracies can mostly likely be linked to the lack of predictive combustion simulation within software as well as heat losses defined within the software not being completely representative of real world experiment conditions. Also, being one dimensional model meant three dimensional effects such as turbulence were not properly accounted for.

8.2 Investigation into the Effect of Bore to Stroke Ratio on the Performance of a Single Cylinder Two-stroke Opposed Piston Engine

In this chapter, first a brief history of the dawn of OP engines and the progress of research into them in the 21st century has been described. A comprehensive 1D thermodynamic modelling of the PAMAR™ single cylinder engine was performed in AVL BOOST to demonstrate fundamental engine performance. The Wiebe, Wiebe 2-Zone and Double Wiebe heat release models were independently analysed. The Double Wiebe is the best choice in AVL BOOST for compression ignition. However, unreliable results were produced because of a lack of information on fuel delivery. The Wiebe 2-Zone model was shown as robust compared to the Wiebe and Double Wiebe models with its utilisation in validating the OP2S engine. Nine

different B/S combinations of the OP2S engine for the same swept volume were investigated after the confidence produced from the validation. The main conclusions of this analysis were that the heat losses increase with the increasing B/S ratio; due to the lower surface area to volume exposed the increase in the ITE and the mechanical efficiency which was observed with increasing the B/S ratios. An improvement in the fuel consumption is also evident. A higher B/S ratio is desirable for applications that require better fuel efficiency.

8.3 Evaluation of the Effect of Variable Compression Ratios' Performance on an Opposed Piston 2-stroke Engine

This chapter discussed the effect of variable compression ratio on OP2S engine performance by modelling and simulating a simple single-cylinder two-stroke opposed piston engine in AVL BOOST. The aim was achieved by completing all the objectives. The results obtained from AVL BOOST indicate a general trend between the analysed parameters and the compression ratio.

In conclusion, the analysis of the results showed that some parameters, such as IMEP, peak pressure, peak temperature and volumetric efficiency, have an effect when increasing the compression ratio. Positive correlations were obtained when analysing IMEP, peak pressure and peak temperature. On the other hand, volumetric efficiency decreased with the increasing of the compression ratio.

In addition, certain parameters, such as specific fuel consumption and mechanical efficiency, were only affected when the engine speed was set at 1500 rpm, and remained constant at an engine speed of 420 rpm. One of the reasons the results remained constant or had very little effect at low speed when increasing the

compression ratio for simulation 1 is because possibly an engine speed of 420 rpm was too low for analysis of engine performance. In future, a higher value of engine speed will be used and more simulations will be carried out to assist with a better comparison.

Finally, AVL BOOST is recommended to model and simulate an OP2S engine, as it is easy and fast to set up the model and furthermore, provide a reliable and accurate simulation of steady and transient engine performance parameters.

8.4 Recommendations for Future Works

Research performed during this work focused on the possible engine specification improvements and their effects on currently available engines. The author would like to recommend the following works for extension of the research on modelling and experimental investigations:

- Obtain more engine performance data at different speeds and loads, including full data of in-cylinder pressure. These should be used to calibrate and validate the models at different engine conditions.

- Improve on the stability of in-cylinder pressure data to make it possible to obtain more reliable heat release data.

- Obtain more engine geometry data, particularly those of inlet and exhaust pipework and flow conditions, to build a more complete engine model that will be useful in optimising the engine design.

List of Publications

1) Alqahtani A. Shokrollahihassanbarough F., Wyszynski M.L., (2015). Thermodynamic Simulation Comparison of AVL BOOST and Ricardo Wave for HCCI and SI engines optimisation. Combustion Engines. 161(2), 68-72. ISSN 2300-9896

2) Alqahtani, A. M., Wyszynski, M. L. ,Mazuro, P. (2016). "Investigation into the effect of bore/stroke ratio on a single cylinder two stroke opposed piston engine." Journal of Kones   23 No 2: 9-16.

3) Alqahtani, A. M., Wyszynski, M. L. ,Mazuro, P, Xu, H. (2017). Evaluation of the effect of variable compression ratios performance on opposed piston 2-stroke engine. Combustion Engines. 171(4), 97-106. DOI: 10.19206/CE-2017-417

4) Shokrollahihassanbarough F., Alqahtani A., Wyszynski M.L. (2015). Thermodynamic simulation comparison of opposed two-stroke and conventional four-stroke engines. Combustion Engines. 162(3), 78-84. ISSN 2300-9896

References

[1]   John Heywood, Internal Combustion Engines Fundamentals. 1988*: McGraw-Hill*.

[2]   MYCO   SYSTEMS   LTD.   Steam   Engine. 2015.http://www.chilternmodelsteam.co.uk/about%20steam%20engines.html

[3]   R.H. Stanglmaier, and Roberts, C.E, Homogeneous Charge Compression Ignition (HCCI): Benefits, Compromises, and Future Engine Applications. *SAE Int. J. Engines*, 1999.

[4]   Z. Peng, Zhao, H., and Ladommatos, N.,, Effects of Air/Fuel Ratios and EGR Rates on HCCI Combustion of n-heptane, a Diesel Type Fuel. *SAE Int. J. Engines*, 2003.

[5]   Richard Stone, Introduction to Internal Combustion Engines. 3rd ed. 1999*: Macmillan*.

[6]   Dale Michael Turner, The Combustion and Emissions Perfomance of Fuel Blends in Modern Combustion Systems. **PhD.**, *Mechanical Engineering*, *University of Birmingham*, 2010

[7]   J Pirault and M Flint, Opposed Piston Engines: Evolution, Use, and Future Applications. 2009, *SAE International, 2009-10-08*.

[8]   Z. Xie, Zhao, Z., and Zhang, Z., Numerical Simulation of an Opposed-Piston Two-Stroke Diesel Engine. *SAE Int. J. Engines, 2015-04-14*, 2015.

[9]   J. Kalke, Opaliński, M., & Szczeciński, M. , Opposed-piston engines: the future of internal combustion engines. . 2014*: PhD Interdisciplinary*.

[10]   Michael Wahl. Achates Power - Fundamentally Better Engines-A Historical Look at Opposed-Piston Engines-Online Data base, http://achatespower.com/opposed-piston-engine-history/. 2011.

[11]   Randy E. Herold Gerhard Regner, Michael H. Wahl, Eric Dion, Fabien Redon, David Johnson, Brian J. Callahan and Shauna McIntyre, The Achates Power Opposed-Piston Two-Stroke Engine: Performance and Emissions Results in a Medium-Duty Application*. SAE Int. J. Engines, 2011-01-2221*, 2011. **4**(3): p. 10.

[12]   G. Regner, Johnson, D., Koszewnik, J., Dion, E. et al., Modernizing the Opposed Piston, Two Stroke Engine for Clean, Efficient Transportation. *SAE Int. J. Engines, 2013-01-09*, 2013. **26**.

[13]   R. Herold, Wahl, M., Regner, G., Lemke, J. et al, Thermodynamic Benefits of Opposed-Piston Two-Stroke Engines*. SAE Int. J. Engines*, 2011. **01**.

[14]   Rishikesh Venugopal, Neerav Abani, and Ryan MacKenzie. Effects of Injection Pattern Design on Piston Thermal Management in an Opposed-Piston Two-Stroke Engine. 2013. *SAE International, 2013-09-24*; 2013-01-2423, 10.4271/2013-01-2423,

[15]   Randy E. Herold Gerhard Regner, Michael H. Wahl, Eric Dion, Fabien Redon, David Johnson, Brian J. Callahan and Shauna McIntyre, The Achates Power Opposed-Piston Two-Stroke Engine: Performance and Emissions Results in a Medium-Duty Application*. SAE Int. J. Engines 2011-01-2221*, 2011.

[16]   M. Opaliński, Mazuro, P. and Wyszyński, M., , Comparison of flow performance in one and three dimensional software for modelling of opposed piston engines. *Archivum Combustions*, 2015. **35**.

[17]   D. Johnson, Wahl, M., Redon, F., Dion, E., McIntyre, S., Regner, G., and Herold, R. Opposed-Piston Two-Stroke Diesel Engine Advantages in meeting higher fuel efficiency and emission standards. in 3rd Aachen Colloquium China Automobile and Engine Technology. 2013.

[18]   Per Risberg, Gautam Kalghatgi, and Hans-Erik Ångstrom. The Influence of EGR on Auto-ignition Quality of Gasoline-like Fuels in HCCI Engines. 2004. *SAE International*; 10.4271/2004-01-2952,

[19]   Marcin Opalinski Jakub Kalke, Paweł Mazuro Experimental test stand for development of an opposed-piston engine and initial results. *Combustion Engines PTNSS*, 2017. **169**(2): p. 7.

[20]   Marcin Opalinski, Andrzej Teodorczyk, and Jakub Kalke, The closed-cycle model numerical analysis of the impact of crank mechanism design on engine efficiency. *Combustion Engines PTNSS*, 2017. **168**(1): p. 8.

[21]   Ricardo WAVE, WAVE Knowledge Center. 2014.

[22]   A. M. Alqahtani, Wyszynski, M. L. , Mazuro, P., Investigation into the effect of bore/stroke ratio on a single cylinder two stroke opposed piston engine. *Journal of Kones*, 2016. **23 No 2**: p. 9-16.

[23]   Alqahtani A. Shokrollahihassanbarough F., Wyszynski M.L, Thermodynamic simulation comparison of opposed two-stroke and conventional four-stroke engines. *Combustion Engines PTNSS*, 2015. **162**(3): p. 6.

[24]   SHOKROLLAHIHASSANBAROUGH F. ALQAHTANI A., WYSZYNSKI M.L., Thermodynamic simulation comparison of AVL BOOST and Ricardo WAVE for HCCI and SI engines optimisation. *Combustion Engines PTNSS*, 2015. **161**(2): p. 5.

[25]   Changlu Zhao Fukang Ma, Fujun Zhang, Zhenfeng Zhao, Zhenyu Zhang, , Zhaoyi Xie and Hao Wang An Experimental Investigation on the Combustion and Heat Release Characteristics of an Opposed-Piston Folded-Cranktrain Diesel Engine *Energies*, 2015. **8**: p. 6365-6381.

[26]   S. Naik, Johnson, D., Koszewnik, J., Fromm, L. et al, Practical Applications of Opposed-Piston Engine Technology to Reduce Fuel Consumption and Emissions. *SAE Int. J. Engines*, 2013. **01**.

[27]   I. and Katrašnik Prah, T., Application of Optimization Techniques to Determine Parameters of the Vibe Combustion Model. *Strojniški vestnik - Journal of Mechanical Engineering*, 2009. **11**: p. 11.

[28]   S.P. Iliev, Devloping of a 1-D Combustion Model and Study of Engine Characteristics Using Ethanol-Gasoline Blends. *Proceedings of the World Congress on Engineering*, 2014. **2**.

[29]   G. Sandu, Cofaru, C., Sacareanu, S., et al., Research of the Engine's Speed Influence on the Intake Process of a Naturally Aspirated Engine. *Bulletin of the Transilvania University of Braşov, Series I: Engineering Sciences*, 2011. **4**(53).

[30]   C. Lee, Goel, S., Babajimopoulos, The Effects of Stroke-to-Bore Ratio on HCCI Combustion. *SAE Technical Paper*, 2010. **01**(0842).

[31]   A. Vassallo, Gopalakrishnan, V., Arrigoni, S., Cavallo, R. et al., Impact of Bore-to-Stroke Ratio Over Light-Duty DI Diesel Engine Performance, Emissions and Fuel Consumption: An Analytical Study Using 1D-CFD Coupled with DOE Methodology. *SAE Technical Paper, 2013-09-08*, 2013. **24**(0013).

[32]   A. Alqahtani, WYszynski M., Mazuro, P., Xu, H, Evaluation of the effect of variable compression ratios performance on opposed piston 2-stroke engine *Combustion Engines PTNSS*, 2017. **171**(4): p. 10.

[33]   G. Regner, Herold, R., Wahl, M., Dion, E. et al., The Achates Power Opposed-Piston Two-Stroke Engine: Performance and Emissions Results in a Medium-Duty Application. *SAE Int. J. Engines*, 2011. **4**(3).

[34]   D. R Lancaster, Kreiger, R. B., and Lienesch, J. H, Measurement and Analysis of Engine Pressure Data. *SAE Int. J. Engines*, 1975.

[35]   D. F. Caris, and Nelson, E. E, A New Look at High Compression Engines. *SAE Trans*, 1959. **67**.

[36]   R.B Krieger and G.L Borman, The Computation of Applied Heat Release for Internal Combustion Engines. *ASME Paper 66-WA/DGP-4; SAE*, 1966.

[37]   M.F.J.; Rai Brunt, H.; Emtage, A.L., The Calculation of Heat Release Energy from Engine Cylinder Pressure Data. *SAE Technical Paper, 1998-02-23*, 1998.

[38]   Richard C. and Seinfeld Flagan, John H., Fundamentals of air pollution engineering, Chapter 4, Internal Combustion Engines. 4 ed. 1988, *Prentice-Hall, Inc. , Englewood Cliffs, New Jersey*.

Appendices

Appendix 5.1. Intake and Exhaust Lifts

Table 7 Intake and Exhaust Lifts

CAD	Low Lift Exhaust	CAD	High Lift Exhaust	CAD	Low Lift Intake	CAD	High Lift Intake
0.4	0	1	0	0.5	0	1	0
0.9	0.03	2	0.12	1	0.03	2	0.12
1.3	0.04	3	0.18	1.6	0.04	3	0.18
1.8	0.05	4	0.24	2.1	0.06	4	0.23
2.2	0.07	5	0.3	2.6	0.07	5	0.29
2.6	0.08	6	0.36	3.1	0.09	6	0.35
3.1	0.09	7	0.42	3.6	0.1	7	0.41
3.5	0.11	8	0.48	4.2	0.12	8	0.47
4	0.12	9	0.54	4.7	0.13	9	0.53
4.4	0.13	10	0.6	5.2	0.15	10	0.58
4.8	0.15	11	0.66	5.7	0.16	11	0.64
5.3	0.16	12	0.72	6.2	0.18	12	0.71
5.7	0.18	13	0.79	6.8	0.2	13	0.78
6.2	0.2	14	0.87	7.3	0.22	14	0.86
6.6	0.22	15	0.96	7.8	0.24	15	0.94
7	0.24	16	1.05	8.3	0.26	16	1.04
7.5	0.26	17	1.15	8.8	0.29	17	1.14
7.9	0.28	18	1.26	9.4	0.31	18	1.24
8.4	0.31	19	1.37	9.9	0.34	19	1.35
8.8	0.33	20	1.49	10.4	0.37	20	1.47
9.2	0.36	21	1.61	10.9	0.4	21	1.59
9.7	0.39	22	1.74	11.4	0.43	22	1.72

10.1	0.42	23	1.86	12	0.46	23	1.84
10.6	0.45	24	1.98	12.5	0.49	24	1.96
11	0.47	25	2.11	13	0.53	25	2.09
11.4	0.5	26	2.23	13.5	0.56	26	2.21
11.9	0.53	27	2.35	14	0.59	27	2.34
12.3	0.56	28	2.48	14.6	0.62	28	2.46
12.8	0.58	29	2.6	15.1	0.65	29	2.59
13.2	0.61	30	2.72	15.6	0.68	30	2.71
13.6	0.64	31	2.85	16.1	0.71	31	2.83
14.1	0.67	32	2.97	16.6	0.74	32	2.96
14.5	0.69	33	3.09	17.2	0.78	33	3.08
15	0.72	34	3.22	17.7	0.81	34	3.21
15.4	0.75	35	3.34	18.2	0.84	35	3.33
15.8	0.78	36	3.46	18.7	0.87	36	3.45
16.3	0.8	37	3.58	19.2	0.9	37	3.58
16.7	0.83	38	3.71	19.8	0.93	38	3.7
17.2	0.86	39	3.83	20.3	0.96	39	3.83
17.6	0.89	40	3.95	20.8	0.99	40	3.95
18	0.91	41	4.08	21.3	1.03	41	4.07
18.5	0.94	42	4.2	21.8	1.06	42	4.2
18.9	0.97	43	4.32	22.4	1.09	43	4.32
19.4	1	44	4.44	22.9	1.12	44	4.44
19.8	1.02	45	4.57	23.4	1.15	45	4.57
20.2	1.05	46	4.69	23.9	1.18	46	4.69
20.7	1.08	47	4.81	24.4	1.21	47	4.82
21.1	1.11	48	4.93	25	1.24	48	4.94
21.6	1.13	49	5.05	25.5	1.27	49	5.06
22	1.16	50	5.17	26	1.31	50	5.19
22.4	1.19	51	5.29	26.5	1.34	51	5.31
22.9	1.21	52	5.4	27	1.37	52	5.43
23.3	1.24	53	5.51	27.6	1.4	53	5.56
23.8	1.26	54	5.63	28.1	1.43	54	5.68

24.2	1.29	55	5.74	28.6	1.46	55	5.8
24.6	1.31	56	5.85	29.1	1.49	56	5.93
25.1	1.34	57	5.95	29.6	1.52	57	6.05
25.5	1.36	58	6.06	30.2	1.55	58	6.17
26	1.38	59	6.17	30.7	1.58	59	6.3
26.4	1.41	60	6.27	31.2	1.62	60	6.42
26.8	1.43	61	6.37	31.7	1.65	61	6.54
27.3	1.45	62	6.47	32.2	1.68	62	6.66
27.7	1.47	63	6.57	32.8	1.71	63	6.78
28.2	1.5	64	6.67	33.3	1.73	64	6.89
28.6	1.52	65	6.76	33.8	1.76	65	7.01
29	1.54	66	6.86	34.3	1.79	66	7.12
29.5	1.56	67	6.95	34.8	1.82	67	7.23
29.9	1.58	68	7.04	35.4	1.85	68	7.34
30.4	1.6	69	7.13	35.9	1.87	69	7.45
30.8	1.62	70	7.22	36.4	1.9	70	7.56
31.2	1.64	71	7.31	36.9	1.93	71	7.66
31.7	1.66	72	7.39	37.4	1.95	72	7.76
32.1	1.68	73	7.47	38	1.98	73	7.86
32.6	1.69	74	7.55	38.5	2	74	7.96
33	1.71	75	7.63	39	2.03	75	8.06
33.4	1.73	76	7.71	39.5	2.05	76	8.16
33.9	1.75	77	7.79	40	2.08	77	8.25
34.3	1.76	78	7.86	40.6	2.1	78	8.34
34.8	1.78	79	7.93	41.1	2.12	79	8.43
35.2	1.8	80	8.01	41.6	2.14	80	8.52
35.6	1.81	81	8.07	42.1	2.17	81	8.61
36.1	1.83	82	8.14	42.6	2.19	82	8.69
36.5	1.84	83	8.21	43.2	2.21	83	8.77
37	1.86	84	8.27	43.7	2.23	84	8.86
37.4	1.87	85	8.33	44.2	2.25	85	8.94
37.8	1.88	86	8.39	44.7	2.27	86	9.01

38.3	1.9	87	8.45	45.2	2.29	87	9.09
38.7	1.91	88	8.51	45.8	2.31	88	9.16
39.2	1.92	89	8.57	46.3	2.32	89	9.23
39.6	1.93	90	8.62	46.8	2.34	90	9.3
40	1.95	91	8.67	47.3	2.36	91	9.37
40.5	1.96	92	8.72	47.8	2.38	92	9.44
40.9	1.97	93	8.77	48.4	2.39	93	9.5
41.4	1.98	94	8.81	48.9	2.41	94	9.57
41.8	1.99	95	8.86	49.4	2.42	95	9.63
42.2	2	96	8.9	49.9	2.44	96	9.69
42.7	2.01	97	8.94	50.4	2.45	97	9.74
43.1	2.01	98	8.98	51	2.47	98	9.8
43.6	2.02	99	9.02	51.5	2.48	99	9.85
44	2.03	100	9.05	52	2.49	100	9.9
44.4	2.04	101	9.09	52.5	2.5	101	9.95
44.9	2.05	102	9.12	53	2.52	102	10
45.3	2.05	103	9.15	53.6	2.53	103	10.04
45.8	2.06	104	9.17	54.1	2.54	104	10.09
46.2	2.06	105	9.2	54.6	2.55	105	10.13
46.6	2.07	106	9.22	55.1	2.56	106	10.17
47.1	2.07	107	9.24	55.6	2.57	107	10.2
47.5	2.08	108	9.26	56.2	2.58	108	10.24
48	2.08	109	9.28	56.7	2.58	109	10.27
48.4	2.09	110	9.3	57.2	2.59	110	10.3
48.8	2.09	111	9.31	57.7	2.6	111	10.33
49.3	2.09	112	9.33	58.2	2.61	112	10.36
49.7	2.09	113	9.34	58.8	2.61	113	10.38
50.2	2.1	114	9.34	59.3	2.62	114	10.41
50.6	2.1	115	9.35	59.8	2.62	115	10.43
51	2.1	116	9.36	60.3	2.63	116	10.45
51.5	2.1	117	9.36	60.8	2.63	117	10.47
51.9	2.1	118	9.36	61.4	2.64	118	10.48

52.4	2.1	119	9.36	61.9	2.64	119	10.49
52.8	2.1	120	9.36	62.4	2.64	120	10.5
53.2	2.1	121	9.35	62.9	2.65	121	10.51
53.7	2.1	122	9.34	63.4	2.65	122	10.52
54.1	2.09	123	9.34	64	2.65	123	10.53
54.6	2.09	124	9.33	64.5	2.65	124	10.53
55	2.09	125	9.31	65	2.65	125	10.53
55.4	2.09	126	9.3	65.5	2.65	126	10.53
55.9	2.08	127	9.28	66	2.65	127	10.53
56.3	2.08	128	9.26	66.6	2.65	128	10.52
56.8	2.07	129	9.24	67.1	2.65	129	10.51
57.2	2.07	130	9.22	67.6	2.64	130	10.5
57.6	2.06	131	9.2	68.1	2.64	131	10.49
58.1	2.06	132	9.17	68.6	2.64	132	10.48
58.5	2.05	133	9.15	69.2	2.63	133	10.47
59	2.05	134	9.12	69.7	2.63	134	10.45
59.4	2.04	135	9.09	70.2	2.62	135	10.43
59.8	2.03	136	9.05	70.7	2.62	136	10.41
60.3	2.02	137	9.02	71.2	2.61	137	10.38
60.7	2.02	138	8.98	71.8	2.61	138	10.36
61.2	2.01	139	8.94	72.3	2.6	139	10.33
61.6	2	140	8.9	72.8	2.59	140	10.3
62	1.99	141	8.86	73.3	2.58	141	10.27
62.5	1.98	142	8.82	73.8	2.58	142	10.24
62.9	1.97	143	8.77	74.4	2.57	143	10.2
63.4	1.96	144	8.72	74.9	2.56	144	10.17
63.8	1.95	145	8.67	75.4	2.55	145	10.13
64.2	1.93	146	8.62	75.9	2.54	146	10.08
64.7	1.92	147	8.57	76.4	2.53	147	10.04
65.1	1.91	148	8.51	77	2.52	148	10
65.6	1.9	149	8.46	77.5	2.5	149	9.95
66	1.88	150	8.4	78	2.49	150	9.9

66.4	1.87	151	8.34	78.5	2.48	151	9.85
66.9	1.86	152	8.28	79	2.47	152	9.8
67.3	1.84	153	8.21	79.6	2.45	153	9.74
67.8	1.83	154	8.15	80.1	2.44	154	9.69
68.2	1.81	155	8.08	80.6	2.42	155	9.63
68.6	1.8	156	8.01	81.1	2.41	156	9.57
69.1	1.78	157	7.94	81.6	2.39	157	9.5
69.5	1.77	158	7.87	82.2	2.38	158	9.44
70	1.75	159	7.8	82.7	2.36	159	9.37
70.4	1.73	160	7.72	83.2	2.34	160	9.3
70.8	1.71	161	7.64	83.7	2.32	161	9.23
71.3	1.7	162	7.56	84.2	2.31	162	9.16
71.7	1.68	163	7.48	84.8	2.29	163	9.09
72.2	1.66	164	7.4	85.3	2.27	164	9.01
72.6	1.64	165	7.32	85.8	2.25	165	8.94
73	1.62	166	7.23	86.3	2.23	166	8.86
73.5	1.6	167	7.14	86.8	2.21	167	8.78
73.9	1.58	168	7.06	87.4	2.19	168	8.69
74.4	1.56	169	6.97	87.9	2.17	169	8.61
74.8	1.54	170	6.87	88.4	2.14	170	8.52
75.2	1.52	171	6.78	88.9	2.12	171	8.43
75.7	1.5	172	6.69	89.4	2.1	172	8.34
76.1	1.48	173	6.59	90	2.08	173	8.25
76.6	1.46	174	6.49	90.5	2.05	174	8.16
77	1.43	175	6.39	91	2.03	175	8.06
77.4	1.41	176	6.29	91.5	2.01	176	7.97
77.9	1.39	177	6.19	92	1.98	177	7.87
78.3	1.37	178	6.09	92.6	1.95	178	7.77
78.8	1.34	179	5.98	93.1	1.93	179	7.67
79.2	1.32	180	5.88	93.6	1.9	180	7.56
79.6	1.29	181	5.77	94.1	1.88	181	7.46
80.1	1.27	182	5.66	94.6	1.85	182	7.35

80.5	1.25	183	5.55	95.2	1.82	183	7.24
81	1.22	184	5.44	95.7	1.79	184	7.13
81.4	1.2	185	5.33	96.2	1.77	185	7.02
81.8	1.17	186	5.21	96.7	1.74	186	6.91
82.3	1.14	187	5.1	97.2	1.71	187	6.79
82.7	1.12	188	4.98	97.8	1.68	188	6.67
83.2	1.09	189	4.87	98.3	1.65	189	6.56
83.6	1.07	190	4.75	98.8	1.62	190	6.44
84	1.04	191	4.63	99.3	1.59	191	6.31
84.5	1.01	192	4.51	99.8	1.56	192	6.19
84.9	0.98	193	4.39	100.4	1.53	193	6.07
85.4	0.96	194	4.27	100.9	1.5	194	5.95
85.8	0.93	195	4.14	101.4	1.47	195	5.83
86.2	0.9	196	4.02	101.9	1.44	196	5.7
86.7	0.87	197	3.9	102.4	1.4	197	5.58
87.1	0.85	198	3.78	103	1.37	198	5.46
87.6	0.82	199	3.66	103.5	1.34	199	5.34
88	0.79	200	3.54	104	1.31	200	5.21
88.4	0.77	201	3.43	104.5	1.28	201	5.09
88.9	0.74	202	3.32	105	1.25	202	4.97
89.3	0.72	203	3.22	105.6	1.22	203	4.85
89.8	0.7	204	3.12	106.1	1.19	204	4.72
90.2	0.68	205	3.04	106.6	1.16	205	4.6
90.6	0.66	206	2.96	107.1	1.13	206	4.48
91.1	0.65	207	2.88	107.6	1.1	207	4.36
91.5	0.63	208	2.81	108.2	1.07	208	4.23
92	0.62	209	2.74	108.7	1.03	209	4.11
92.4	0.6	210	2.67	109.2	1	210	3.99
92.8	0.58	211	2.6	109.7	0.97	211	3.87
93.3	0.57	212	2.54	110.2	0.94	212	3.74
93.7	0.55	213	2.47	110.8	0.91	213	3.62
94.2	0.54	214	2.4	111.3	0.88	214	3.5

94.6	0.52	215	2.33	111.8	0.85	215	3.37
95	0.51	216	2.26	112.3	0.82	216	3.25
95.5	0.49	217	2.19	112.8	0.79	217	3.13
95.9	0.48	218	2.12	113.4	0.76	218	3.01
96.4	0.46	219	2.06	113.9	0.73	219	2.88
96.8	0.45	220	1.99	114.4	0.69	220	2.76
97.2	0.43	221	1.92	114.9	0.66	221	2.64
97.7	0.42	222	1.85	115.4	0.63	222	2.51
98.1	0.4	223	1.78	116	0.6	223	2.39
98.6	0.38	224	1.71	116.5	0.57	224	2.27
99	0.37	225	1.65	117	0.54	225	2.14
99.4	0.35	226	1.58	117.5	0.51	226	2.02
99.9	0.34	227	1.51	118	0.48	227	1.9
100.3	0.32	228	1.44	118.6	0.45	228	1.78
100.8	0.31	229	1.37	119.1	0.42	229	1.65
101.2	0.29	230	1.31	119.6	0.39	230	1.53
101.6	0.28	231	1.24	120.1	0.36	231	1.42
102.1	0.26	232	1.17	120.6	0.33	232	1.31
102.5	0.25	233	1.1	121.2	0.3	233	1.2
103	0.23	234	1.04	121.7	0.28	234	1.1
103.4	0.22	235	0.97	122.2	0.25	235	1.01
103.8	0.2	236	0.9	122.7	0.23	236	0.93
104.3	0.19	237	0.83	123.2	0.21	237	0.85
104.7	0.17	238	0.77	123.8	0.2	238	0.78
105.2	0.16	239	0.7	124.3	0.18	239	0.72
105.6	0.14	240	0.64	124.8	0.17	240	0.66
106	0.13	241	0.58	125.3	0.15	241	0.59
106.5	0.12	242	0.51	125.8	0.13	242	0.53
106.9	0.1	243	0.45	126.4	0.12	243	0.46
107.4	0.09	244	0.39	126.9	0.1	244	0.4
107.8	0.07	245	0.32	127.4	0.08	245	0.33
108.2	0.06	246	0.26	127.9	0.07	246	0.26

108.7	0.04	247	0.19	128.4	0.05	247	0.2
109.1	0.03	248	0.13	129	0.03	248	0.13
109.6	0.01	249	0.06	129.5	0.02	249	0.07
110	0	250	0	130	0	250	0